Parallel processing in the mammalian olfactory bulb

by

Matthew A. Geramita

Bachelor of Science, Biophysics, University of Michigan, 2008

Submitted to the Graduate Faculty of

The Kenneth P. Dietrich School of Arts and Sciences in partial fulfillment

of the requirements for the degree of

Doctor of Philosophy

University of Pittsburgh

2016

UNIVERSITY OF PITTSBURGH

DIETRICH SCHOOL OF ARTS AND SCIENCES

This dissertation was presented

by

Matthew A. Geramita

It was defended on

June 9, 2016

and approved by

Elias Aizenman, Ph.D.

Alison L. Barth, Ph.D.

Brent Doiron, Ph.D.

Sandra J. Kuhlman, Ph.D.

Kerry J. Ressler, M.D.,Ph.D.

Thesis Advisor: Nathan N. Urban, Ph.D.

Parallel processing in the mammalian olfactory bulb

Matthew A. Geramita

University of Pittsburgh, 2016

PARALLEL PROCESSING IN THE MAMMALIAN OLFACTORY BULB

Matthew A. Geramita, Ph.D.

University of Pittsburgh, 2016

Splitting sensory information into parallel pathways is a common strategy in sensory systems. Yet, it is not well understood how circuits in these parallel pathways are composed to maintain or even enhance the encoding of specific stimulus features. In this dissertation, we investigate the parallel pathways formed by mitral and tufted cells (MCs and TCs) of the olfactory system and characterize the emergence of feature selectivity in these cell types via distinct patterns of connectivity to local inhibitory interneurons.

Chapter 2 explores differences in feedforward circuitry onto MCs and TCs. We find that MCs display longer latency spiking that is more strongly dependent on stimulus intensity than TCs. Longer latency spiking in MCs is a consequence of weaker excitatory and stronger inhibitory currents, mediated by periglomerular cells, onto MCs compared to TCs.

Chapter 3 describes the causes and consequences of lateral inhibition differences between MCs and TCs. We find that MCs are affected by lateral inhibition at intermediate firing rates, while TCs are affected at lower firing rates. These differences arise, in part, due to differential recruitment of morphologically distinct classes of granule cells by MCs and TCs. Using simulations, we show that these differences in lateral inhibition allow TCs and MCs to perform odor discriminations best in separate concentration ranges.

Together, the experiments described here suggest that differences in odor-evoked responses between MCs and TCs are a consequence of distinct patterns of connectivity to multiple populations of inhibitory interneurons.

TABLE OF CONTENTS

LIST OF TABLES IX

LIST OF FIGURES X

PREFACE XIII

1.0 INTRODUCTION 1

1.1 Olfactory sensory neurons 3

1.1.1 Nasal epithelium 3

1.1.2 From the nose to the olfactory bulb 4

1.2 Cell types of the olfactory bulb 5

1.2.1 Mitral and tufted cells 6

1.2.2 Periglomerular cells 9

1.2.3 Superficial short-axon cells 9

1.2.4 Granule cells 10

1.3 Goals of the dissertation 12

2.0 DIFFERENCES IN PERIGLOMERULAR CELL MEDIATED FEED-FORWARD INHIBITION ONTO MITRAL AND TUFTED CELLS LEAD TO DISTINCT MODES OF INTENSITY CODING 17

2.1 Introduction 17

2.2 Materials and Methods 19

2.2.1 Slice preparation 19

2.2.2 Cell classification 20

2.2.3 Electrophysiology 20

2.2.4 Data analysis and statistics 22

2.3 Results 22

2.3.1 Mitral and tufted cells encode the intensity of olfactory sensory neuron stimulation differently 22

2.3.2 TCs respond to OSN stimulation with stronger excitatory and weaker inhibitory currents than MCs 28

2.3.3 MCs receive stronger PGC-mediated inhibition than TCs 32

2.3.4 Blocking PGC-mediated, but not GC-mediated inhibition, affects spike latencies in MCs but not TCs. 34

2.4 Discussion 40

3.0 DISTINCT LATERAL INHIBITORY CIRCUITS DRIVE PARALLEL PROCESSING OF SENSORY INFORMATION IN THE MAMMALIAN OLFACTORY BULB 46

3.1 Introduction 46

3.2 Materials and methods 48

3.2.1 Slice preparation 48

3.2.2 Cell identification and morphological analyses 49

3.2.3 Electrophysiology 50

3.2.4 Data analysis 51

3.2.5 Computational model 52

3.3 Results 55

3.3.1 MCs receive stronger and more asynchronous lateral inhibitory currents than TCs 55

3.3.2 Lateral inhibition affects intermediate firing rates in MCs and low firing rates in TCs 61

3.3.3 Differences in the excitability of anatomically defined subclasses of GCs account for differences in the effective activity range of lateral inhibition onto MCs and TCs69

3.3.4 Differences in lateral inhibition between MCs and TCs translate into differences in stimulus encoding 83

3.4 Discussion 92

4.0 GENERAL DISCUSSION 99

4.1 Summary of findings 99

4.2 Finding better markers for MCs and TCs 102

4.3 Do MCs and TCs mediate different behaviors? 104

4.4 Feedback from the cortex 107

4.5 Segregation of lateral inhibition 108

4.6 Plasticity of lateral inhibition..... 109

4.7 General conclusions 112

APPENDIX A: POSTNATAL ODOR EXPOSURE INCREASES THE STRENGTH OF INTER-GLOMERULAR LATERAL INHIBITION ONTO OLFACTORY BULB TUFTED CELLS. 113

BIBLIOGRAPHY 128

LIST OF TABLES

Table 1: Morphological properties of GCs 78

Table 2: Action potential properties of GCs 78

Table 3: Spike train properties of GCs 78

Table 4: Passive membrane properties of GCs 79

Table 5: Spontaneous synaptic event properties of GCs 79

LIST OF FIGURES

Figure 1: Olfactory bulb anatomy with relevant cell types and tissue layers 16

Figure 2: Examples that MCs and TCs encode the intensity of olfactory sensory neuron stimulation differently. 25

Figure 3: Summary statistics indicating that MCs and TCs encode the intensity of olfactory sensory neuron stimulation differently. 26

Figure 4: Optical activation of a single glomeruli in olfactory bulb sections from OMP-ChR2:EYFP mice 27

Figure 5: Examples showing that TCs respond to electrical stimulation of OSNs with stronger excitatory and weaker inhibitory currents than MCs. 30

Figure 6: Summary statistics indicating that TCs respond to electrical stimulation of OSNs with stronger excitatory and weaker inhibitory currents than MCs. 31

Figure 7: MCs receive stronger PGC-mediated inhibition than TCs. 33

Figure 8: Examples showing that blocking GC-mediated inhibition does not alter firing rates or spike latencies in MCs or TCs. 36

Figure 9: Summary statistics indicating that blocking GC-mediated inhibition does not alter firing rates or spike latencies in MCs or TCs. 37

Figure 10: Examples showing that blocking PGC-mediated inhibition alters spike latencies in MCs but not TCs. 38

Figure 11: Summary statistics indicating that blocking PGC-mediated inhibition alters spike latencies in MCs but not TCs. 39
Figure 12: Summary of differences in feed-forward circuitry onto MCs and TCs 45
Figure 13: MCs receive stronger lateral inhibition than TCs. 58
Figure 14: Glomerular layer circuits cannot explain lateral inhibition differences between MCs and TCs. 59
Figure 15: Distance dependence of lateral inhibition onto MCs and TCs. 60
Figure 16: Examples show a TC and MC affected by lateral inhibition at low and intermediate firing rates, respectively. 63
Figure 17: MCs and TCs can sustain high firing rates for long periods 64
Figure 18: Summary results show that TCs are influenced by lateral inhibition at low rates while MCs are influenced at intermediate rates. 65
Figure 19: Distance dependence of lateral inhibition onto MCs and TCs. 66
Figure 20: Examples of FI curves with and without photostimulation of the M72. 67
Figure 21: Differences in ADLI are maintained on physiologically relevant timescales 68
Figure 22: Example of recordings from superficial GCs following glomerular activation. 74
Figure 23: Example of recordings from deep GCs following glomerular activation. 75
Figure 24: Synaptic and intrinsic differences between superficial and deep GCs regulate recruitment following glomerular activation. 76
Figure 25: Morphological analysis of superficial and deep GCs. 77
Figure 26: Proposed mechanism of ADLI in mitral (MCs) and tufted cells (TCs). 80
Figure 27: Increasing GC excitability shifts the effective activity range of lateral inhibition in MCs to lower frequencies. 81

Figure 28: DHPG has no effect on MC excitability. 82
Figure 29: MCs and TCs discriminate between odors best in separate concentration ranges. 88
Figure 30: Procedure used to create the odors that served as inputs to simulated mitral and tufted cell networks. 89
Figure 31: Subtractive or divisive lateral inhibition does not improve discrimination accuracy. 90
Figure 32: Visual processing example of how the multiple parallel neuron populations can simultaneously enhance the contrast of high and low intensity images. 91
Figure 33: Postnatal exposure to the M72 ligand, acetophenone, increases the strength of M72-mediated lateral inhibition onto TCs, but not MCs..... 121
Figure 34: Statistics indicating that postnatal exposure to the M72 ligand, acetophenone, increases the strength of M72-mediated lateral inhibition onto TCs, but not MCs. 123
Figure 35: Postnatal exposure to the M72 ligand, acetophenone, increases the strength of M72-mediated lateral inhibition onto TCs, but not MCs..... 124

PREFACE

The work presented in this dissertation is based on three manuscripts.

Chapter 2 is based on:

Geramita, M. and Urban, N.N. (submitted). “Differences in periglomerular cell mediated feed-forward inhibition onto mitral and tufted cells lead to distinct modes of intensity coding.”

Chapter 3 is based on:

Geramita, M., Burton S.D., and Urban, N.N. (submitted). "Distinct lateral inhibitory circuits drive parallel processing of sensory information in the mammalian olfactory bulb."

Appendix A is based on:

Geramita, M. and Urban, N.N. (submitted). “Postnatal odor exposure increases the strength of inter-glomerular lateral inhibition onto olfactory bulb tufted cells.”

All of the experiments presented in this thesis were conducted by Matthew Geramita, except those presented in Figures 22-25, which were conducted by Shawn D. Burton.

1.0 INTRODUCTION

All mammals, from platypus to humans and everything in between, spend their entire lives sensing, interpreting and acting on a barrage of information about the external world. Their survival depends on it. Each sensory system is structured in a way that allows it to process a specific aspect of the environment. As humans, we see photons of light at distinct wavelengths and either stop or speed through traffic lights; we feel pressure moving around our ear and swat that pesky fly; we hear oscillations in air pressure and run to answer the phone; we smell sets of chemicals wafting from the kitchen and salivate in anticipation of chocolate chip cookies. All other mammals respond in analogously idiosyncratic ways to similar types of stimuli.

How the mammalian brain senses, interprets and initiates an action to respond to these stimuli is one of the most fascinating and important questions in neuroscience today. Broadly, for each sense, a primary sensory organ translates external stimuli into patterns of action potentials that are processed by multiple areas of the brain and ultimately translated into a coordinated motor response. This dissertation answers questions that involve the intermediate processing steps required for this to happen. Which aspects of action potential patterns, such as their rate or timing, encode the identity of a sensory stimulus? How do neurons in upstream brain areas decode information passed on from lower level brain areas? How do inhibitory interneurons shape the way sensory information is represented in populations of neurons? Most importantly

for this dissertation, how do sensory systems encode multiple features of a stimulus simultaneously?

The visual system is one example of a sensory system that encodes multiple features of a stimulus simultaneously. When we see, we are extracting information about color, brightness, motion, shape and depth, all at the same time. Similarly, our somatosensory system simultaneously extracts information about pain, temperature, itch and texture. Each of these systems, and potentially others, uses parallel populations of neurons to encode individual sensory features that are ultimately combined into a unified perception incorporating all features. This organization allows individual types of neurons to specialize, which, in many instances, means each neuron type will have specific properties and patterns of connectivity that will ultimately allow it to perform more its specific task most efficiently. This question – how local circuitry within sensory areas shapes information so that individual features of a stimulus emerge in parallel classes of output neurons – will be the focus of this dissertation.

Here, we explore how parallel processing emerges in the olfactory bulb. Why use the olfactory system? 1) Olfaction, more than any other sense, guides the behavior of mice, and mice are important model organisms for leveraging recent advances in optogenetics and virology to test how individual neuron types affect behavior. 2) The olfactory system is shallower than other sensory systems, meaning that information must only pass through two layers of neurons (rather than four layers in the visual system, for instance) to reach the cortex. Consequently, understanding how local inhibitory circuitry affects sensory processing at each layer of the hierarchy is more tractable in the olfactory system. 3) Parallel streams of information emerge at the second layer of the olfactory system. Each of the two distinct classes receives input from a source (in the first layer) in which multiple features are encoded. This implies that

representations of specific sensory features in the second layer of cells emerge solely due to differences in how the cells are embedded within the local circuitry of the olfactory bulb. 4) Finally, the idea that the olfactory bulb splits information into parallel streams of information is relatively new, despite the wide acceptance of parallelization of sensory information in the visual and somatosensory systems. This dissertation aims to reverse the long held dogma that a single class of neurons encodes all aspects of odor information.

In this dissertation, we explore how differential connectivity to local olfactory bulb inhibitory interneurons allows mitral and tufted cells, the two types of olfactory bulb output neurons, to encode particular odor features in parallel. Chapter 2 describes how periglomerular cells differentially inhibit mitral and tufted cells so that spike latencies in mitral cells, but not tufted cells, vary with odor intensity. Chapter 3 shows how lateral inhibition differentially influences mitral and tufted cells due to distinct connectivity to separate populations of granule cells. We show that these differences in lateral inhibition ultimately allow mitral and tufted cells to perform odor discriminations best in separate odor concentration ranges. Together, the data presented here provide strong evidence that the local inhibitory circuitry of the olfactory bulb differentially affects mitral and tufted cells and ultimately allows them to perform distinct roles in odor processing.

1.1 OLFACTORY SENSORY NEURONS

1.1.1 Nasal epithelium

Odor processing begins when odors enter the nose and bind to receptors on olfactory

sensory neurons (OSNs), which reside in the olfactory epithelium. OSN dendrites express G-protein coupled receptors (GPCRs), called olfactory receptors, which bind odors and begin a signaling cascade that results in spikes that propagate throughout the OSN. The cascade begins when G_{olf} protein activates adenylyl-cyclase resulting in an increase in cAMP concentrations and subsequent activation of the cyclic nucleotide gated (CNG) channels in the receptor (Ronnett, Cho et al. 1993, Buck 1996). Opening of the CNG channels allow sodium and calcium to enter the OSN and cause depolarization and action potential generation (Zufall, Leinders-Zufall et al. 2000).

There are approximately 1300 odorant receptors in mice (Zhang and Firestein 2002), and each OSN expresses only one odorant receptor type (Ngai, Chess et al. 1993, Ngai, Dowling et al. 1993, Ressler, Sullivan et al. 1993, Vassar, Ngai et al. 1993) so that the olfactory receptive field of an OSN is dictated by the specific olfactory receptor expressed. Olfactory receptors vary widely in their receptive fields – some are activated by many odors, others by only a few. Conversely, a single odorant can activate multiple OSN types, so that a particular odor can be defined by the set of OSN types that it activates.

1.1.2 From the nose to the olfactory bulb

OSN axons relay odor information to the olfactory bulb where OSNs of a particular type coalesce into spherical structures call glomeruli (Ressler, Sullivan et al. 1994, Mombaerts, Wang et al. 1996, Mombaerts, Wang et al. 1996). Specific glomeruli (defined by the OSN type) target precise spatial locations on the bulb that are remarkably conserved across animals (Soucy, Albeanu et al. 2009). Because odors activate particular sets of OSNs, the spatial pattern of

activated glomeruli contains odor information. Consequently behaviorally important tasks such as odor discrimination or recognition can be restated as a problem of decoding activity-patterns across the two-dimensional sheet of glomeruli in the olfactory bulb (Uchida, Poo et al. 2014). For instance, similar odors activate similar spatial patterns of glomeruli (Uchida, Takahashi et al. 2000). Simple decoding strategies can discriminate between odors using only information about the spatial pattern of activated glomeruli (Johnson and Leon 2000).

An important related question is whether nearby glomeruli exhibit similar odor response profiles (i.e., is the olfactory bulb chemotopically organized?). Early studies found that different functional groups and carbon chain lengths activated glomeruli within distinct domains of the olfactory bulb (Johnson and Leon 2000, Uchida, Takahashi et al. 2000, Meister and Bonhoeffer 2001, Mori, Takahashi et al. 2006). This fractured topography showed coarse spatial biases on the scale of millimeters. However more recent studies found no finer spatial topography – pairs neighboring glomeruli were no more similar in their response profiles than distant pairs (Soucy, Albeanu et al. 2009). Whether chemotopy exists in the olfactory bulb is important when studying the role of inhibitory interneurons. How inhibitory interneurons can facilitate contrast enhancement in circuits that lack topography will be an important question addressed in this later in this introduction and in Chapter 3.

1.2 CELL TYPES OF THE OLFACTORY BULB

A diagram of the relevant tissue layers and cell types of the olfactory bulb can be found in Figure 1**.**

1.2.1 Mitral and tufted cells

Mitral and tufted cells are the two types of excitatory output neurons that send odor information out of the bulb. Mitral cells reside in the mitral cell layer while tufted cells reside throughout the external plexiform layer. Each mitral and tufted cell receives excitatory input from a single glomerulus via an apical dendrite that branches repeatedly to form a tuft within the glomerulus. In addition to a single apical dendrite, mitral and tufted cells receive multiple lateral dendrites tangentially throughout the external plexiform layer where they make inhibitory synaptic inputs from granule cells via reciprocal dendrodendtric synapses(Rall, Shepherd et al. 1966). Compared with mitral cells, tufted cells have fewer and shorter lateral dendrites (Mori, Kishi et al. 1983, Orona, Rainer et al. 1984, Burton and Urban 2014) that innervate separate strata of the external plexiform layer (Mori, Kishi et al. 1983, Orona, Rainer et al. 1984) indicating that lateral inhibitory circuits onto mitral and tufted cells may be segregated. Mitral and tufted cell axons project to a largely overlapping cortical areas. Tufted cells axons innervate the anterior olfactory nucleus, the anterior piriform cortex, and the olfactory tubercle, while mitral cells project to the anterior and posterior piriform cortex, the olfactory tubercle, the anterior olfactory nucleus, the lateral entorhinal cortex, the nucleus of the lateral olfactory tract and the cortical amygdaloid nucleus (Nagayama, Enerva et al. 2010, Igarashi, Ieki et al. 2012).

Excitation onto mitral and tufted cells within the glomerulus is a multi-step process mediated by a variety of factors. Following OSN activation, glutamate directly excites the distal tuft of mitral and tufted cells as well as external tufted cells – an intrinsically bursting excitatory interneuron (Hayar, Karnup et al. 2004, Hayar, Karnup et al. 2004, Liu and Shipley 2008, Liu and Shipley 2008). Glutamate release from OSNs synchronizes external tufted cell bursting

within the glomerulus, which triggers glutamate release from the apical dendrites of external tufted cells and induces a long-lasting depolarization in mitral and tufted cells(Carlson, Shipley et al. 2000). Therefore excitation onto mitral and tufted cells occurs in two stages, the initial monosynaptic excitation from OSNs followed by a longer-lasting (~500 ms) wave of excitation mediated by external tufted cells. Inputs from external tufted cells, as well as gap junctions and AMPA autoreceptors(Schoppa and Westbrook 2002, Christie, Bark et al. 2005, Ma and Lowe 2010) synchronize homotypic mitral and tufted cells cells (mitral/tufted cells that receive input from the same glomerulus) (Schoppa and Westbrook 2001). Compared with mitral cells tufted cells receive strong direct excitation (Gire, Franks et al. 2012, Burton and Urban 2014) from OSNs and are more intrinsically excitable (Burton and Urban 2014).

How do mitral and tufted cells represent odorant information? As mentioned above, at the level of OSNs, odor information is represented by the spatial map of glomerular activation. Because mitral and tufted cells receive excitatory input from a single glomerulus, the spatial map of mitral and tufted cell activity similarly contains odor information. While firing rates in mitral and tufted cells change in response to odors in awake animals (Rinberg, Koulakov et al. 2006, Davison and Katz 2007, Bathellier, Carleton et al. 2008), the timing of spikes also changes and is thought to relay odorant information as well. One of the main influences of spike timing in mitral and tufted cells is respiration. Animals sniff at 2-3 Hz during slow breathing and 7-10 Hz during active exploration (Shusterman, Smear et al. 2011, Wachowiak 2011). In awake mice, mitral and tufted cells reliably spike at temporally precise phases of the sniff cycle (Chaput 1986, Cury and Uchida 2010, Shusterman, Smear et al. 2011). Importantly, animals can be trained to discriminate between ORN activation at different phases of the sniff cycle (Smear, Shusterman et al. 2011). Additionally, information about odor identity can be decoded more effectively using

the fine scale temporal structure of odor-evoked responses across the sniff cycle than with the total number spikes evoked throughout the sniff (Fantana, Soucy et al. 2008, Cury and Uchida 2010). This fine scale temporal structure of spikes across mitral and tufted populations evolves over time. Consequently, the spike patterns evoked by similar odors become less decorrelated over time (Bathellier, Buhl et al. 2008, Cury and Uchida 2010). Granule cells drive this decorrelation (Gschwend, Abraham et al. 2015) and are crucial to the animal's ability to discriminate between similar odors (Abraham, Spors et al. 2004, Abraham, Egger et al. 2010, Gschwend, Abraham et al. 2015). The mechanisms that allow granule cells to decorrelate mitral and tufted cells will be discussed below and will be the focus of Chapter 3.

Despite differences between mitral and tufted cell axon and dendrite innervation patterns and morphologies, the field has long considered them to be functionally equivalent neuron types. However, emerging evidence shows that mitral and tufted cells exhibit distinct activity *in vivo*, suggesting that each cell type encodes distinct aspects of olfactory information. For instance, compared with mitral cells, tufted cells respond to lower concentrations odors (Igarashi, Ieki et al. 2012, Kikuta, Fletcher et al. 2013), respond earlier in the sniff cycle to odors (Fukunaga, Berning et al. 2012, Igarashi, Ieki et al. 2012); display odor-evoked responses that are more strongly correlated to OSN activity (Adam, Livneh et al. 2014) and vary less with concentration (Fukunaga, Berning et al. 2012, Igarashi, Ieki et al. 2012). Additionally, mitral and tufted cells are influenced by cortical feedback differently. Feedback from the piriform cortex decorrelates representations in mitral cells, but not tufted cells (Otazu, Chae et al. 2015). Additionally feedback from the raphe nucleus excites tufted cells but bidirectionally modulates mitral cells leading to improved pattern separation of mitral cell, but not tufted cell, odor representations (Kapoor, Provost et al. 2016).

1.2.2 Periglomerular cells

Periglomeruluar cells are small axonless GABAergic neurons that project a single apical dendrite, which receives excitatory and inhibitory input from a single glomerulus (Pinching and Powell 1971, Pinching and Powell 1971, Pinching and Powell 1971, Kosaka and Kosaka 2010). About half of periglomeular cells receive direct excitation from OSNs while the other half receive excitation from external tufted cells (Hayar, Karnup et al. 2004, Hayar, Shipley et al. 2005). Additionally, PGCs are molecularly heterogeneous (Kosaka, Toida et al. 1998, Parrish-Aungst, Shipley et al. 2007, Kiyokage, Pan et al. 2010). Periglomerular cells provide feedforward inhibition onto mitral and tufted cells that peaks approximately 100ms following OSN activation and have been proposed to mediate differences in spike latency between mitral and tufted cells *in vivo* (Fukunaga, Berning et al. 2012). In Chapter 2, the question of whether mitral and tufted cells receive different amounts of periglomerular cell mediated inhibition is explored.

1.2.3 Superficial short-axon cells

Short-axon cells are a class of dopaminergic/GABAergic interneuron that receives excitatory input from external tufted cells of multiple glomeruli and send axons to multiple glomeruli (Pinching and Powell 1971, Pinching and Powell 1971, Pinching and Powell 1971, Aungst, Heyward et al. 2003, Hayar, Karnup et al. 2004, Kiyokage, Pan et al. 2010, Kosaka and Kosaka 2010, Kosaka and Kosaka 2011, Liu, Plachez et al. 2013). Axon of short-axon cells release both GABA and dopamine onto external tufted cells (Liu, Plachez et al. 2013, Whitesell, Sorensen et al. 2013). The co-release of dopamine and GABA onto external tufted cells leads to

a hyperpolarization followed by a dopamine-mediated depolarization (Liu, Plachez et al. 2013, Whitesell, Sorensen et al. 2013, Banerjee, Marbach et al. 2015). Functionally, short-axon cells implement gain control and decorrelation of odor representations in mitral and tufted cells (Banerjee, Marbach et al. 2015). Whether mitral and tufted cells receive direct input from short-axon cells is unknown and will be addressed in Chapter 3.

1.2.4 Granule cells

Granule cells reside in the granule cell layer, deep to the mitral cell layer. These cells lack an axon and project a prominent apical dendrite vertically into the EPL and smaller basal dendrites into the granule cell layer. Granule cells can be divided into two distinct classes based on their pattern of dendritic targeting – those that innervate a deep vs. a superficial lamina of the EPL (Mori, Kishi et al. 1983, Orona, Scott et al. 1983) – indicating that each class of granule cell may preferentially connect to either mitral or tufted cells.

Glutamate released from mitral and tufted cell lateral dendrites binds to AMPA and NMDA receptors on GCs: AMPA receptors mediate fast depolarization of the spine and NMDA receptors provide prolonged depolarization (Isaacson and Strowbridge 1998). GABA release from vesicles occurs in a calcium-dependent manner and is asynchronous and considerably delayed with respect to mitral or tufted cell depolarization, leading to a slow time course for dendrodendritic inhibition (Kapoor and Urban 2006).

GCs are capable of three different modes of GABA release. (1) A local mode, independent of APs, which is restricted to individual spines: In this local mode, single spines are depolarized; experience a rise in calcium mediated by NMDARs, voltage-dependent calcium-channels and internal stores; and release GABA onto the mitral and tufted cell that provided the

initial synaptic input (recurrent inhibition) (Egger, Svoboda et al. 2003, Egger, Svoboda et al. 2005). (2) A global, AP-independent mode, mediated by a low-threshold calcium spike (LTS) that is triggered by sub-AP-threshold depolarization: This LTS spreads throughout the GC and depends on low threshold voltage-dependent (LVA) calcium channels. This mode explains lateral inhibition between mitral or tufted cells in the presence of TTX (Isaacson and Strowbridge 1998). (3) A global, AP-dependent mode that consists of a sodium AP evoked followed by a long lasting depolarization and influx of calcium evoked by synaptic activation: The long lasting depolarization requires the NMDARs, LVA calcium channels and nonselective cation conductance I(CAN) channels (Egger 2008).

These unique dendrodendritic synapses facilitate a variety of olfactory bulb computations. Granule cells are important for generating oscillations (Lagier, Carleton et al. 2004, Bathellier, Lagier et al. 2006, Lagier, Panzanelli et al. 2007) and synchronizing (Giridhar and Urban 2012, Fukunaga, Herb et al. 2014) and decorrelating (Arevian, Kapoor et al. 2008, Gschwend, Abraham et al. 2015) mitral and tufted cell representations. Stimulating granule cells decorrelates mitral and tufted cell activity patterns and improves behavioral discrimination of similar olfactory stimuli (Abraham, Egger et al. 2010, Gschwend, Abraham et al. 2015). However, an important question is how are granule cell-mediated inhibitory connections between mitral and tufted cells specified in order to allow decorrelation in a circuit that lacks topography?

Prior work(Arevian, Kapoor et al. 2008) proposed a possible answer to this question when describing activity-dependent lateral inhibition. Activity-dependent lateral inhibition refers to the phenomenon by which mitral cells are only affected by lateral inhibition when firing at intermediate firing rates (25-75 Hz). Consequently, neurons with similar firing rates, rather than similar spatial locations, become decorrelated, so that the distribution of activity (i.e. the

histogram of firing rates) becomes wider. Due to the extensive lateral dendrites of individual mitral and tufted cells, which have the potential to reach over two-thirds of the olfactory bulb(Egger and Urban 2006), granule cells have the potential to connect spatial distant pairs of mitral cells. Functionally, odor that evoke similar spatial representation will become less correlated through activity-dependent lateral inhibition because of an increase in the separation between cell with high firing rates and those firing at intermediate rate.

Why are only intermediate firing rates influenced by lateral inhibition? Consider mitral cells A and a connected mitral cell B. When mitral cell A fires at low rates, no additional granule cells are recruited when cell B spikes, so no lateral inhibition is evoked onto cell A. When cell A is firing at intermediate firing rates, additional granule cells are activated when cell B fires, so lateral inhibition is generated and the firing rate of A is reduced. When cell A is firing at high rates, all shared granule cells are maximally recruited so that cell B spiking is unable to activate any additional granule cells or generate additional lateral inhibition. Whether activity-dependent lateral inhibition acts similarly in tufted cells will be addressed in Chapter 3.

1.3 GOALS OF THE DISSERTATION

Sensory systems often use parallel neural pathways to encode different components of sensory stimuli. Yet, how circuits in these parallel pathways are composed to maintain or even enhance the encoding of specific stimulus features is poorly understood. This question is particularly interesting in the olfactory system because the distinct outputs of mitral cells (MCs) and tufted cells (TCs) are generated from initially homogeneous sources and so must consequently arise from differences in connectivity with local circuitry. In this thesis we will

explore which aspects of the olfactory bulb circuit are responsible for these differences in odor-evoked activity between MCs and TCs.

Chapter 2 describes differences in feed-forward circuitry onto MCs and TCs. Recent work has explored differences in how the latency of odor-evoked responses differs between MCs and TCs because response latency has the potential to encode behaviorally relevant information(Cury and Uchida 2010, Shusterman, Smear et al. 2011, Smear, Shusterman et al. 2011, Haddad, Lanjuin et al. 2013). TCs respond to odors hundreds of milliseconds earlier in the sniff cycle and show more concentration invariant odor-evoked response latencies than MCs(Fukunaga, Berning et al. 2012, Igarashi, Ieki et al. 2012). These studies suggest that MCs may use spike latency to encode concentration-specific information while TCs may encode concentration-independent information. In light of these emerging differences in the latency of MC and TC responses, determining the circuit-level mechanisms that drive these differences is critical. Chapter 2 describes experiments that will test whether, in acute olfactory bulb slices, MCs and TCs response to olfactory stimulation at different latencies. Then we will test whether differences in spike latencies between MCs and TCs are driven, in part, by differences in feed-forward excitatory and/or inhibitory currents. Finally we will test which population of inhibitory interneurons, granule cells or periglomerular cells, are responsible for differences in feed-forward inhibition onto MC and TCs.

Chapter 3 describes the causes and consequences of lateral inhibition differences between mitral and tufted cells. Throughout the brain lateral inhibitory circuits enhance contrast and facilitate discrimination by decorrelating neural responses(Hirsch and Gilbert 1991, Urban 2002). In the olfactory bulb, lateral inhibition occurs between pairs of MCs and TCs via reciprocal dendrodendritic synapses with inhibitory granule cells(Rall, Shepherd et al. 1966).

Prior work has shown that lateral inhibition most strongly affects MCs firing at intermediate rate because coincident input is required for the activation of GCs(Arevian, Kapoor et al. 2008). This activity-dependent regulation of the strength of lateral inhibition onto MCs decorrelates MCs responses to similar stimuli more effectively than other forms of inhibition(Arevian, Kapoor et al. 2008). However the effects of lateral inhibition onto TCs has yet to be explored. Chapter 3 describes experiments that test whether the strength and timing of lateral inhibitory currents differ onto MCs and TCs. Then we will determine whether lateral inhibition affects different ranges of firing rates between MCs and TCs. We next test the hypothesis that differences in the excitability of anatomically distinct subclasses of granule cells cause differences in activity-dependent lateral inhibition onto MCs and TCs. Finally we use simulations to determine the consequences of differences in activity-dependent lateral inhibition on coding.

Appendix A provides a preliminary study of how early postnatal odor exposure affects lateral inhibition onto MCs and TCs. Lateral inhibition is modulated by a variety of inhibitory interneuron subtypes that include superficial short axon cells (sSACs) (Aungst, Heyward et al. 2003, Liu, Plachez et al. 2013, Whitesell, Sorensen et al. 2013, Banerjee, Marbach et al. 2015), external plexiform layer interneurons (EPL-INs) (Huang, Garcia et al. 2013, Kato, Gillet et al. 2013, Miyamichi, Shlomai-Fuchs et al. 2013) and granule cells (GCs) (Arevian, Kapoor et al. 2008, Fukunaga, Herb et al. 2014, Gschwend, Abraham et al. 2015). These circuits influence MC/TC activity in a variety of ways that include controlling gain (Banerjee, Marbach et al. 2015), decorrelating odor representations (Arevian, Kapoor et al. 2008, Gschwend, Abraham et al. 2015), modulating spike timing (Fukunaga, Herb et al. 2014) and synchronizing gamma band oscillations (Lagier, Carleton et al. 2004, Lagier, Panzanelli et al. 2007, Lepousez and Lledo 2013, Fukunaga, Herb et al. 2014). The effects of sensory experience have been studied most

extensively in GCs, as previous work has shown that prior odor exposure influences GC survival (Lemasson, Saghatelyan et al. 2005, Saghatelyan, Roux et al. 2005, Alonso, Viollet et al. 2006, Lepousez, Valley et al. 2013), morphology (Saghatelyan, Roux et al. 2005, Yoshihara, Takahashi et al. 2012) and *in vivo* odor responses (Kato, Chu et al. 2012). Whether activity-dependent changes in interneurons leads to changes in inter-glomerular lateral inhibition onto MCs and TCs is unknown. Here we test whether early postnatal exposure to acetophenone, a ligand known to activate a specific (M72) glomerulus alters the lateral inhibition mediated by the activated glomerulus onto MCs and TCs.

Together the experiments described in this dissertation suggest that differences in odor-evoked responses between MCs and TCs are a consequence of distinct patterns of connectivity to multiple populations of inhibitory interneurons.

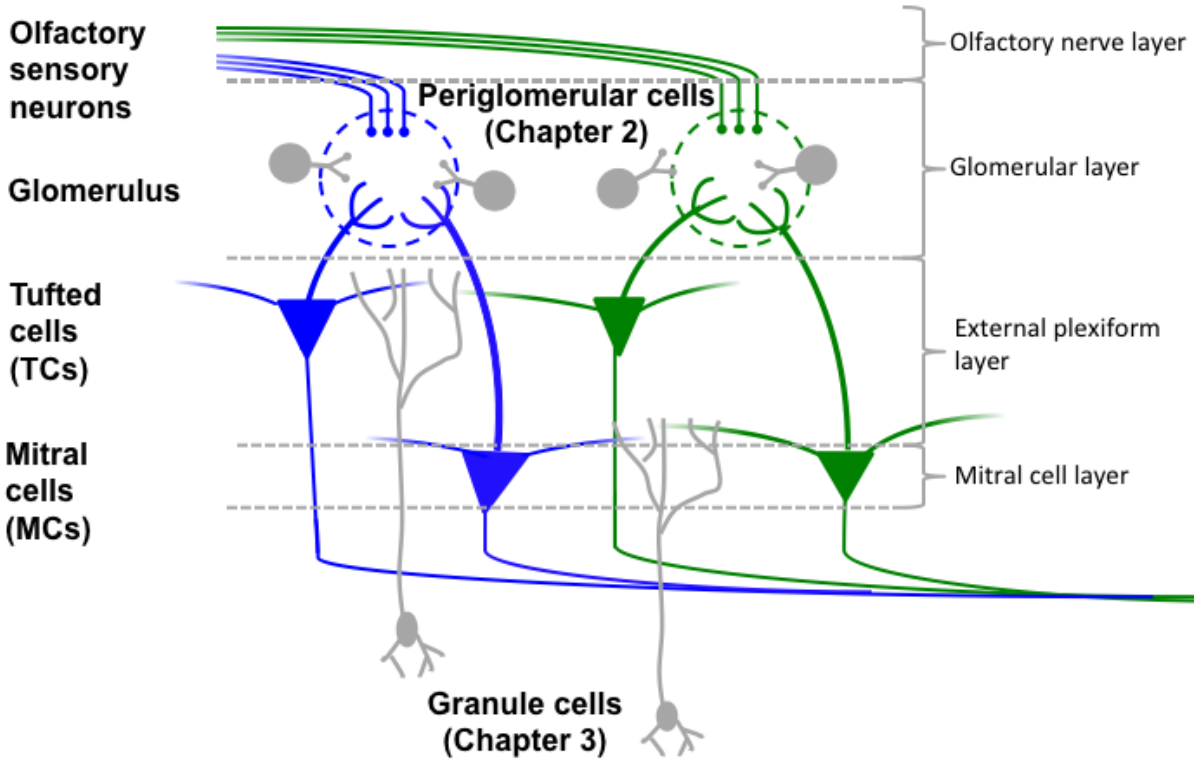

Figure 1: Olfactory bulb anatomy with relevant cell types and tissue layers

2.0 DIFFERENCES IN PERIGLOMERULAR CELL MEDIATED FEED-FORWARD INHIBITION ONTO MITRAL AND TUFTED CELLS LEAD TO DISTINCT MODES OF INTENSITY CODING

2.1 INTRODUCTION

In multiple sensory systems, separate neuron types encode distinct features of sensory stimuli. Yet, olfaction has historically been viewed differently: mitral cells (MCs) and tufted cells (TCs), the two types of principal neurons of the olfactory bulb, have been thought to play identical roles in odor coding. This view has prevailed despite clear differences in the locations of their cell bodies and in the patterns of their dendritic arbors and axonal projections(Mori, Kishi et al. 1983, Orona, Rainer et al. 1984, Nagayama, Enerva et al. 2010, Igarashi, Ieki et al. 2012). Recently, however, several studies have identified functional differences between MCs and TCs that suggest that the olfactory system segregates olfactory information into parallel pathways, much like in other sensory systems. For instance, MCs and TCs are differentially modulated by other brain areas, including the raphe nucleus(Kapoor, Provost et al. 2016) and the piriform cortex(Otazu, Chae et al. 2015). Additionally, MCs and TCs respond differently to odors.

The strongest evidence that MCs and TCs play different roles in odor coding comes from studies exploring differences in odor-evoked responses. Compared to MCs, TCs are less

frequently inhibited by odors (Nagayama, Takahashi et al. 2004), respond to lower concentration odors(Igarashi, Ieki et al. 2012, Kikuta, Fletcher et al. 2013), and have responses that are more highly correlated with olfactory sensory neuron (OSN) input(Adam, Livneh et al. 2014). Additionally, recent work has explored differences in how the latency of odor-evoked responses differs between MCs and TCs because response latency has the potential to encode behaviorally relevant information(Cury and Uchida 2010, Shusterman, Smear et al. 2011, Smear, Shusterman et al. 2011, Haddad, Lanjuin et al. 2013). TCs respond to odors hundreds of milliseconds earlier in the sniff cycle and show more concentration invariant odor-evoked response latencies than MCs(Fukunaga, Berning et al. 2012, Igarashi, Ieki et al. 2012). These data suggest that MCs may use spike latency to encode concentration-specific information while TCs may encode concentration-independent information.

In light of these emerging differences in the latency of MC and TC responses, determining the circuit-level mechanisms that drive these differences is critical. Compared to MCs, TCs are more intrinsically excitable(Burton and Urban 2014) and receive stronger olfactory sensory neuron (OSN) input at minimal stimulation intensities(Gire, Franks et al. 2012, Burton and Urban 2014), which suggests that a combination of intrinsic and synaptic differences drive differential responses to changes in concentration. Relatively little is known about how differences in inhibition between MCs and TCs also contribute to latency differences. OSN stimulation evokes strong intra-glomerular inhibition mediated by periglomerular cells (PGCs) onto MCs(Shao, Puche et al. 2012). However whether differences in the strength of these PGC-mediated inhibitory circuits onto MCs and TCs contribute to differences in the latency of MC and TC responses remains controversial. Computational models predict that differential input from PGCs may drive differences in spike latency between MCs and TCs(Fukunaga, Berning et

al. 2012). Other work, however, has shown that strength of PGC-mediated inhibitory currents onto MCs and TC are similar when OSNs are stimulated at weak intensities(Najac, Sanz Diez et al. 2015). Additionally, the relative influence of PGCs and granule cells (GCs) in shaping odor-evoked firing rates in MCs and TCs remains unclear(Cleland 2010, Fukunaga, Herb et al. 2014, Gschwend, Abraham et al. 2015). Therefore, a systematic investigation of how both GC- and PGC- mediated inhibitory currents onto MCs and TCs vary with stimulus intensity is needed.

Here, using whole-cell recordings of MCs and TCs in acute olfactory bulb slices, we find that MCs display longer latency spiking that is more strongly dependent on stimulus intensity than TCs. We find that longer latency spiking in MCs is a consequence of weaker excitatory and stronger inhibitory currents onto MCs compared to TCs. Stronger inhibitory currents onto MCs than TCs are PGC-mediated, so blocking PGC-mediated, but not GC-mediated, inhibition led to more reliable and shorter latency responses in MCs, but not TCs. These data suggest that differences in PGC-mediated inhibition, along with differences in intrinsic excitability and excitatory input, work cooperatively to allow TCs to respond to OSN stimulation earlier than MCs.

2.2 MATERIALS AND METHODS

2.2.1 Slice preparation

Postnatal day 16 – 23 C57BL/6 and OMP-ChR2-YFP(Smear, Shusterman et al. 2011) mice were anaesthetized with isoflurane and decapitated. Brains were dissected into ice-cold oxygenated solution containing (in mM): 125 NaCl, 25 glucose, 2.5 KCl, 25 $NaHCO_3$, 1.25

NaH_2PO_4, 7 $MgCl_2$ and 0.5 $CaCl_2$. Horizontal slices (310 μm thick) of the MOB were prepared using a vibratome (VT1200S; Leica, Nussloch, Germany) and recovered for 15–30 min in 37°C oxygenated Ringer solution that was identical to the dissection solution except for lower Mg^{2+} concentrations (1 mM $MgCl_2$) and higher Ca^{2+} concentrations (2 mM $CaCl_2$). Prior to recording, slices were stored in room temperature oxygenated Ringer solution until recording.

2.2.2 Cell classification

TCs were identified as those cells residing completely in the superficial half of the EPL with large somas (>10 μm in diameter). All TCs had at least 1 lateral dendrite and did not display the rhythmic bursting characteristic of external tufted cells(Hayar, Karnup et al. 2004, Antal, Eyre et al. 2006, Liu and Shipley 2008). MCs were identified as large cells located in the mitral cell layer (MCL). Cells with ambiguous identities – those with somata that resided partially in the MCL – were excluded from analysis.

2.2.3 Electrophysiology

M/TCs were visualized using infrared differential interference contrast video microscopy. Throughout the recording process, slices were continuously superfused with 37°C oxygenated Ringer solution. Current clamp recordings were made from individual cells using electrodes filled with (in mM) 120 potassium gluconate, 2 KCl, 10 HEPES, 10 sodium phosphocreatine, 4 Mg-ATP, 0.3 Na_3GTP, 0.2 EGTA, 0–0.025 Alexa Fluor 594 (Life Technologies, Carlsbad, CA, USA) and 0.2% Neurobiotin (Vector Labs, Burlingame, CA, USA). Voltage clamp recordings were made using electrodes filled with (in mM): 140 Cs-gluconate, 10 HEPES, 2 KCl, 10

sodium phosphocreatine, 3 Mg-ATP, and 0.3 Na_3GTP,0.025 Alexa Fluor 594 (Life Technologies, Carlsbad, CA, USA) and 0.2% Neurobiotin (Vector Labs, Burlingame, CA, USA). All data were low-pass filtered at 4 kHz and digitized at 10 kHz using a MultiClamp 700A amplifier (Molecular Devices, Sunnyvale, CA, USA) and an ITC-18 acquisition board (Instrutech, Mineola, NY, USA) controlled by custom software written in Igor Pro (WaveMetrics, Lake Oswego, OR, USA). For electrical stimulation of OSNs, a monopolar glass electrode was filled with Ringer solution and connected to a stimulus isolation unit (World Precision Instruments, Sarasota, FL, USA) controlled by TTL pulses from the ITC-18 acquisition board. For optogenetic stimulation, slices were illuminated (10ms light pulse) by a 470nm LED (pE-100, CoolLed, UK) directed through a 60x water-immersion objective centered on a single glomerulus with a closed field stop(Burton and Urban 2015). All data were low-pass filtered at 4 kHz and digitized at 10 kHz using a MultiClamp 700A amplifier (Molecular Devices, Sunnyvale, CA, USA) and an ITC-18 acquisition board (Instrutech, Mineola, NY, USA) controlled by custom software written in Igor Pro (WaveMetrics, Lake Oswego, OR, USA).

Electrical and light stimulation intensities were chosen as follows. First the minimum intensity needed to evoke reliable spiking (for current-clamp experiments) or excitatory currents (for voltage-clamp experiments) was determined. Reliability was defined as the presence of at least 1 spike or excitatory currents in over 80% of trials. To the find the maximum stimulation intensity, the electrical or light intensity was increased until a plateau in the number of spikes or the size of excitatory currents was reached. The middle stimulation intensity was defined as halfway between the minimum and maximum intensities. Lastly, the final two intensities were chosen as halfway between the minimum and middle intensities and the middle and maximum intensities. Measurements of spiking or synaptic currents were repeated 7 times at each

stimulation intensity. MCs and TCs were held at resting membrane potential throughout the current-clamp recordings.

2.2.4 Data analysis and statistics

For current-clamp experiments, peri-stimulus time histograms (PSTHs) were computed by summing spikes across trials and smoothing with a 150 ms-wide Gaussian filter. The maximum firing rate referenced throughout the manuscript is calculated as the peak of the PSTH. The latency to reliable spiking was calculated in each cell by binning spikes in 10ms bins and finding the percentage of trials on which the cell spiked in each time bin. 'Time to reliable spiking' was defined as the first time bin after stimulation in which the cell spiked in over 80% of trials.

Significance between MCs and TCs when metrics of spike latency were plotted vs. PSTH peak was determined by fitting the dependence of latency on rate for each cell to an exponential function to determine τ. Then τ's were compared between MCs and TCs using unpaired t-tests.

2.3 RESULTS

2.3.1 Mitral and tufted cells encode the intensity of olfactory sensory neuron stimulation differently

To determine how MCs and TCs respond to changes in stimulus intensity, we recorded membrane in single MCs and TCs in olfactory bulb slices following electrical stimulation of the

olfactory nerve layer adjacent to the cell's home glomerulus at multiple intensities (Figure 2**a-c**). Five intensities for each cell were chosen to sample the entirety of each cell's sensory-evoked dynamic range. First, the weakest stimulation intensity that elicited reliable spiking was found (min. intensity). Then the stimulation intensity was increased until a plateau in the maximum number of sensory-evoked spikes was evoked (max. intensity). The third stimulation intensity (mid. intensity) was defined as the intensity halfway between the min. and max. intensity, while the fourth and fifth intensities were chosen as halfway between min. and mid. intensities and mid. and max. intensities, respectively. This approach allowed between-cell comparisons at each relative intensity.

Given prior work showing that both spike latencies and firing rates of principal neurons vary with odor concentration(Cang and Isaacson 2003, Fukunaga, Berning et al. 2012, Igarashi, Ieki et al. 2012, Sirotin, Shusterman et al. 2015), we compared how spike latencies and firing rates varied with stimulation intensity in MCs and TCs. The total number of action potentials (Figure 3**a**) in a 2s interval following stimulation increased with intensity ($p=1.52e-12$; 2-way ANOVA) but did not differ between MCs and TCs. Compared with MCs, however, TCs exhibited significantly higher firing rates, as measured by the peak in the PSTH (Figure 3**b**). Therefore, MCs and TCs are both capable of using firing rate to encode information about OSN stimulation intensity.

Next we explored whether spike latency, as assessed by three different metrics, varied with OSN stimulation intensity in either MCs or TCs. First we found that the latency to PSTH peak decreased with stimulation intensity in MCs, but not TCs (Figure 3**c**). To better compare spike latency with *in vivo* data, we plotted the latency to PSTH peak vs. peak firing rate (PSTH peak) and similarly found that the dependence of spike latency on firing rate is significantly

different between MCs and TCs (Figure 3**d** – see Methods). Additionally, using 1st spike latency (Figure 3**e**) and the time to reliable spiking (Figure 3**f** – see Methods) as measures of latency similarly showed that latencies in MCs vary more strongly with peak firing rate than latencies in TCs. Additionally, at low firing rates (< 20 Hz), many fewer MCs than TCs exhibit reliable spike timings (Figure 3**g**), which corroborates *in vivo* data that MC response latencies are not reliable at low odor concentrations(Igarashi, Ieki et al. 2012). Therefore while both MCs and TCs have the potential to encode information about the intensity of glomerular activation in their firing rates, only MCs are capable of using spike latency to encode intensity information.

One potential confound to these experiments is the possibility that MC and TC apical dendrites are directly excited by electrical stimulation at strong stimulation intensities. Therefore we performed an analogous experiment in OMP-ChR2-YFP mice(Smear, Shusterman et al. 2011), in which we photostimulated (10 ms pulse) the home glomerulus of the recorded cell at five light intensity chosen as described above (Figure 4**a**). We found that while the number of spikes increases in MCs and TCs (Figure 4**b**), firing rates in TCs are significantly higher than in MCs (Figure 4**c**). Additionally, spike latency in MCs, but not in TCs, showed a strong dependence on firing rate. Latency to PSTH peak (Figure 4**d**), 1st spike latency (Figure 4**e**) and latency to reliable spiking (Figure 4**f**) all significantly differed between MCs and TCs. Additionally fewer MCs than TCs showed reliable spike timing at low photostimulation intensities (Figure 4**g**). Finally, the peak firing rates and latencies in MCs and TCs were comparable between experiments using electrical and photostimulation of OSNs, indicating that direct electrical stimulation of MC or TC apical dendrites did not significantly influence our results. Therefore, our *in vitro* data corroborates prior *in vivo* findings that MCs and TCs have

the potential to use distinct strategies for encoding concentration(Fukunaga, Berning et al. 2012, Igarashi, Ieki et al. 2012).

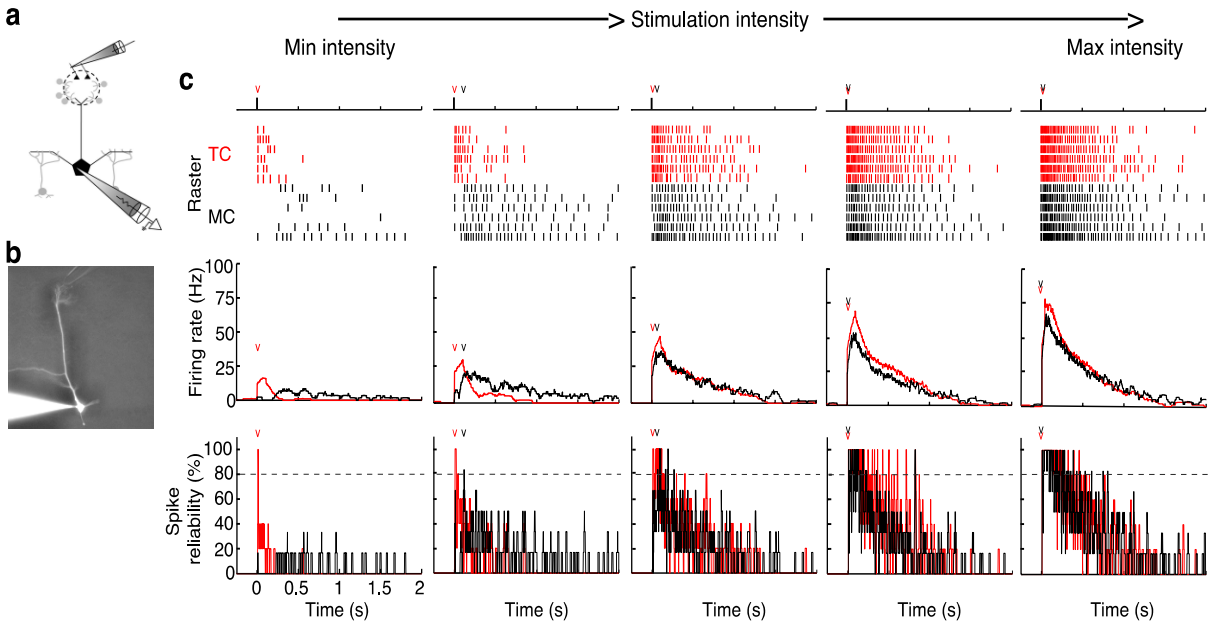

Figure 2: Examples that MCs and TCs encode the intensity of olfactory sensory neuron stimulation differently.

(**a-b**) Schematic (**a**) and examples (**b**) of experimental setup. Spiking responses to electrical stimulation (10 µs) of OSNs at five intensities was recorded in either mitral (**b – TOP**) or tufted (**b – bottom**) cells (OSN – olfactory sensory neurons; PGCs – periglomerular cells; GCs – granule cells; M/TCs – mitral or tufted cells). (**c**) Example of spike rasters (TOP), PSTHs (MIDDLE) and spike time reliability plots (BOTTOM) for a MC (black) and TC (red) across 5 stimulation intensities (see Materials and Methods). Plots of spike time reliability depict the percentage of trials in which the cell fired an action potential during each 10 ms time bin following OSN stimulation ('v' represents the first time bin following OSN stimulation during which spike timing was more than 80% reliable).

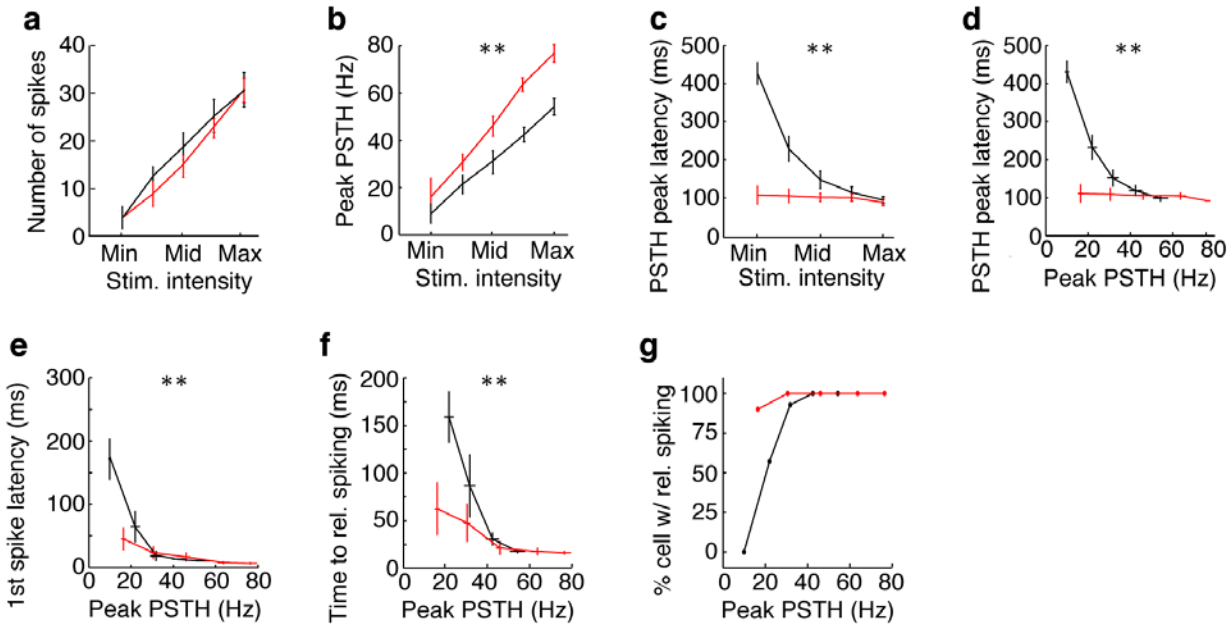

Figure 3: Summary statistics indicating that MCs and TCs encode the intensity of olfactory sensory neuron stimulation differently.

Statistics from data collected from experiments described in **Figure 2.1.** (**a**) MCs and TCs respond to OSN stimulation with similar numbers of spikes (p=0.911), (**b**) however TCs respond with higher firing rates – measured as the peak of the PSTH – than MCs (p=8.8e-16). (**c-g**) TCs respond to low intensity OSN stimulation at shorter latencies than MCs. (**c-d**) Latency to PSTH peak is shorter in TCs than in MCs when plotted vs. stimulation intensity (**c**; p=1.58e-9) or PSTH peak (**d**; p=1.15e-5). (**e-f**) 1st spike latency (**e**; p=0.007) and time to first reliable spike (**f**; p=0.0083) are also shorter in TCs than MCs at low stimulation intensities. (**g**) At low stimulation intensities, a larger percentage of TCs than MCs show reliable spike timing. Data taken from 14 MCs and 20 TCs. Significance was assessed in a,b,c using 2-way ANOVA and in **d,e,f** as unpaired t-test comparing τ's derived from exponential fit from data in each cell. Asterisks (**) in **a-g** indicate significant ($p<0.05$) differences between MCs and TCs.

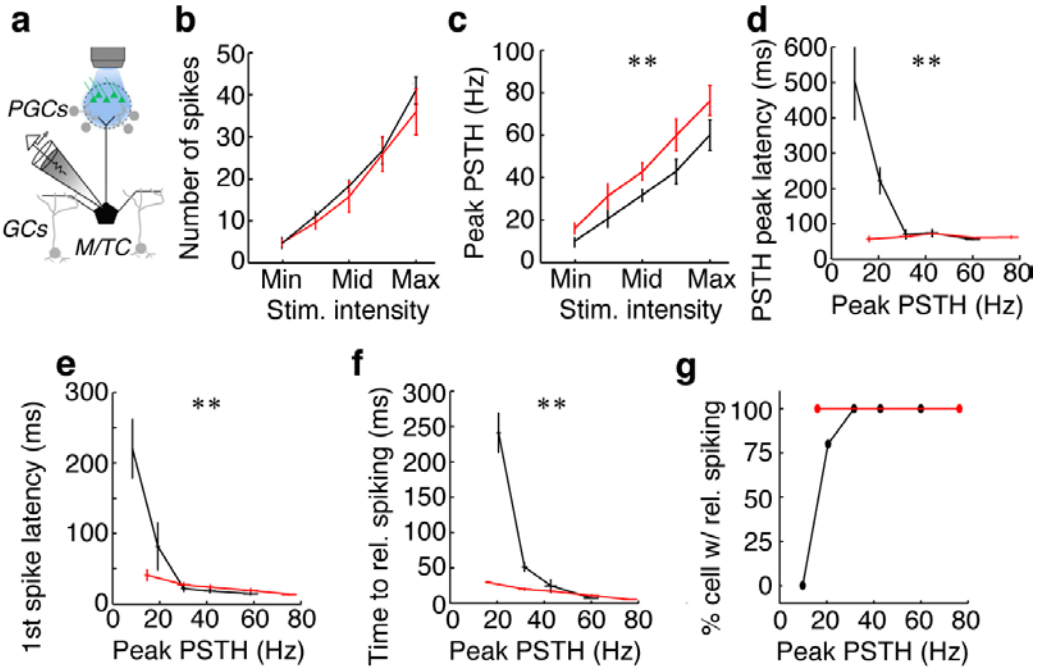

Figure 4: Optical activation of a single glomeruli in olfactory bulb sections from OMP-ChR2:EYFP mice.

(**a**) Schematic of experimental setup analogous to the one used in Figure 1. Spiking in single MCs or TCs in response to photostimulation (10 ms) of a single glomerulus at five intensities. MCs and TCs respond to OSN photostimulation with similar numbers of spikes (**b**; p=0.4), however TCs responded with higher firing rates than MCs (**c**; p=1.83e-10). Additionally, TCs responded to low intensity OSN photostimulation with shorter latencies than MCs as assessed by the time to PSTH peak (**d**; p=0.0045), first spike latency (**e**; p=0.0023) and time to first reliable spike (**f**; p=0.004). (**g**) A larger percentage of TCs than MCs display reliable spike timing. Data taken from 5 MCs and 5 TCs. Significance was assessed in b,c using 2-way ANOVA and in **d,e,f** as unpaired t-test comparing τ's derived from exponential fit from data in each cell. Asterisks (**) in **b-g** indicate significant (p<0.05) differences between MCs and TCs.

2.3.2 TCs respond to OSN stimulation with stronger excitatory and weaker inhibitory currents than MCs

To determine potential sources of these differences in how MCs and TCs respond to changes in stimulus intensity, we measured both excitatory and inhibitory currents following electrical stimulation of OSNs across five stimulation intensities (Figure 5**a,b**). Previously, our group and others have shown that MCs receive stronger excitation than TCs at minimal stimulation intensities(Gire, Franks et al. 2012, Burton and Urban 2014). However, evidence for differences in feed-forward inhibition is mixed(Fukunaga, Herb et al. 2014, Najac, Sanz Diez et al. 2015). Therefore we measured both excitatory and inhibitory currents across five stimulation intensities in MCs and TCs. We found that both the peak amplitude (Figure 6**a TOP**) and charge (Figure 6**b TOP**; calculated as the integral across 1s following stimulation) of feed-forward inhibition onto MCs is larger than onto TCs. However, while the peak amplitude of excitation is significantly larger in TCs than in MCs (Figure 6**a BOTTOM**), charge transferred did not differ between MCs and TCs (Figure 6**b BOTTOM**). Consequently, the E/I ratio is significantly lower in MCs than in TCs (Figure 6**d TOP**). These E/I ratios, calculated across the first second after stimulation likely allow TCs to fire at higher rates than MCs across all stimulation intensities. However it cannot explain why the latency of spiking in MCs, but not TCs, is much longer at low stimulation intensities than at high stimulation intensities.

Given prior work indicating that PGCs play an important role in regulating response latency in MCs and that PGC-mediated feedforward inhibition is confined to the first 150ms after OSN stimulation(Shao, Puche et al. 2012, Najac, Sanz Diez et al. 2015), we limited our analysis of excitatory and inhibitory charge transfer and E/I ratio to the first 150ms following OSN stimulation. Similar to the findings described above for the 0-1000ms time window, we

find that inhibitory (Figure 6**c TOP**), but not excitatory (Figure 6**c BOTTOM**), charge transferred during the 0-150ms time window is significantly larger in MCs than TCs. Additionally, the E/I ratio in this 0-150ms time window is significantly higher in TCs than in MCs (Figure 6**d BOTTOM**). This difference in E/I ratio is largest at low stimulation intensities; E/I ratio is approximately 1 in MCs and over 6 in TCs at minimal stimulation intensities. Consequently, longer latency spiking in MCs than TCs at these low intensities is predominantly driven by large inhibitory currents during the first 150ms after stimulation. Finally, we analyzed how the latency to the peak amplitudes of inhibition and excitation change across stimulation intensities. While the latency to the peak of inhibition does not vary with stimulation intensity ($p=0.60$; 2-way ANOVA) or between MCs and TCs (Figure 6**e**), the latency to the peak of excitation does vary with stimulation intensity ($p=1.10e-5$; 2-way ANOVA) and between MCs and TCs (Figure 6**f**). Interestingly, in TCs, the peak of excitation precedes the peak of inhibition at all intensities. However, in MCs, excitation leads inhibition at high stimulation intensities but lags inhibition at low intensities (Figure 6**g**). This shift from excitation lagging inhibition to excitation leading inhibition likely reflects prior work showing that at weak stimulation intensities, MCs primarily receive indirect excitation from external tufted cells (ETCs)(Gire, Franks et al. 2012) and that at higher intensities, MCs receive both indirect and direct excitation from OSNs(De Saint Jan and Westbrook 2007, De Saint Jan, Hirnet et al. 2009, Najac, De Saint Jan et al. 2011).

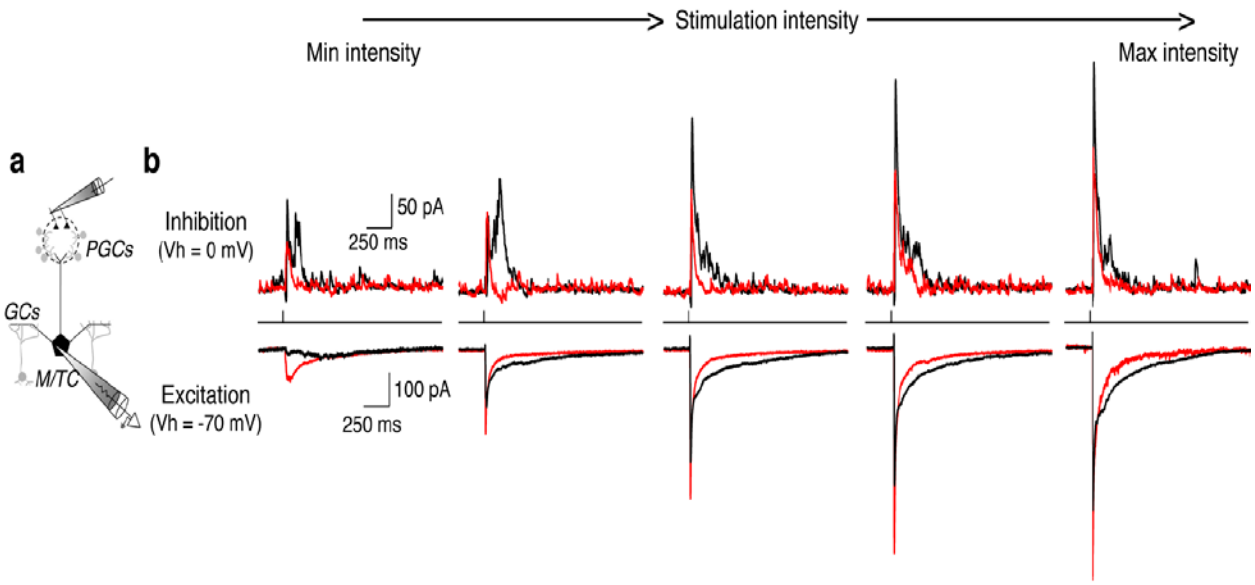

Figure 5: Examples showing that TCs respond to electrical stimulation of OSNs with stronger excitatory and weaker inhibitory currents than MCs.

(**a-b**) Excitatory (V_h= -70 mV) and inhibitory (V_h=0 mV) currents were measured in single MCs or TCs following electrical stimulation of OSNs at five intensities. (**b**) Examples of inhibitory (TOP) and excitatory (BOTTOM) currents at each of the five stimulation intensities in one example MC (black) and TC (red).

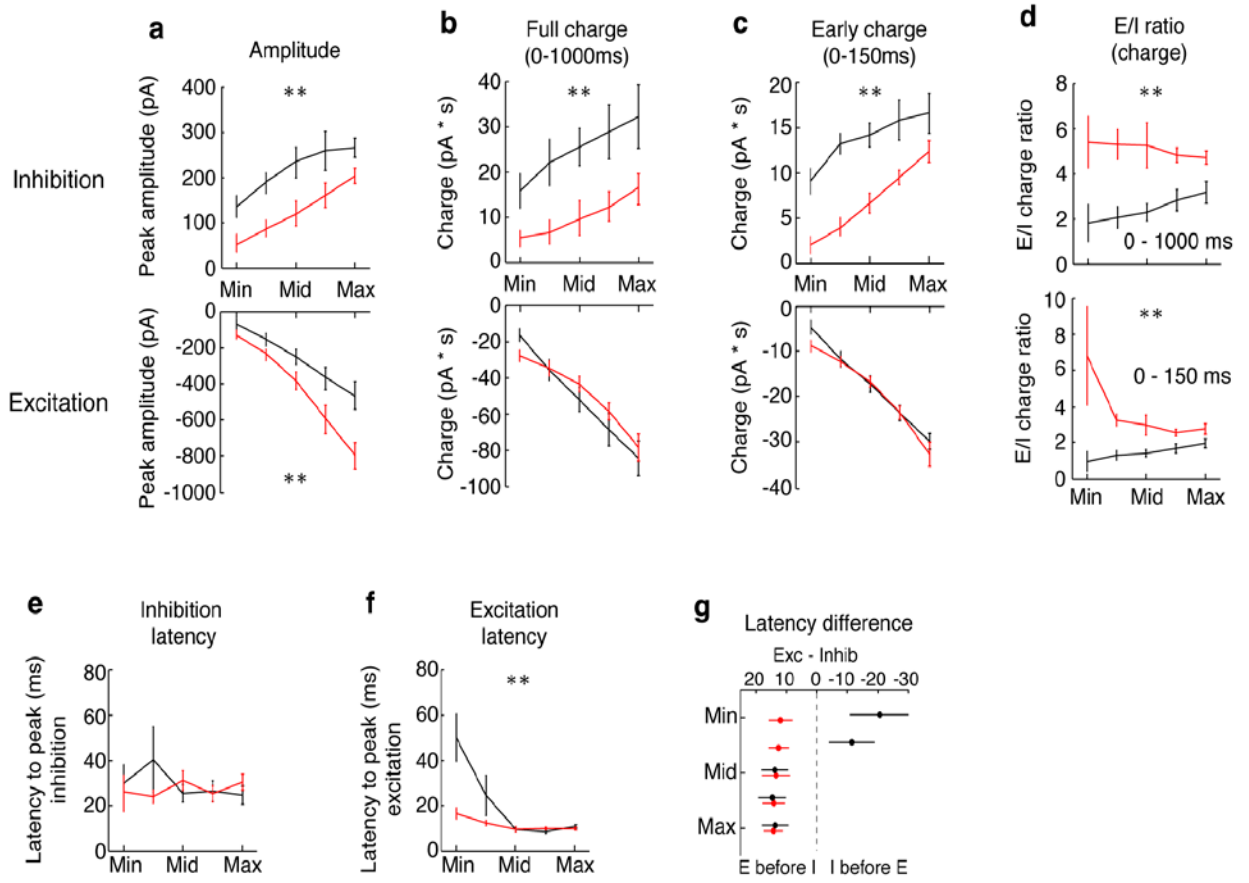

Figure 6: Summary statistics indicating that TCs respond to electrical stimulation of OSNs with stronger excitatory and weaker inhibitory currents than MCs.

Statistics from data collected from experiments described in **Figure 2.4.** (**a-c**) Comparisons of inhibitory (TOP) and excitatory current peak amplitude (**a**), charge in 1s following stimulation (**b**) and charge in first 150ms following stimulation (**c**) between MCs and TCs. Compared to TCs, inhibitory currents in MCs have larger peak amplitudes (p=5.36e-18) and charge transferred in the 1s following stimulation (p=3.16e-8) and the first 150ms following stimulation (p=7.56e-10). However, excitatory currents in MCs have larger peak currents (p=4.58e-14) but similar charge transferred in the 1s following stimulation (p=0.47) and the first 150ms following stimulation (p=0.18) compared with TCs. (**d**) The ratio of excitatory to inhibitory currents is larger in TCs than in MCs when calculated as the ratio of charge transferred during 1s after stimulation (TOP; p=4.2e-7) or during the 1st 150ms after stimulation (BOTTOM; p=0.0005). (**e-f**) The latency to the peak of inhibitory currents does not differ between MCs and TCs (**e**; p=0.40), however the latency to the peak of excitatory currents differs between MCs and TCs (**f**; p=0.001). (**g**) At all five intensities, the peak of excitatory currents precedes inhibition in TCs. However, in MCs, excitation lags inhibition at the weakest two intensities but leads inhibition at the strongest three intensities. Data taken from 8 MCs and 8 TCs and plotted as mean ± s.e.m. Significance was assessed in all panels using 2-way ANOVA. Asterisks (**) in **a-g** indicate significant (p<0.05) differences between MCs and TCs.

2.3.3 MCs receive stronger PGC-mediated inhibition than TCs

To directly test whether larger inhibitory currents onto MCs and TCs are mediated by PGCs, we measured PGC-mediated inhibitory currents by photostimulating the home glomerulus of the recorded MC/TC in OMP-ChR2 mice while limiting GC-mediated inhibition by blocking mGluR1s (LY36785, 100μM) and NMDARs (AP-5, 25μM) as previously described (Figure 7**a,b**)(Najac, Sanz Diez et al. 2015, Geramita, Burton et al. submitted). Because the differences in spike timing are greatest at minimal stimulation intensities, we compared PGCs-mediated currents between MCs and TCs at the minimum intensity needed to elicit reliable excitatory currents. PGC-mediated inhibitory currents are larger in amplitude in MCs than in TCs (Figure 7**e**). There were no differences between MCs and TCs in the latency to the peak of inhibition (Figure 7**f**) or the duration of inhibition (Figure 7**g** – see Methods). Additionally, we measured excitatory currents and found that blockade of NMDARs and mGluRs did not affect the amplitude or duration of excitatory currents in either MCs or TCs (Figure 7**c,d**). Similar to the results from electrical stimulation experiments, excitatory currents are larger (Figure 7**h**) and peak at shorter latencies (Figure 7**i**) in TCs than in MCs. Therefore, at minimal stimulation intensities, MCs receive weaker and longer latency excitatory inputs and stronger PGC-mediated inhibitory currents compared with TCs.

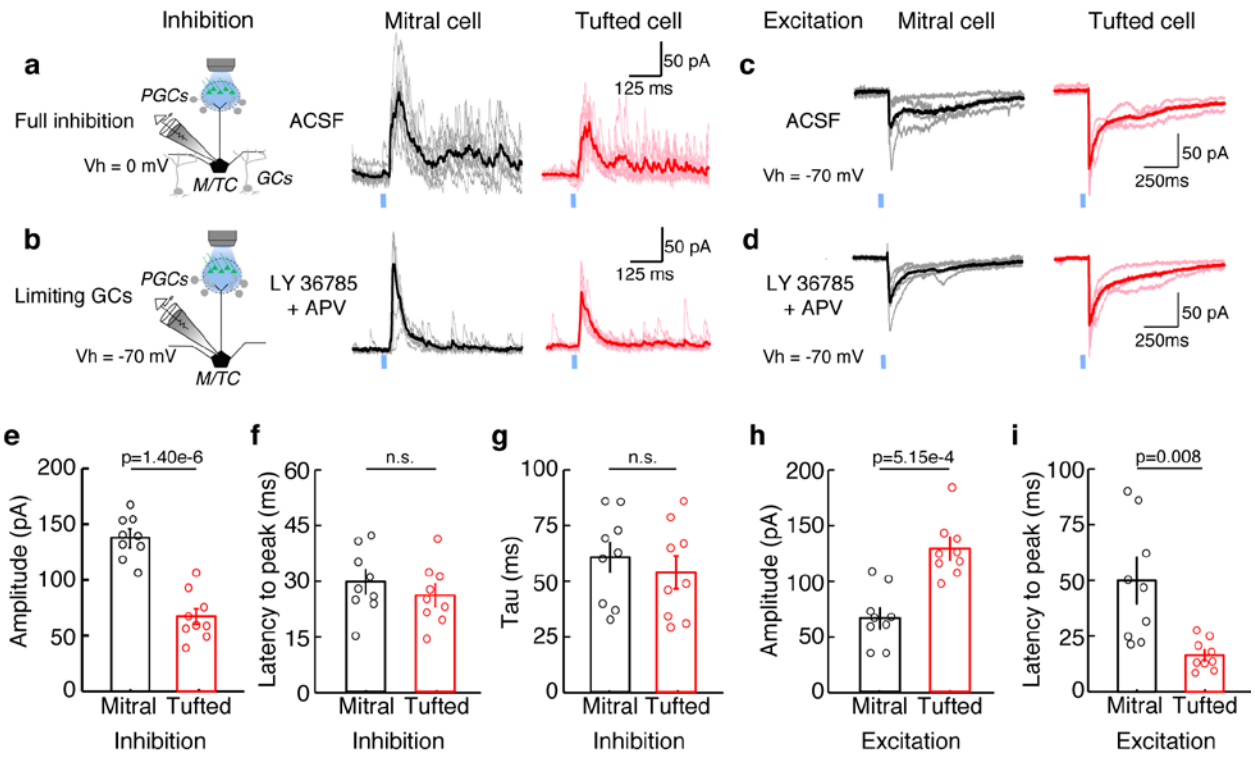

Figure 7: MCs receive stronger PGC-mediated inhibition than TCs.

Inhibitory (**a-b**) and excitatory (**c-d**) currents in MCs and TCs were measured before and after limiting GC-mediated inhibition by blocking mGluRs (LY36785, 100 μM) and NMDARs (APV, 25 μM). Currents were evoked using photostimulation in OMP-ChR2-YFP mice at minimal stimulation intensities. (**e**) The peak amplitude of PGC-mediated inhibition is larger in MCs than in TCs (p=1.40e-6). (**f-g**) The latency to peak of inhibition (**f**; p=0.56) and the duration of inhibition (**g**; p=0.89; comparing exponential decay constants of currents) did not differ between MCs and TCs. (**h**) The peak amplitude of excitatory currents are larger in TCs than in MCs (p=5.15e-4). (**i**) The latency to the peak of excitatory currents is longer in MCs than in TCs (p=0.006). Data taken from 9 MCs and 9 TCs and plotted as mean ± s.e.m. Significance was assessed in all panels using paired t-tests.

2.3.4 Blocking PGC-mediated, but not GC-mediated inhibition, affects spike latencies in MCs but not TCs.

Next we tested how blocking specific inhibitory interneuron subtypes affected spiking in MCs and TCs. First we measured spiking elicited by electrically stimulating OSNs at three different intensities (min., max. and mid.) before and after limited GC-mediated inhibition by blocking NMDARs and mGluRs (Figure 8**a,b**). Limiting GC-mediated inhibition did not significantly affect the number of spikes (Figure 9**a**), the maximum firing rate (Figure 9**b**), or the latency of spiking – as measured by either latency to PSTH peak (Figure 9**c**) or the latency to reliable spiking (Figure 9**d**) in either MCs or TCs at any of the three stimulation intensities. While we cannot rule out the possibility that GCs contribute to M/TC spike timing and synchrony, our results suggest that GCs do not strongly influence peak firing rates or spike latencies following OSN stimulation.

To test whether blocking PGCs differentially affect spiking in MCs and TCs, we measured spiking elicited by electrically stimulating OSNs at three different intensities before and after puffing gabazine into the recorded cell's home glomerulus (Figure 10**a-d**). After blocking PGC-mediated inhibition, in MCs, the total number of spikes (Figure 11**a**) elicited increased at all three stimulation intensities. However, in TCs, the number of spikes increased only at the lowest stimulation intensity. Additionally, the maximal firing rate increased at all three stimulation intensities (Figure 11**b**) in both MCs and TCs. Increases in firing rate despite the lack of changes in the total number of spikes in TCs at mid. and max. intensities in TCs implies that the timing of spikes is redistributed following PGC blockade. While PGC-mediated inhibition increased peak firing rates by similar amounts in MCs and TCs at the lowest

stimulation intensity (Figure 11**c LEFT**), increases in peak firing rates were significantly larger MCs than in TCs at the stronger two stimulation intensities (Figure 11**c MIDDLE, RIGHT**).

PGC-mediated inhibition also affected spike latency more strongly in MCs than in TCs. At the weakest two stimulation intensities, the latency to PSTH peak became significantly shorter in MCs but not in TCs after blocking PGCs (Figure 11**d**). Additionally, spike timing in MCs became more reliable at the weakest stimulation intensity after blocking PGC-mediated inhibition. Before blocking PGC-mediated inhibition, zero of the four MCs showed reliable spike timing, however after puffing gabazine in the glomerulus, spike timing in all four MCs became reliable and the latency to reliable spiking became comparable to TCs (Figure 11**e LEFT**). Additionally, the latency to reliable timing became shorter in MCs at the middle intensity after blocking PGC-mediated inhibition but did change in TCs at any of the three stimulation intensities (Figure 11**e**). Therefore PGC-mediated inhibition more strongly regulates the reliability and latency of spike timing in MCs than in TCs.

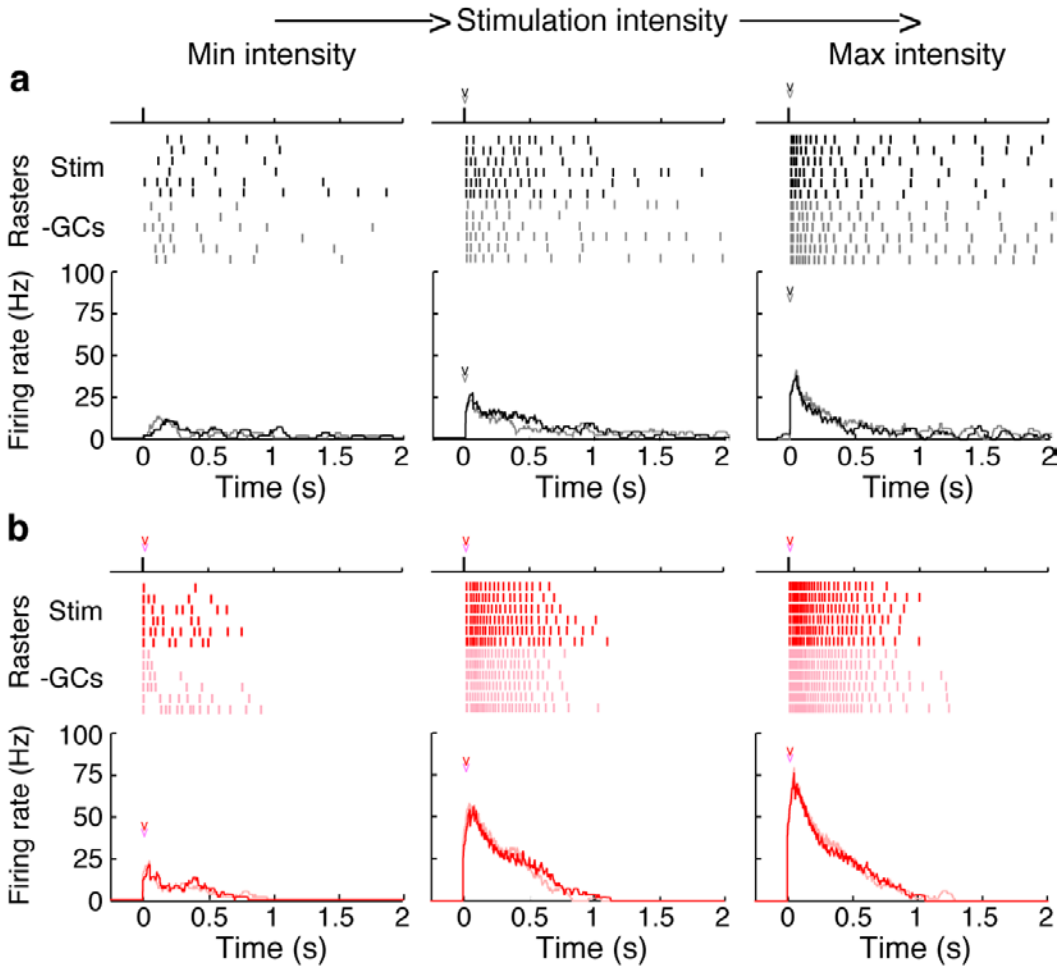

Figure 8: Examples showing that blocking GC-mediated inhibition does not alter firing rates or spike latencies in MCs or TCs.

(**a**-**b**) Example spike rasters following electrical stimulation of OSNs at three intensities in a MC (**a**) and TC (**b**) before (black/red) and after (gray/pink) limiting GC-mediated inhibition by blocking mGluRs (LY36785) and NMDARs (APV).

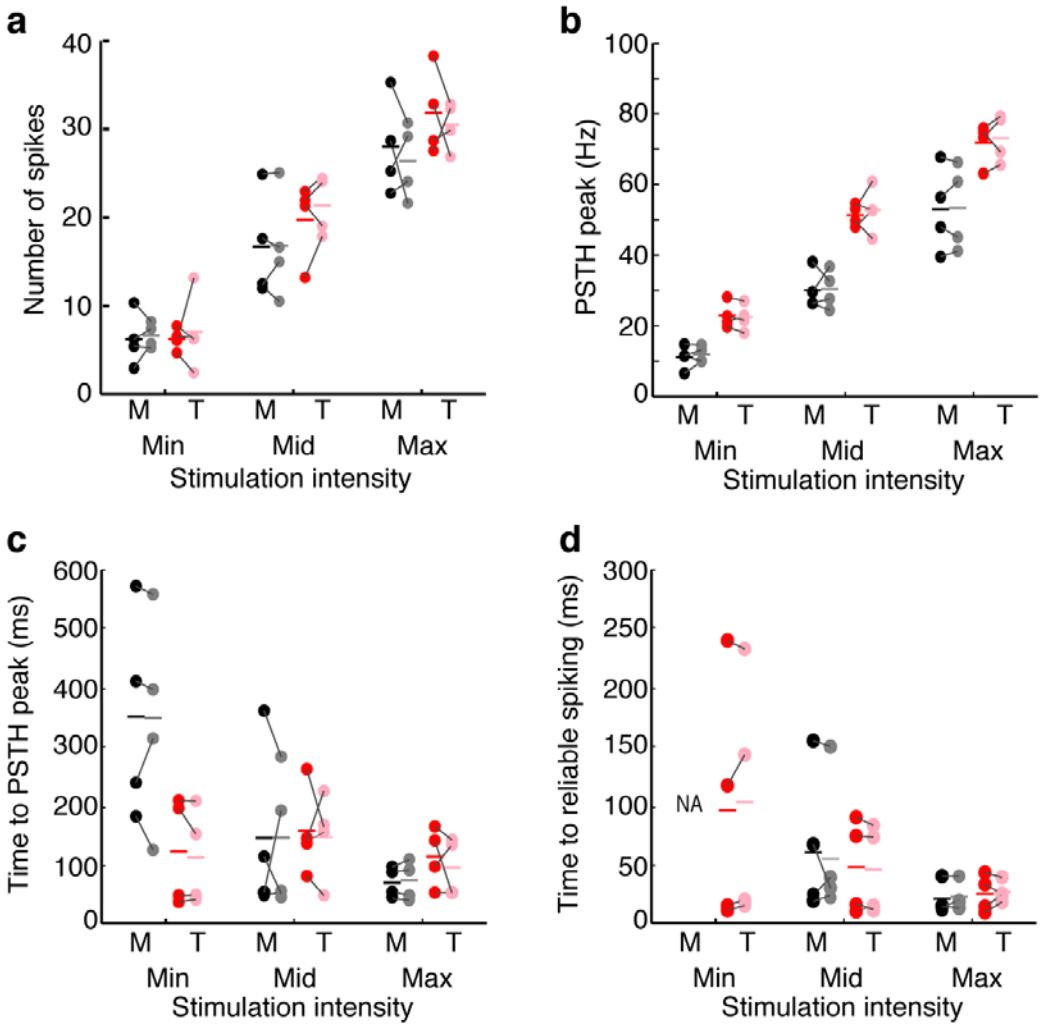

Figure 9: Summary statistics indicating that blocking GC-mediated inhibition does not alter firing rates or spike latencies in MCs or TCs.

Statistics from data collected from experiments described in **Figure 2.7**. (**a**) GC-mediated inhibition does not affect the number of spikes in either MCs (Min – p=0.72; Mid – p=0.97; Max – p=0.57) or TCs (Min – p=0.73; Mid – p=0.29; Max – p=0.64). (**b**) GC-mediated inhibition does not affect peak firing rates (PSTH peak) in either MCs (Min – p=0.49; Mid – p=0.91; Max – p=0.81) or TCs (Min – p=0.56; Mid – p=0.67; Max – p=0.62). (**c-d**) GC-mediated inhibition does not affect response latency as measured by the time to PSTH peak (**c**) in either MCs (Min – p=0.93; Mid – p=0.97; Max – p=0.58) or TCs (Min – p=0.44; Mid – p=0.79; Max – p=0.53) or the time to reliable spiking (**d**) in either MCs (Min – NA; Mid – p=0.67; Max – p=0.29) or TCs (Min – p=0.38; Mid – p=0.50; Max – p=0.73). Data taken from 4 MCs and 4 TCs. Significance was assessed in all panels using paired t-tests.

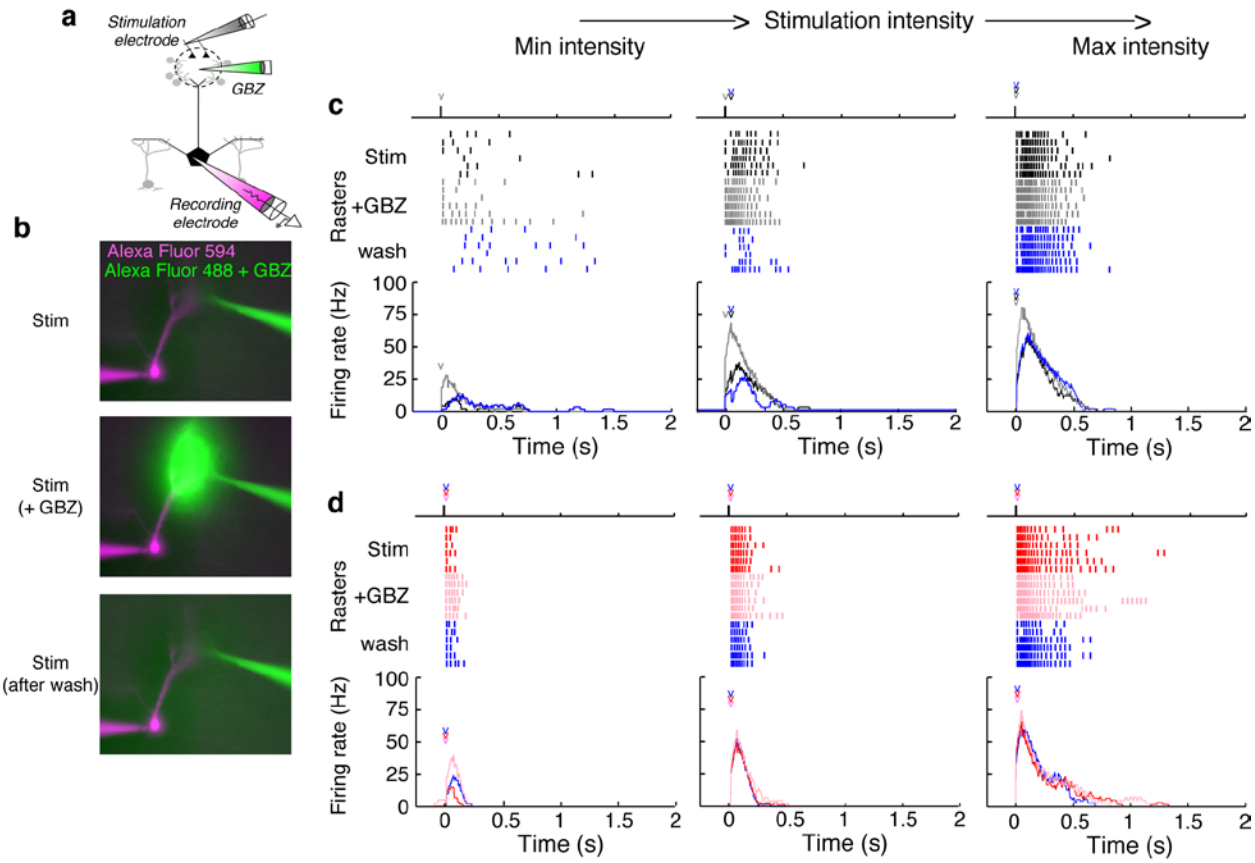

Figure 10: Examples showing that blocking PGC-mediated inhibition alters spike latencies in MCs but not TCs.

(**a-b**) Spikes were measured before and after puffing gabazine in the recorded cell's home glomerulus to limit PGC-mediated inhibition. (**c-d**) Spike rasters in a MC (**c**) and TC (**d**) before (black/red), during (gray/pink) and after (blue) blocking PGCs.

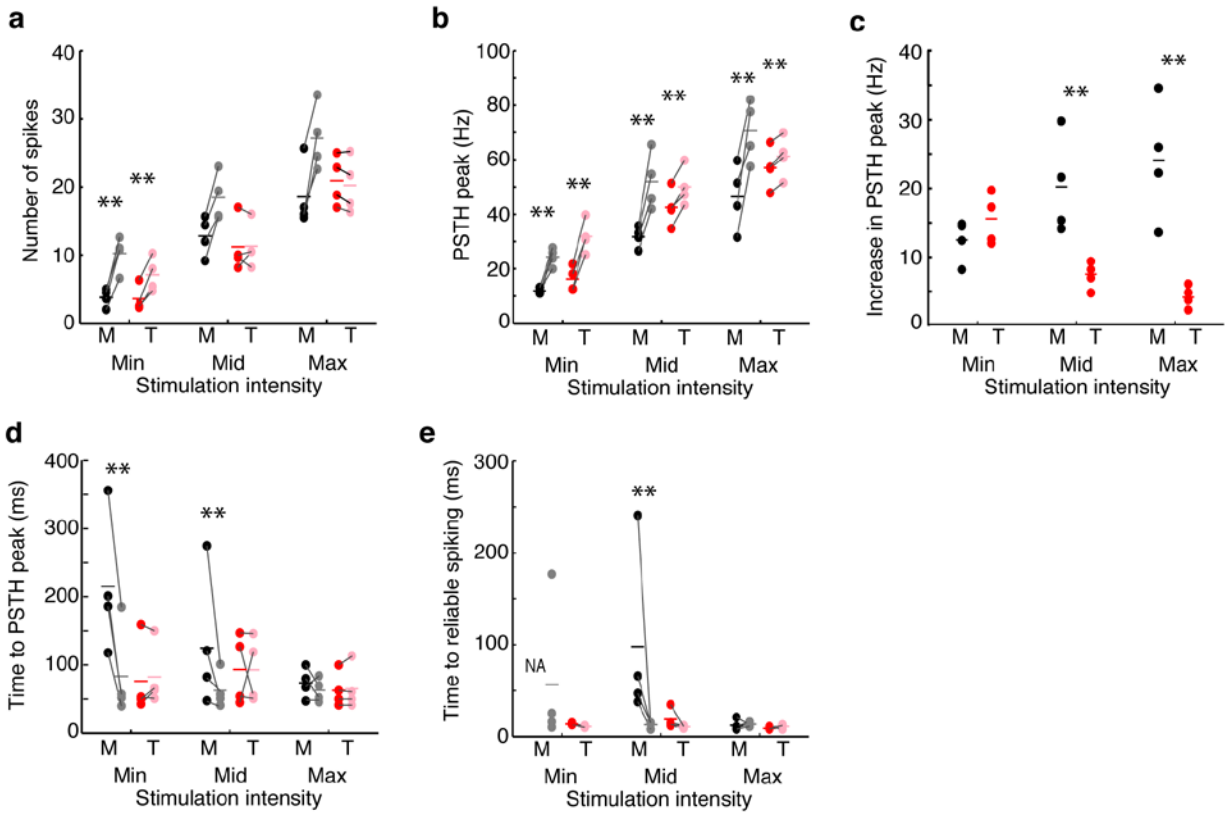

Figure 11: Summary statistics indicating that blocking PGC-mediated inhibition alters spike latencies in MCs but not TCs.

Statistics from data collected from experiments described in **Figure 2.9.** (**a**) Blocking PGCs increased the number of spikes in MCs at all three stimulation intensities (Min – p=0.003; Mid – p=0.005; Max – p=0.0075) and in TCs at the weakest intensity (Min – p=0.0078; Mid – p=0.91; Max – p=0.12). (**b**) Blocking PGCs increased the firing rate, as measured by the peak of the PSTH, at all three intensities in both MCs (Min – p=0.0039; Mid – p=0.011; Max – p=0.012) and TCs (Min – p=0.0027; Mid – p=0.037; Max – p=0.0023). (**c**) However firing rates were more strongly affected by blocking PGCs in MCs than in TCs at the strongest two intensities (Min – p=0.22; Mid – p=0.014; Max – p=0.0039). (**d**) Blocking PGCs reduced the latency to the PSTH peak in MCs at the weakest two intensities (Min – p=0.007; Mid – p=0.018; Max – p=0.56) but did not affect the latency in TCs (Min – p=0.43; Mid – p=0.98; Max – p=0.48). (**e**) The latency to reliable spiking did not change in TCs following PGC blockade (Min – p=0.09; Mid – p=0.13; Max – p=0.57), however, in MCs, the timing of responses in all four MCs became reliable at the weakest intensity and latency was reduced at the middle (p=0.03), but not the maximum (p=0.75), intensity. Data taken from 4 MCs and 4 TCs. Significance was assessed in all panels using paired t-tests. Asterisks (**) in **a-e** indicate significant (p<0.05) differences between MCs and TCs.

2.4 DISCUSSION

Here we show that MCs, but not TCs, show long latency responses at weak stimulation intensities that shorten with increasing intensity. We find that these differences are likely due to stronger inhibitory currents and weaker excitatory currents onto MCs than onto TCs (Figure 12). Differences in inhibition are largest during the first 150ms after stimulation and are mediated by PGCs. Additionally, we show that after blocking PGCs-mediated, but not GC-mediated inhibition, the latency of responses in MCs becomes shorter and more reliable.

These data support an emerging view that MCs and TCs are differentially influenced by glomerular layer sources of inhibition, which cause differences in spike latency between MCs and TCs(Fukunaga, Berning et al. 2012, Fukunaga, Herb et al. 2014). We corroborate prior work and show that at weak stimulation intensities, MCs primarily receive indirect excitatory input from external tufted cells (ETCs) that peaks approximately 50ms after stimulation(De Saint Jan and Westbrook 2007, De Saint Jan, Hirnet et al. 2009, Gire and Schoppa 2009, Najac, De Saint Jan et al. 2011, Smear, Shusterman et al. 2011, Gire, Franks et al. 2012, Najac, Sanz Diez et al. 2015). As the stimulation intensity increases, direct connections from OSNs onto MCs are recruited and the latency to the peak of excitation shortens. TCs, on the other hand, receive strong and direct excitation from OSNs at all stimulation intensities, and, consequently, the peak of excitation does not vary with stimulation intensity. In both MCs and TCs, inhibitory currents peak approximately 30ms after stimulation. Therefore, in TCs, the peak of excitation precedes inhibition regardless of stimulation intensity. In MCs, however, the peak of excitation lags inhibition at weak stimulation intensities but leads inhibition at higher stimulation intensities. Stronger PGC-mediated inhibitory currents onto MCs than TCs work cooperatively with these

differences in the source and relative strength of excitation to cause the latency of MC spiking to vary with stimulation intensity.

Stronger PGC-mediated inhibition onto MCs than TCs may be explained by multiple mechanisms. PGC synapses onto MCs may be stronger or more numerous than synapses onto TCs. Alternatively, separate populations of PGCs may preferentially target MCs and TCs. Subsets of PGCs have been identified both functionally and molecularly. Functionally, PGCs are classified by whether they receive excitation from OSNs or ETCs(Hayar, Karnup et al. 2004, Shao, Puche et al. 2009). Additionally, PGCs are molecularly heterogeneous ((Kosaka, Toida et al. 1998, Parrish-Aungst, Shipley et al. 2007, Kiyokage, Pan et al. 2010). Expressing channelrhodpsin in specific subpopulations of PGCs will be vital for determining the sources of these differences in PGC-mediated inhibition between MCs and TCs.

Whether animals use latency to determine odor concentration is an unanswered question that will play an important role in interpreting these data. While prior work has shown that animals can be trained to use latency to encode behaviorally relevant information(Smear, Shusterman et al. 2011), whether animals normally use latency to encode concentration-specific information is unknown. If MCs do encode concentration with spike latency, then the concentration-invariance of TC latency(Fukunaga, Berning et al. 2012, Igarashi, Ieki et al. 2012) suggests that TCs may play in important role in identifying odors across a wide range of odor concentrations. However, if animals do not use latency to determine odor concentration, and instead exclusively use firing rates, then an alternative purpose for long latency spiking in MCs is needed. For instance, odor identity may be encoded by MC spike latency(Hopfield 1995, Brody and Hopfield 2003). Therefore, while the absolute latency of MC spiking may vary with concentration, the relative differences in MC latency across the population remains constant so

that the representation of odor identity remains concentration invariant. Alternatively, MCs and TC may be responsible for encoding olfactory information in separate concentration ranges and only cells spiking early in the sniff cycle may be encoding task-specific information. This view implies that intrinsic and circuit-level factors that cause long latency spiking in MC serves to reduce redundant spikes early in the sniff cycle. Data showing that spike latency in MCs is unreliable at low stimulus intensities(Igarashi, Ieki et al. 2012) and that TCs have lower odor thresholds(Nagayama, Takahashi et al. 2004, Kikuta, Fletcher et al. 2013) implies that at least at low odor concentrations, odor information is primarily encoded by TCs. Finally, other aspects of olfactory bulb circuitry support concentration-specific ranges for MCs and TCs. For instance, differences in the sources and effects of lateral inhibition on MCs and TCs allow each to best perform odor discriminations in separate concentrations ranges(Geramita, Burton et al. submitted). Future experiments exploring how odor identification or discrimination at low concentrations is affected by either chemical or optical silencing of TCs will be needed to determine the extent to which MCs and TCs contribute to encoding olfactory information at low vs. high odor concentrations.

What are other consequences of stronger PGC-mediated inhibition onto MCs? Blocking PGC-mediated inhibition more strongly inhibits firing rates in MCs than in TCs, indicating that PGCs may play a critical role in the higher firing rates observed in TCs *in vitro* and *in vivo*(Nagayama, Takahashi et al. 2004, Igarashi, Ieki et al. 2012). While weaker input from PGCs and stronger excitation allows a larger dynamic range of excitatory responses in TCs than in MCs, PGCs may also be responsible for the more robust inhibitory responses observed *in vivo* in MCs(Nagayama, Takahashi et al. 2004). Indeed, both computational and *in vivo* work suggest that feed-forward inhibition mediated by PGCs is the most likely explanation for odor-evoked

inhibition commonly observed in MCs(Cleland 2010, Fukunaga, Berning et al. 2012, Fukunaga, Herb et al. 2014). Functionally these differences in PGC-mediated inhibition onto MCs and TCs may play an important role in decorrelating firing rates between MCs and TCs that project to the same glomerulus (i.e. homotypic M/TCs). Future in vivo experiments that monitor how homotypic MCs and TCs respond to odor will be vital for determining how TCs respond to odors that inhibit MCs. In addition to driving decorrelation of homotypic MC and TC firing rates, it is temping to speculate that differences in PGC-mediated inhibition between homotypic MCs may be one mechanism, in addition to other known intrinsic differences(Padmanabhan and Urban 2010), responsible for heterogeneous odor responses between homotypic MCs(Dhawale, Hagiwara et al. 2010). Supporting this idea, blocking PGC-mediated inhibition *in vitro* reduces spike time variability in MCs(Najac, Sanz Diez et al. 2015). Future studies measuring odor-evoked responses in homotypic MCs before and after blocking inhibition from various interneuron subtypes may help resolve the circuit-level mechanisms behind unique temporal dynamics in individual MCs.

Segregating sensory information presented in specific intensity ranges in parallel neuron types is a common strategy in sensory systems. The data presented here and elsewhere strongly indicate that MCs and TCs are responsible for encoding odor information presented at high and low concentrations, respectively. Similarly, distinct touch receptors in the skin respond to tactile stimulation in separate pressure ranges. Additionally, rods and cones encode visual information in largely separate intensity ranges. Given these similarities, it is temping to draw further analogies between sensory systems. For instance in visual system, three separate light intensity ranges have been described based on the type of photoreceptors that mediate vision in each range. In low light intensity conditions, scotopic vision is mediated by rods, while in high

intensity light conditions, photopic vision is mediated by cones. Mesopic vision is consequently defined as the intermediate range of light intensities in which visual information is encoded by both rods and cones. Because both rods and cones relay information through separate neural pathways in the retina and have distinct temporal responses, modeling how these signals are combined at these intermediate light intensity levels becomes quite challenging(Stockman and Sharpe 2006). Moving forward, determining whether three analogous ranges of odor concentration can be defined based on the responses of MCs and TCs will be vital. Given the added complexities of understanding olfactory coding in concentration regimes when both MCs and TCs are activated, it will be important to determine how each population encodes odors in isolation by studying responses in concentration ranges that only engage MCs or TCs.

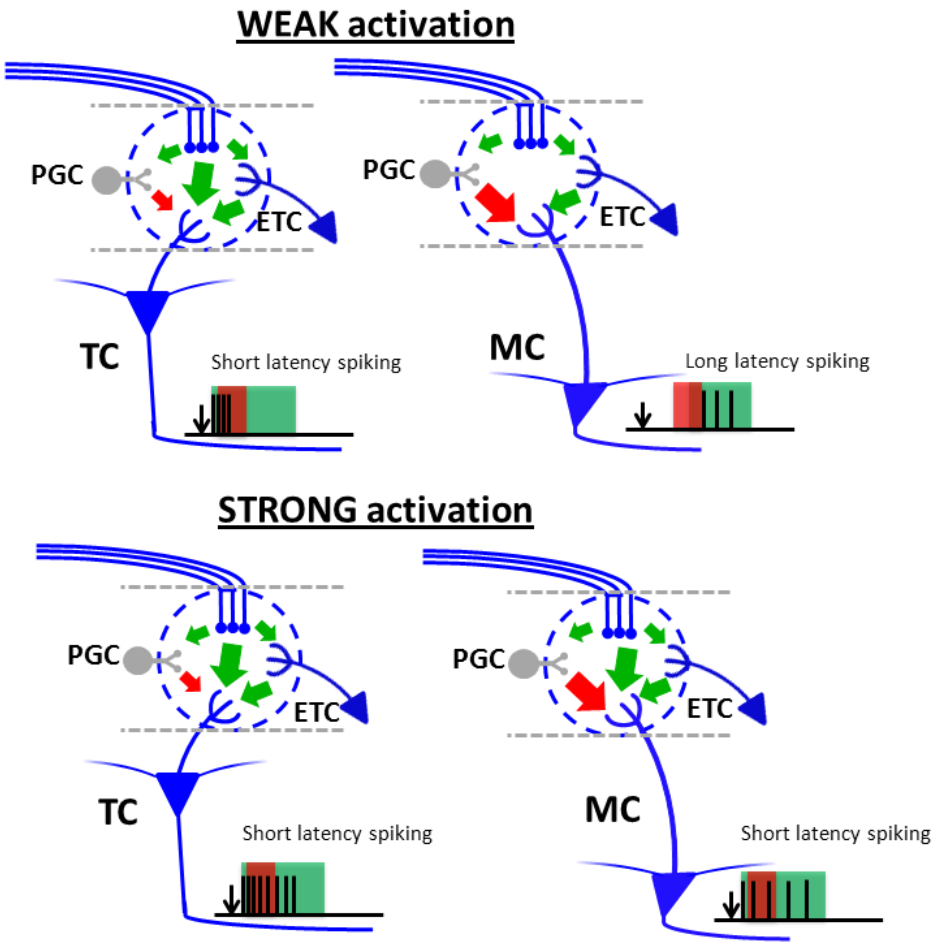

Figure 12: Summary of differences in feed-forward circuitry onto MCs and TCs

3.0 DISTINCT LATERAL INHIBITORY CIRCUITS DRIVE PARALLEL PROCESSING OF SENSORY INFORMATION IN THE MAMMALIAN OLFACTORY BULB

3.1 INTRODUCTION

Brain sensory systems use parallel pathways to encode different components of sensory information. Motion and color are segregated in the visual system(Merigan and Maunsell 1993, Callaway 2005), sound location and tonal pattern are processed in parallel pathways in the auditory system(Lomber and Malhotra 2008), and pain and itch are conveyed by distinct pathways in the somatosensory system(Davidson and Giesler 2010, Ross 2011). How local circuits support feature selectivity in these parallel streams remains poorly understood. This issue is of particular interest when considering brain areas in which distinct outputs are generated from initially homogeneous sources, such as in the olfactory system.

In the mammalian olfactory bulb, firing of olfactory sensory neurons (OSNs) excites two classes of projection neurons – mitral cells and tufted cells (MCs and TCs). While long viewed as essentially equivalent neuron classes, emerging evidence shows that MCs and TCs exhibit distinct activity *in vivo*(Nagayama, Takahashi et al. 2004, Fukunaga, Berning et al. 2012, Igarashi, Ieki et al. 2012, Adam, Livneh et al. 2014, Otazu, Chae et al. 2015), suggesting that MCs and TCs encode complementary aspects of olfactory information. For instance, TCs

respond to lower odor concentrations than MCs(Igarashi, Ieki et al. 2012, Kikuta, Fletcher et al. 2013), suggesting that TCs are involved in processing near-threshold stimuli. Consistent with this notion of parallel pathways, MCs and TCs project their axons to many non-overlapping regions(Nagayama, Enerva et al. 2010, Igarashi, Ieki et al. 2012). Recent work has begun to explore the circuit-level origins of these functional differences in odor-evoked activity. For instance, TCs are more intrinsically excitable and receive stronger OSN-mediated excitation than MCs(Gire, Franks et al. 2012, Burton and Urban 2014). Whether other elements of the olfactory bulb circuit account for differences in MC vs. TC odor-evoked activity is unknown.

Throughout the brain, lateral inhibitory circuits enhance contrast and facilitate discrimination of similar stimuli by decorrelating neural responses(Hirsch and Gilbert 1991, Urban 2002, Gschwend, Abraham et al. 2015). In the olfactory bulb, lateral inhibition occurs between pairs of MCs or TCs via reciprocal dendrodendritic synapses with inhibitory granule cells (GCs)(Schoppa and Urban 2003, Egger and Urban 2006). Previously, we have shown that lateral inhibition most strongly affects MCs firing at intermediate rates because coincident input is required for the activation of GCs(Arevian, Kapoor et al. 2008). This activity-dependent regulation of the strength of lateral inhibition onto MCs decorrelates MC responses to similar input more effectively than subtractive or divisive forms of inhibition(Arevian, Kapoor et al. 2008). Lateral inhibition onto TCs is largely unexplored, but the marked differences in MC and TC odor-evoked activity suggest that lateral inhibition onto TCs may operate differently.

Here, we show that optogenetic activation of a single, gene-targeted glomerulus elicits larger and more asynchronous lateral inhibitory currents in nearby MCs than in TCs. Moreover, this same photostimulation paradigm inhibits spiking differently in MCs and TCs. While MCs are affected by lateral inhibition at intermediate firing rates (~50 Hz), TCs are affected when

firing at low firing rates (<25Hz). This difference arises, in part, due to differential recruitment of morphologically distinct classes of GCs by MCs and TCs. Finally, we use simulations to explore how these circuit-level differences between MCs and TCs influence odor discrimination. Specifically the combination of activity-dependent lateral inhibition at both low and intermediate rates enables TCs and MCs to collectively encode odors better than either population alone and supports novel computations that are unlikely to occur with a single neuron type.

3.2 MATERIALS AND METHODS

3.2.1 Slice preparation

For MC and TC recordings, postnatal day 16 – 23 M72-ChR2-YFP(Smear, Resulaj et al. 2013) mice were anaesthetized with isoflurane and decapitated into ice-cold oxygenated dissection solution containing (in mM): 125 NaCl, 25 glucose, 2.5 KCl, 25 $NaHCO_3$, 1.25 NaH_2PO_4, 7 $MgCl_2$ and 0.5 $CaCl_2$. Sagittal slices (280 μm thick) of the MOB were prepared using a vibratome (VT1200S; Leica, Nussloch, Germany). Slices recovered for 15–30 min in 37°C oxygenated Ringer solution that was identical to the dissection solution except for lower Mg^{2+} concentrations (1 mM $MgCl_2$) and higher Ca^{2+} concentrations (2 mM $CaCl_2$). Slices were then stored in room temperature oxygenated Ringer solution until recording. For MC and TC recordings in OMP-ChR2-YFP mice, horizontal slices (280 μm thick) were prepared from postnatal 17-21 mice. For GC recordings, equivalent methods were used to prepare horizontal slices (310 μm) of the MOB from postnatal day 18-28 C57BL/6, Thy1-YFP-G(Feng, Mellor et

al. 2000) albino C57BL/6J, and heterozygous OMP-ChR2-YFP(Smear, Shusterman et al. 2011) mice using a vibratome (5000mz-2, Campden).

3.2.2 Cell identification and morphological analyses

TCs were identified as those cells with large somas (>10 μm in diameter) that reside completely in the EPL. Cell bodies resided in the superficial half of the EPL. All TCs included in our final dataset had at least 1 lateral dendrite and did not display the rhythmic bursting characteristic of external tufted cells(Hayar, Karnup et al. 2004, Antal, Eyre et al. 2006, Liu and Shipley 2008). MCs were identified as large cells located in the mitral cells layer (MCL). 'Displaced MCs(Mori, Kishi et al. 1983)' or 'internal TCs(Igarashi, Ieki et al. 2012)', those cells with somata that only partially reside in the mitral cell layer were excluded from analysis due to their ambiguous identity as MCs or TCs. GCs located in the MCL or GC layer were distinguished from other cell types and classified as sGCs or dGCs as previously described(Burton and Urban 2015). Specifically, GCs were classified as dGCs if their apical dendritic gemmules were visibly concentrated in the deep half of the EPL, while GCs were classified as sGCs if their apical dendritic gemmules were visibly concentrated in the superficial half of the EPL. Cell morphologies were reconstructed under a 100X oil-immersion objective and analyzed with Neurolucida (MBF Bioscience). Anatomical positions of GC apical dendritic gemmules were manually identified from 3D reconstructions using custom software written in Matlab (Mathworks).

3.2.3 Electrophysiology

Cells were visualized using infrared differential interference contrast video microscopy. For MC and TC recordings, slices were continuously superfused with 37°C oxygenated Ringer solution that contained 0.2 mM Mg^{2+} unless otherwise noted. Current clamp recordings were made from individual cells using electrodes filled with (in mM) 120 potassium gluconate, 2 KCl, 10 Hepes, 10 sodium phosphocreatine, 4 Mg-ATP, 0.3 Na_3GTP, 0.2 EGTA, 0–0.25 Alexa Fluor 594 (Life Technologies, Carlsbad, CA, USA) and 0.2% Neurobiotin (Vector Labs, Burlingame, CA, USA). Voltage clamp recordings were made using electrodes filled with (in mM): 140 Cs-gluconate, 10 HEPES, 2 KCl, 10 sodium phosphocreatine, 3 Mg-ATP, and 0.3 Na_3GTP.

M72 photostimulation was provided by a 250 μm multimode optical fiber (Thorlabs) coupled to a high-intensity light emitting diode (M470F1; Thorlabs) and driver (DC2100: Thorlabs) controlled by TTL pulses. For photostimulation in OMP-ChR2-YFP, slices were illuminated with 100ms light pulses by a xenon arc lamp directed through an YFP filter set and 60x water-immersion objective centered on a single glomerulus. Photostimulation was confined to single glomeruli by closing the field stop as previously described(Burton and Urban 2015). All data were low-pass filtered at 4 kHz and digitized at 10 kHz using a MultiClamp 700A amplifier (Molecular Devices, Sunnyvale, CA, USA) and an ITC-18 acquisition board (Instrutech, Mineola, NY, USA) controlled by custom software written in Igor Pro (WaveMetrics, Lake Oswego, OR, USA).

For GC recordings, slices were continuously superfused with warmed oxygenated Ringer's solution (temperature measured in bath: 32ºC) containing 1 mM Mg^{2+} and 2 mM Ca^{2+}. Current clamp recordings were made as described above. Voltage clamp recordings were made using electrodes filled with either the Cs-based solution supplemented with 10 mM QX-314 and

0.2% Neurobiotin or the K-based solution. To examine GC activity following activation of a single glomerulus, extracellular stimulation of olfactory sensory neuron fibers within a single glomerulus was performed as previously described(Burton and Urban 2015).

3.2.4 Data analysis

Lateral inhibitory currents were measured in 5 trials at a holding potential of +10 mV. Analysis of IPSCs was performed using custom Matlab (Mathworks) analysis software. The presence or absence of IPSCs was calculated by taking the average trace of 5 trials and finding the mean and standard deviation of the trace during the second prior to photostimulation. Then the baseline current (mean of the second prior to photostimulation) was subtracted from each trace. IPSCs evoked through lateral inhibition were present if positive deflections of the current trace exceeded 3*s.d. for longer than 10 ms in the 500 ms time window following M72 photostimulation.

Lateral inhibitory currents were split into early and late phases and the peak current amplitude and charge transfer were calculated in each. Charge transfer was calculated as the integral of the current trace in either the early phase (0-250ms) or late phase (250-1500ms) following photostimulation.

The effect of lateral inhibition on spiking was measured by performing FI curves in MCs and TCs via somatic current injection of increasing amplitudes. At each current step (500 ms), we measured the number of action potentials evoked with and without M72 photostimulation (10 ms pulses at 15 Hz). Two full FI curves (a full FI curve is defined as having current steps with and without photostimulation) were performed on each cell and the average change in firing rate at each current step was calculated and used for the presented analysis. Lateral inhibition was

defined to have a significant effect on a cell if there was a greater than 10% decrease in firing rate in at least 2 consecutive current steps.

Intrinsic biophysical properties of GCs, including passive membrane, action potential, and spike train properties were calculated as previously described(Burton and Urban 2015).

3.2.5 Computational model

Models of odors and olfactory bulb circuitry were developed in Matlab (Mathworks). Code is freely available and can be attained by contacting the corresponding author. The scheme for generating odor panels and individual odor trials is depicted in Figure 30. Each odor is represented by the spatial pattern of a 15 x 10 array of pixels (ie glomeruli). For each odor presented at a particular concentration ($I_{presentation}$), we first made Odor 1. To do this, we randomly sampled 1/3 of pixels to represent non-activatable (NA) pixels that are not responsive to odors, regardless of concentration. Next a concentration threshold (T_i) was sampled from a uniform distribution between 0 and 1000 for each activatable pixel (T_i = U([0,1000]). Activatable pixels were then divided into ON and OFF pixels. ON pixels were defined as having $T_i < I_{presentation}$, while OFF pixels are ones where $T_i > I_{presentation}$. Each ON pixel then got a mean activation intensity sampled from a normal distribution ($I_{base} = N(I_{presentation},50)$).

The next step in the construction of the odor panel was to make an arbitrary number of other odors that are 90% similar to Odor 1. To make these odors, we enforced a set of rules.

1) Each pixel in Odor 1 had a 10% probability of changing.

2) For each NA pixel that was chosen to change:

- P(NA – NA) = 1/3

- P(NA – ON) = 2/3

-If a NA pixel became an ON pixel, it received an activation intensity. $I_{base}=N(I_{presentation},50)$

3) For each ON pixel that was chosen to change:

- P(ON – NA) = 1/3

-P(ON – ON) = 2/3

-if an ON pixel remained ON, it received a new activation intensity. $I_{base}=N(I_{presentation},50)$

4) For each OFF pixel that was chosen to change:

- P(OFF – OFF) = 1

The last step in odor panel construction was to add noise to create trial-to-trial variability. To do this, we enforced a set of rules for sampling the activation strength of each pixel on each trial.

1) The strength of activation of NA and OFF pixels: $I_{trial} = U([0,1000])$

2) The strength of activation of ON pixels: $I_{trial} = N(I_{base},5)$

These odors became the glomerular input for olfactory bulbs composed of either MC or TCs. Each MC/TC was represented by a continuous firing rate variable, v. Each neuron received a leak current, an inhibitory current and an excitatory current input from 1 pixel (eqn. 1). The excitatory current was calculated by passing the pixel activation strength through a sigmoid. Two differences between MCs and TCs, higher excitability and increased excitatory input are reflected by increased slope (0.007 for MCs and 0.01 for TCs) and reduced midpoint (500 for MCs and 350 for TCs) of the TC sigmoid. MCs/TCs were randomly connected to 75/60% of other MC/TCs, reflecting the shorter extent of lateral dendrites in TCs compared with MCs(Igarashi, Ieki et al. 2012, Burton and Urban 2014). Inhibition was calculated as the product of the sum of network activity, u(t) (eqn. 5), and a Gaussian function that determines which

range of firing rates are influenced by lateral inhibition (eqn 3,4). The center and width of the MC and TC Gaussian distribution are based on differences in the range of rates influenced by lateral inhibition in our data.

(1) $t\frac{dv}{dt} = stim(t) - leak(t) - inhib(t)$

(2) $leak = g_l * (v(t) - E_l)$

(3) $inhib_{tufted}(t) = g_i * u(t) * e^{-\frac{(v(t)-\mu t)^2}{\sigma t}}$, μ_t=10, σ_t=350

(4) $inhib_{mitral}(t) = g_i * u(t) * e^{-\frac{(v(t)-\mu m)^2}{\sigma m}}$, μ_m=50, σ_m=500

(5) $inhib_{subtractive}(t) = g_i * u(t)$

(6) $inhib_{divisive}(t) = g_i * v(t)$

(7) $u(t) = \sum_{n=1}^{T} v_n(t), where\ T\ is\ the\ number\ of\ connected\ MCs\ or\ TCs$

(8) $stim(t) = f(\text{Itrial}), where\ f\ is\ a\ sigmoid$

One of N odors from the panel was presented to the MC or TC bulb on each of 2000 trials. The MC or TC outputs from half of the trials are used to train a naïve Bayes classifier which was then used to predict which odor is being presented on the remaining half of trials. The percent correct is used as the discrimination accuracy for that odor panel. For simulations, we constructed 100 odor panels at each concentration. Concentrations in Figure 29 are plotted as the percent of maximum concentration. The maximum concentration was defined as the concentration that evokes maximum firing rates in MCs and TCs, which in our models is set at 100 Hz – a rate often observed *in vivo.* A sigmoidal transfer function was used to translate glomerular inputs into MC/TC outputs so that odor concentrations could be defined in terms of MC/TC firing rates while not make any explicit comparisons to actual odor concentrations. Significance in discrimination accuracy between output neuron configurations was determined in

2 steps. First, we conducted one-way ANOVA tests (corrected for multiple comparisons – ie the number of odor concentrations tested) on the discrimination accuracy of the three output neuron configurations at each odor concentration. At concentrations with significant ANOVA tests, we performed post-hoc t-tests to determine whether one particular output neuron configuration was significantly better than the other two. The results of the post-hoc t-tests determine the highlighted areas of Figure 29**.**

The simulations used to generate the data in Figure 29**k-m**, in which 2 output neurons receive inputs from 1 glomerulus required additional connectivity rules. For bulbs containing only MCs or TCs, each of the two cell that input from the same glomerulus receive inhibition from a random set of other neurons. In bulbs containing both MCs and TCs, inhibition remained segregated, that is TCs/MCs only received inhibition from a random set of other TCs/MCs. Additionally, for all 3 output neuron configurations, neurons projecting to the same glomerulus did not inhibit one another. The simulations used to generate the data in Figure 32, in which one input image served as input to 2 separate populations that only differed in the range of ADLI. For each population, each pixel in the image provided into to one neuron.

3.3 RESULTS

3.3.1 MCs receive stronger and more asynchronous lateral inhibitory currents than TCs

To analyze lateral inhibition, we optically activated M72-expressing OSN axons in acute slices from M72-ChR2-YFP mice(Smear, Resulaj et al. 2013) while recording from MCs or TCs innervating nearby glomeruli (Figure 13**a,b)**. This approach allows specific and selective

activation of a single, genetically-identified glomerulus across animals, eliminating an important potential source of variability. MCs and TCs showed reliable lateral inhibition following a 10 ms light pulse (Figure 13**c,d**), and similar proportions of MCs (10/17 – 59%) and TCs (9/15 – 60%) received lateral inhibitory currents. The MCs and TCs recorded were similar distances from the M72 glomerulus, and lateral inhibition did not vary within this limited range of distances in either MCs or TCs (Figure 15). To examine early and late components of the inhibitory responses onto MCs and TCs, we separated early (<250 ms after stimulation) and late (>250 ms after photostimulation) components of the inhibitory currents. The peak amplitude of early inhibition was larger in MCs than in TCs (Figure 13**e**), while the charge transferred of early phase inhibition was not significantly different (Figure 13**f**). Additionally, both the peak amplitude and charge transferred of late phase inhibition (>250ms) was significantly larger in MCs than in TCs. MCs also receive a smaller proportion of total inhibition during the early phase than TCs, indicating that inhibition is more asynchronous onto MCs than onto TCs. Collectively, these results demonstrate that lateral inhibitory currents are larger and more asynchronous onto MCs than onto TCs.

We also explored two potential causes of cell-to-cell variability in lateral inhibition. The strength of lateral inhibition onto MCs and TCs did not depend on whether the apical dendrite was truncated during the slicing procedure, indicating that lateral inhibition originating in the glomerular layer(Aungst, Heyward et al. 2003, Liu, Plachez et al. 2013, Whitesell, Sorensen et al. 2013, Banerjee, Marbach et al. 2015) did not significantly contribute to the differences in lateral inhibition studied here. Variability from slice-to-slice did contribute to variability in the strength of inhibition. However, for MCs and TCs recorded in the same slice, the same relationships in peak amplitude and charge transferred for both early and late phase inhibition

were observed as in the larger data set. Specifically, early and late phase peak amplitude, but only late phase charge transferred, was significantly higher in MCs than in TCs measured in the same slice (Figure 13**g**).

To confirm that these results are not specific to the M72 glomerulus, we performed an analogous experiment in OMP-ChR2-YFP mice(Smear, Shusterman et al. 2011) by photostimulating a single unidentified glomerulus (100 ms pulses) in the medial olfactory bulb (Figure 14**a-b**). Previously we have shown that we can limit photostimulation to single glomeruli in OMP-ChR2YFP mice(Burton and Urban 2015). Similar to the results obtained using M72-ChR2-YFP mice, we find that only the peak amplitude of the early phase of inhibition is larger in MCs while both the amplitude and charge transferred of the late phase of inhibition are larger in MCs (Figure 14**c,d**). Together these two experiments indicate that lateral inhibition is larger and more asynchronous onto MCs than onto TCs.

Finally, using photostimulation of a single glomerulus in OMP-ChR2-YFP mice, we tested whether GCs contribute similar proportions of lateral inhibition onto MCs and TCs using a Figure 14previously described strategy(Najac, Sanz Diez et al. 2015) to differentiate between GC- vs. non-GC-mediated inhibition onto MCs and TCs. We recorded lateral inhibition before and after limiting GC-mediated inhibition by bath applying NMDAR antagonist APV (25 μM) and mGluR antagonist LY36785 (100 μM). Using this pharmacological approach, we found that GCs contribute similar proportions of lateral inhibition onto MCs and TCs (Figure 14**e**). Additionally, in MCs and TCs in which the apical dendrite had been truncated, all lateral inhibition was blocked after limiting GC-mediated inhibition (Figure 14**b,e**). In contrast, small inhibitory currents remained after limiting GC-mediated inhibition in MCs and TCs with intact apical dendrites (Figure 14**b,e**). Removing cells with cut apical dendrites and redoing the

analysis presented in Figure 14**e** similarly shows that GCs contribute similar proportions of lateral inhibition onto MCs and TCs. These observations indicate that glomerular layer circuits make small and uniform contributions to lateral inhibition in MCs and TCs and thus are not the primary source of differences in lateral inhibition between MCs and TCs.

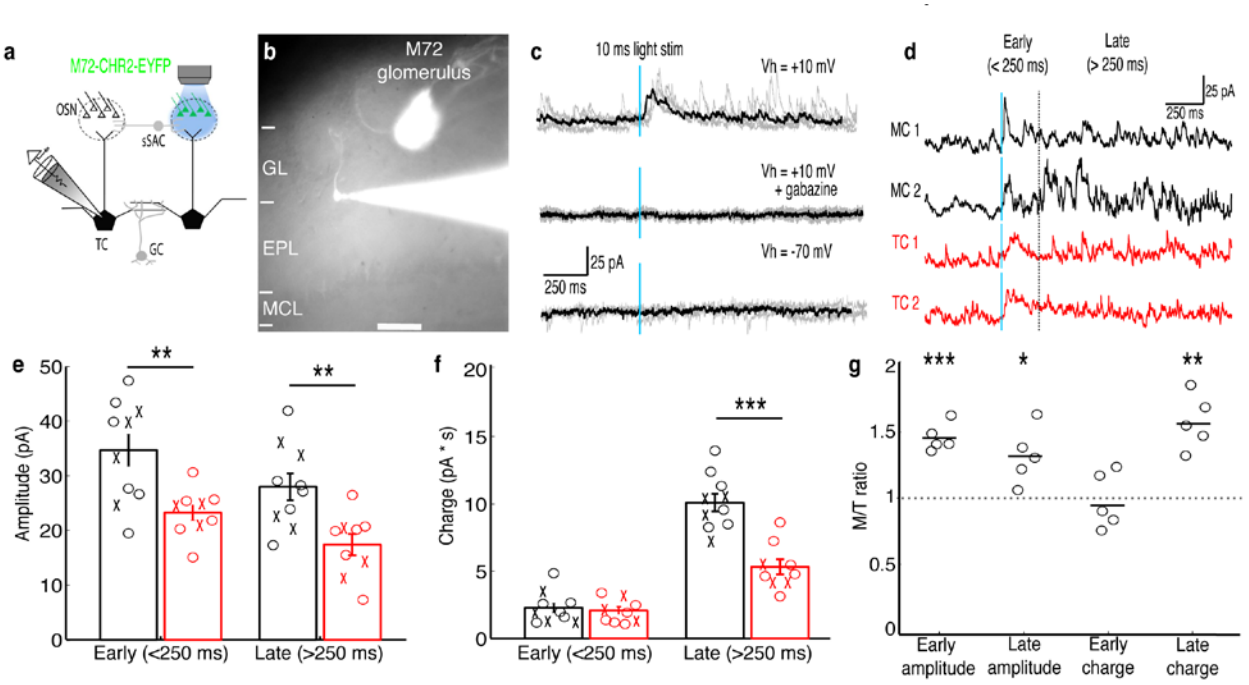

Figure 13: MCs receive stronger lateral inhibition than TCs.

(**a-b**) Schematic and example of recording from a TC that projects to a glomerulus near the M72 glomerulus to measure lateral inhibition in M72-ChR2-YFP mice (GL: glomerular layer, EPL: external plexiform layer, MCL: mitral cell layer). (**c**) Light stimulation evoked reliable inhibitory currents in recorded TC (TOP; 5 trials – grey, average – black) that are abolished by gabazine (MIDDLE) but did not evoke excitatory currents (BOTTOM). (**d**) Examples of average inhibitory currents in 2 MCs and 2 TCs. Inhibitory responses were grouped into early phase (<250 ms) and late phase (>250 ms). (**e**) The peak amplitude was significantly larger in MCs (n=10) than in TC (n=10) during both the early and late phases of inhibition. (**f**) Charge transferred was significantly larger in MCs than TCs during the late phase only. ('x' indicates cells lacking apical dendrites). (**g**) MCs and TC recorded sequentially in the same slice (n=5 slices) show similar differences in inhibiton. Data are presented as mean ± s.e.m. Statistical tests

in **e,f** were two-tailed, unpaired t tests and tests in **g** were paired t tests. (***** p<0.05, ****** p<0.01, ******* p<0.001)

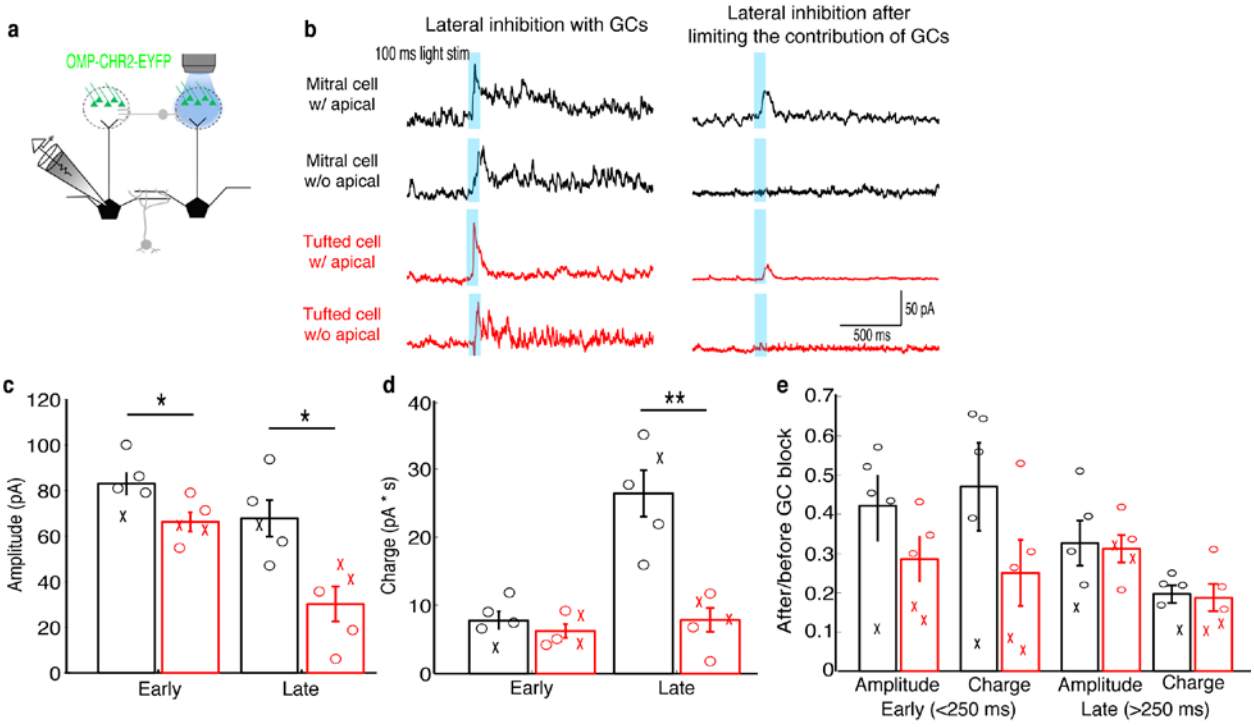

Figure 14: Glomerular layer circuits cannot explain lateral inhibition differences between MCs and TCs.

(**a-b**) Analogous experiment to those performed in M72-ChR2 mice measuring lateral inhibition in OMP-ChR2-YFP mice before and after limiting GC-mediated inhibition by bath applying APV and LY36785. (**c,d**) Similar differences in the peak amplitude (**c**) and charge (**d**) in MCs (n=5) and TCs (n=5) were found. (**e**) Ratio of early and late phase amplitude and charge after and before limiting GC-mediated inhibition. Data are presented as mean ± s.e.m. Statistical tests in **c-e** were two-tailed (***** p<0.05, ****** p<0.01, ******* p<0.001)

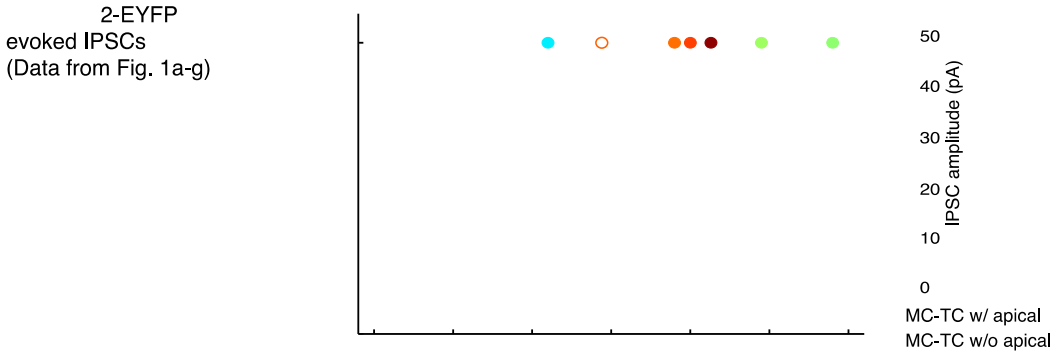

Figure 15: Distance dependence of lateral inhibition onto MCs and TCs.

(a-d) Lateral distance dependence of inhibitory current amplitude from data taken from Figure 1a-g. (**a**) Map of where recorded MCs and TCs resided with respect to the M72 glomerulus. TC position on the y axis is the relative distance between the glomerular layer and the mitral cell layer (MCL). Unfilled circles indicate MC/TCs that lack an apical dendrite. (**b-c**) Plot of lateral inhibition amplitude vs absolute lateral distance from the M72 glomerulus in MCs (**b;** r=0.17, p=0.52) and TCs (**c;** r=0.25, p=0.36). (**d**) Plot of lateral inhibition amplitude vs relative radial distance from the M72 glomerulus in TCs (r=-0.09, p=0.76). Significance determined using Pearson's correlation.

3.3.2 Lateral inhibition affects intermediate firing rates in MCs and low firing rates in TCs

We next explored how lateral inhibition influences MC and TC spiking. To do this, we stimulated MCs and TCs by step current injection and measured firing rates to constructed input-output curves in cells near the M72 glomerulus. On interleaved trials we activated M72 OSN axons via photostimulation (Figure 16**,**Figure 18). We used a duration of step current injection matching the physiological duration of firing observed following *in vivo* odor delivery(Patterson, Lagier et al. 2013) or *in vitro* glomerular activation(Najac, Sanz Diez et al. 2015) (Figure 17). Similar proportions of MCs (16/25 – 64%) and TCs (12/18 – 67%) were affected by lateral inhibition (see **Methods**), and unaffected cells were excluded from further analysis. Additionally, MCs and TCs were similar distances from the M72 glomerulus (Figure 19). Similar to our previous results using paired MC recordings(Arevian, Kapoor et al. 2008), MC firing rates were reduced by lateral inhibition selectively when MCs fired at intermediate rates, although inhibition was observed at more than double the rate observed in paired recordings. For example, the MC in Figure 16**b,e** was affected by lateral inhibition while firing between 27 – 76 Hz. Likewise, across a population of 16 MCs, rates between 34 ± 11 Hz and 79 ± 22 Hz were affected by lateral inhibition (Figure 18**a-e,** Figure 20**a-c**). Surprisingly, TCs were influenced by

lateral inhibition only when firing at low rates. The example TC in Figure 16**c,d,f** was affected by lateral inhibition while firing between 5 – 42 Hz, and across a population of 12 TCs, rates between 10 ± 4 Hz and 43 ± 8 Hz were affected by lateral inhibition (Figure 18**a-e,** Figure 20**d-f**). Both the lower and upper bounds of the effective activity range of lateral inhibition (i.e. the range of firing rates over which lateral inhibition reduces firing rates) were significantly lower in TCs than in MCs (Figure 18**e**).

The average fractional reduction in firing rate was much larger in TCs than in MCs (Figure 18**c**), though the absolute firing rate decrease was not significantly different (MC: -8.2 ± 2.5 Hz n=16, vs TC: -8.8 ± 3.2 Hz n=12) (Figure 18**d,f**). Similar to the findings reported above, neither the effective activity range of lateral inhibition nor the decrease in absolute firing rate depended on whether the cell had an intact apical dendrite. Additionally, these effects of lateral inhibition on firing rate were present even in short timescales matching a single 4 Hz sniff (Figure 21). Collectively, our results demonstrate that lateral inhibition is functionally distinct in MCs and TCs.

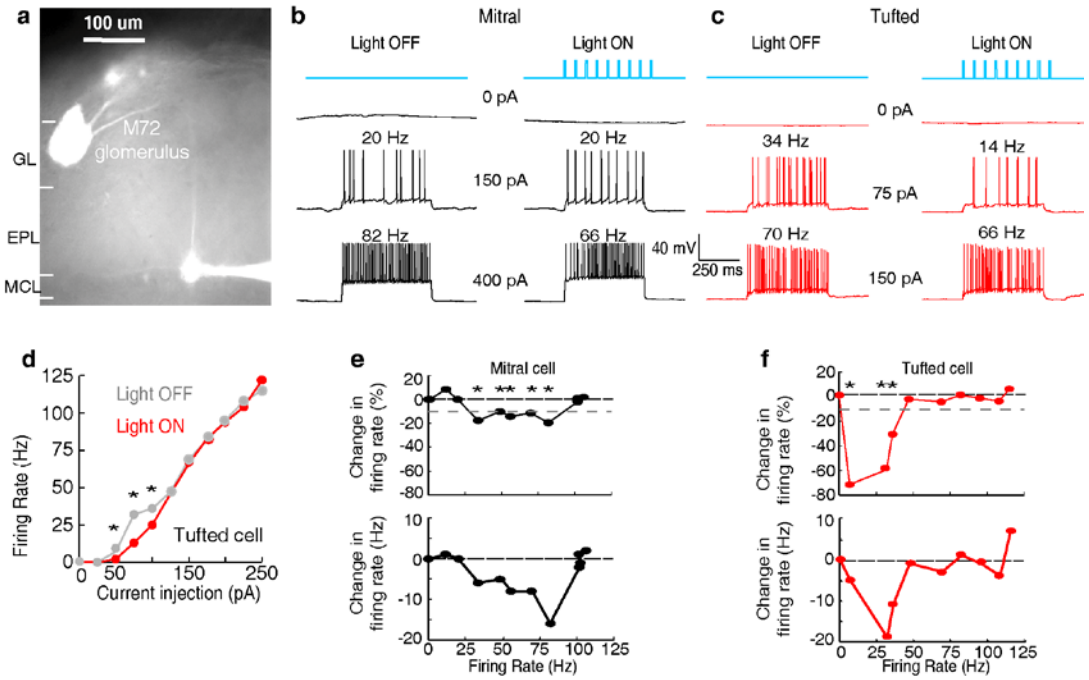

Figure 16: Examples show a TC and MC affected by lateral inhibition at low and intermediate firing rates, respectively.

(GL: glomerular layer, EPL: external plexiform layer, MCL: mitral cell layer). (**a**) Fluorescent image of a recorded MC that projects to a glomerulus near the M72 glomerulus. (**b-f**) The impact of lateral inhibition on one example MC (**b, e**) and one example TC (**c, d, f**) was assessed by constructing FI curves for each cell via somatic current injections of increasing amplitudes. At each current step, the number of action potentials evoked with and without M72 photostimulation was determined (10 ms pulses at 15 Hz). (**b-c**) Examples of voltage traces in a MC (**b**) or TC (**c**) at 2 different firing rates with and without M72 photostimulation. (**d**) The effect of lateral inhibition is illustrated by comparing the FI curves for the light off (grey) versus light on (red) trials in the TC. (**e-f**) Plots of the percent decrease in firing rate (TOP) or absolute firing rate (BOTTOM) in light on trials for a MC (**e**) or TC (**f**). Asterisks signify firing rates that are reduced by more than 10% in at least 2 consecutive light on trials.

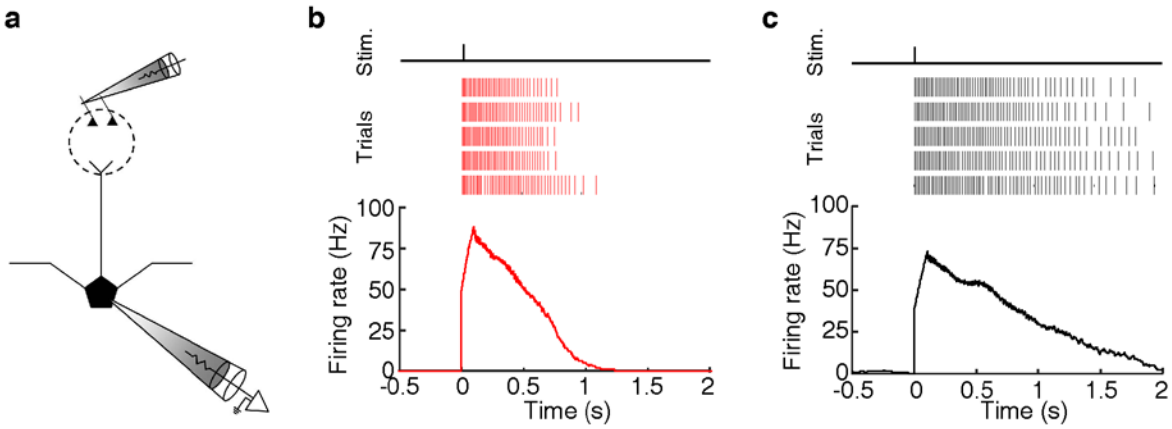

Figure 17: MCs and TCs can sustain high firing rates for long periods

(**a-c**) MCs and TCs can sustain high firing rates (>50 Hz) for long periods (>500 ms) following glomerular stimulation. (**a**) Schematic of experiment in which we electrically stimulated the home glomerulus of a MC or TC. (**b-c**) Spike raster (TOP) and PSTH (BOTTOM) of the response in one MC (**b**) and one TC (**c**) to a single electrical pulse (100 μA, 600 μs) to the OSN layer.

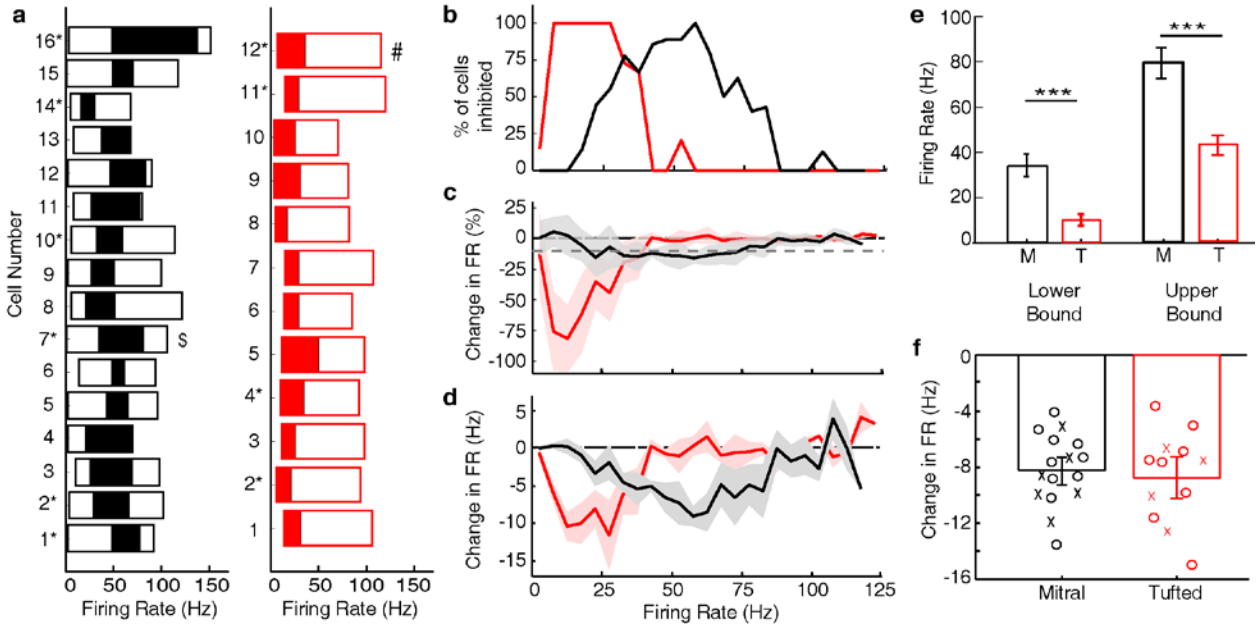

Figure 18: Summary results show that TCs are influenced by lateral inhibition at low rates while MCs are influenced at intermediate rates.

(**a**) The range of firing rates that are significantly influenced by lateral inhibition is plotted with respect to the firing rate in light off trials. Outer rectangle for each cell indicates the total range of firing rates evoked during light off trials. Inner (shaded) rectangle indicates the range of firing rates that are reduced during light on trials. Asterisks indicate cells that lack apical dendrites. ($ - MC used in Fig 2, # - TC used in Fig 2). (**c**) Percentage of cells that are significantly inhibited is plotted with respect to the firing rate in light off trials. (**c-d**) Average decrease in firing rate (**c** – plotted as percent, **d** – plotted as Hz) across the population of MCs (black) and TCs (red). Grey dotted line in **c** represents the 10% threshold used to indicate significant inhibition. Shaded areas represent s.d. **(e)** The lower (LEFT, unpaired t-test, $p=2.8\times10^{-7}$) and upper bound (RIGHT, unpaired t-test, $p=1.7\times10^{-5}$) of the range of rates affected by lateral inhibition are significantly lower in TCs compared to MCs. (**f**) There is no change in the average decrease in firing rate (Hz) between MCs and TCs (unpaired t test, p=0.87). In **f**, decreases in firing rate were calculated as the average decrease across all significantly affected firing rates. Data are presented as mean ± s.e.m.

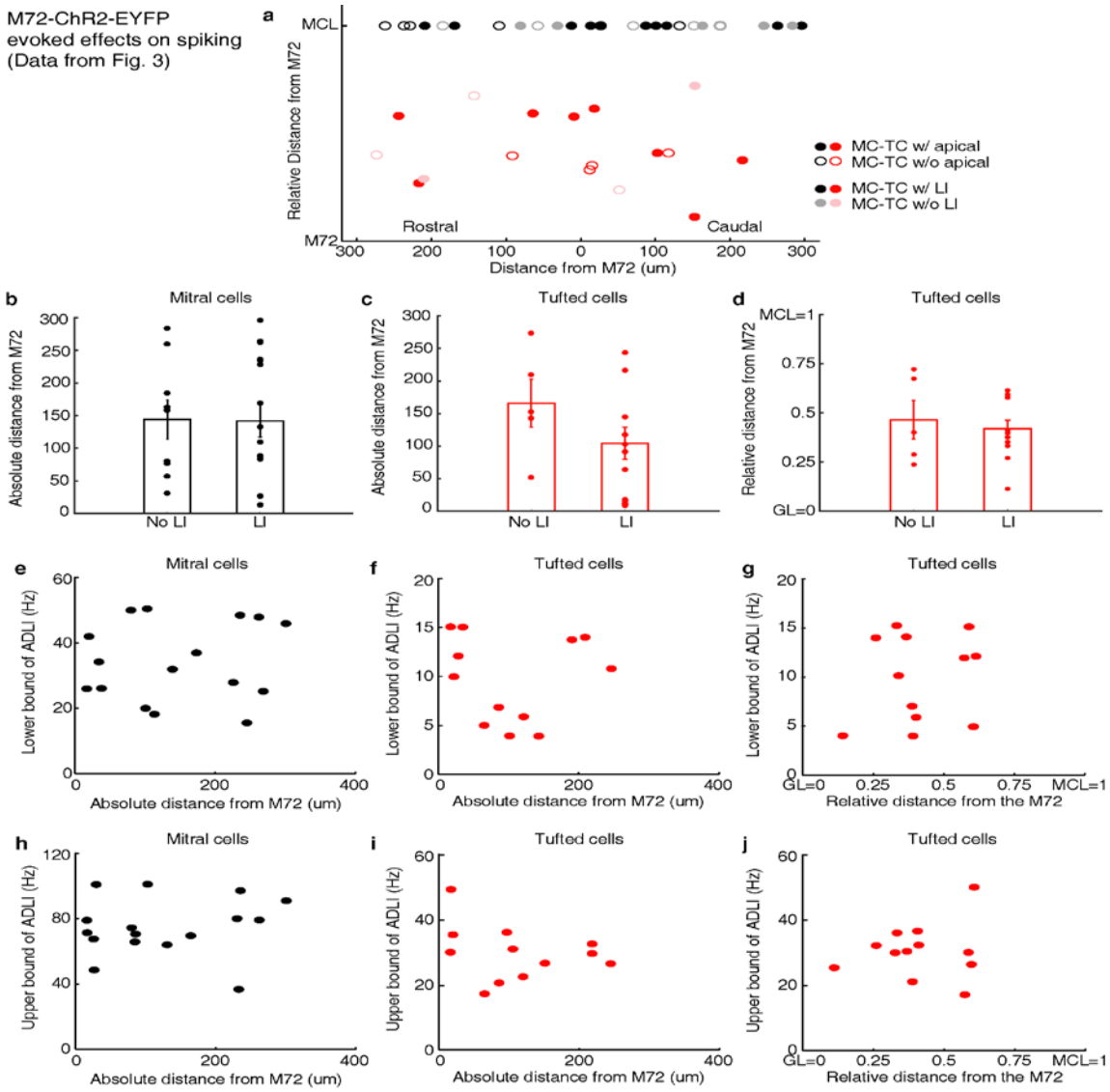

Figure 19: Distance dependence of lateral inhibition onto MCs and TCs.

(a-d) Lateral distance dependence of effect of lateral inhibition on spiking from data taken from Figure 3. (**a**) Map of where recorded MCs and TCs resided with respect to the M72 glomerulus. TC position on the y axis is the relative distance between the glomerular layer and the mitral cell layer (MCL). Unfilled circles indicate MC/TCs that lack an apical dendrite. (**b-c**) Plot of lateral inhibition amplitude vs. absolute lateral distance from the M72 glomerulus in MCs (**b,** p=0.28; unpaired t-test) and TCs (**c,** p=0.31; unpaired t-test) with and without lateral inhibition. (**d**) Plot of lateral inhibition amplitude vs. relative radial distance from the M72 glomerulus in TCs (p=0.62; unpaired t-test) with and without lateral inhibition. (**e-f**) Plot of lower bound of ADLI vs absolute distance from the M72 glomerulus in MCs (**e** – r=0.16, p=0.56) and TCs (**f** – r=0.005, p=0.99). (**g**) Plot of lower bound of ADLI vs. relative distance from the M72 glomerulus in TCs (r=0.20, p=0.54). (**h-j**) Same as **e-g**, only with the upper bound of ADLI (**h** – r=0.21, p=0.44; **i** – r=-0.30, p=0.34; **j** – r=0.11, p=0.72). In **e-j**, significance was determined using Pearson's correlation. Error bars in **b-d** indicate mean ± SEM.

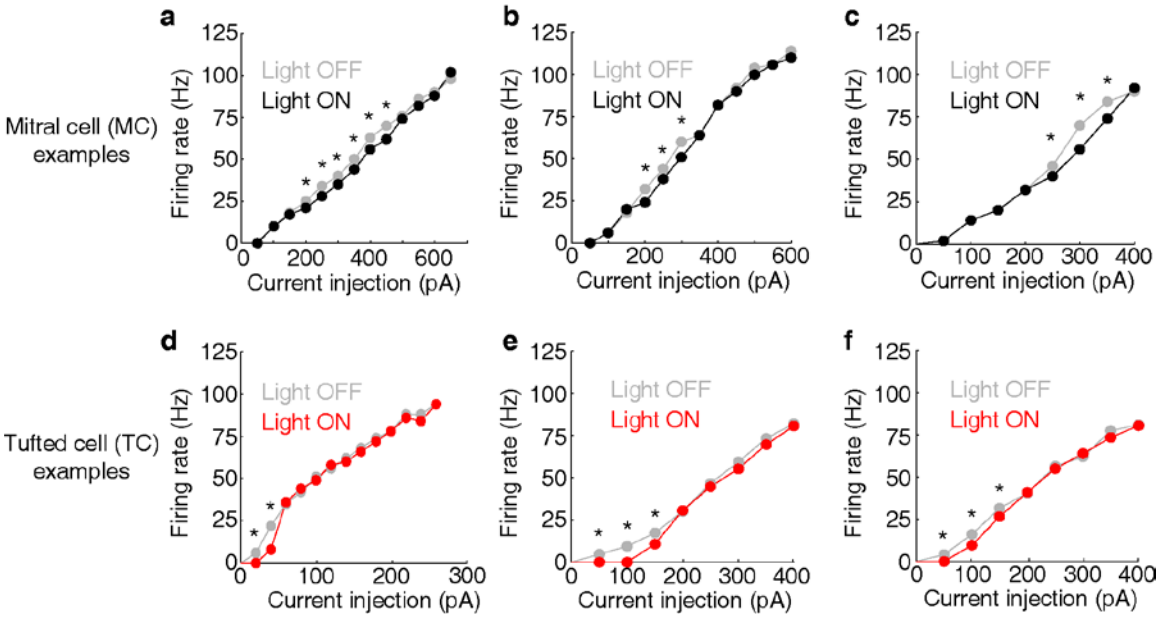

Figure 20: Examples of FI curves with and without photostimulation of the M72.

(a-c) Current intensity vs. firing rate (FI curve) is plotted in 3 MCs in light off (grey) and light on (black) conditions. **(d-f)** Same as a-c, only in 3 TCs. Asterisks indicate current intensities in which the firing rate during light on conditions is reduced by more than 10% compared to light off conditions – indicating significant effects of lateral inhibition.

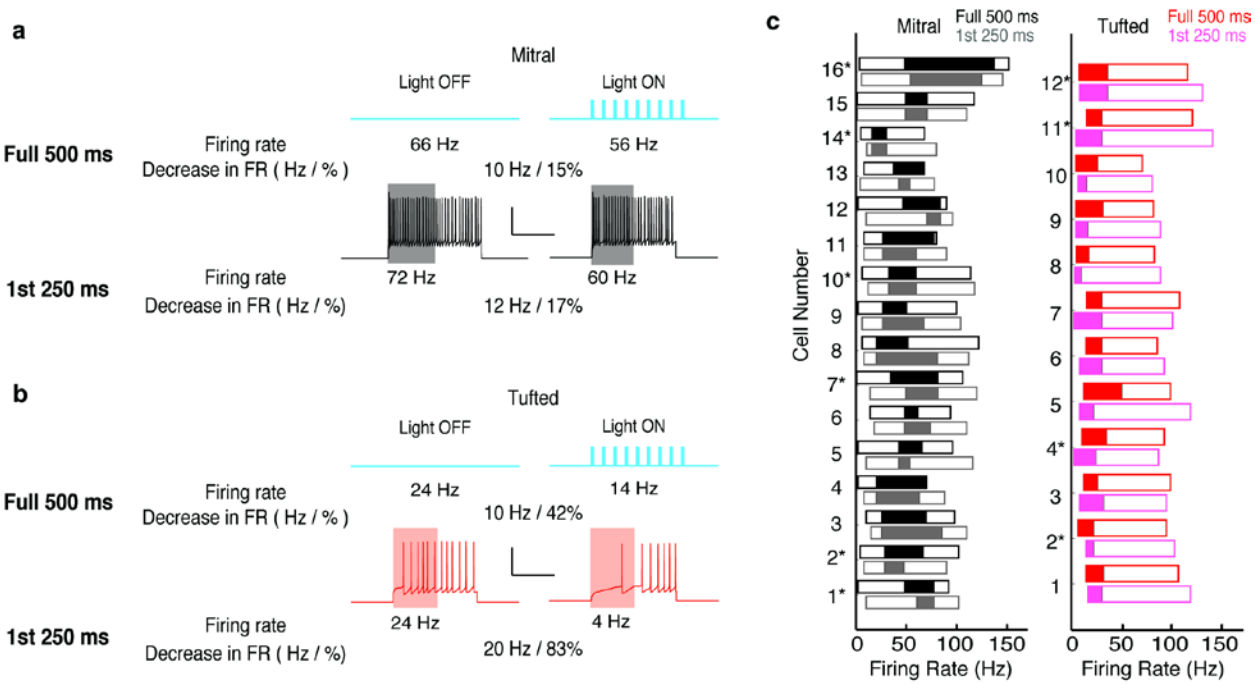

Figure 21: Differences in ADLI are maintained on physiologically relevant timescales

(**a-c**) The effects of lateral inhibition found in Figures 2-3 are maintained on the physiologically relevant timescale of a single 4 Hz (250 ms) sniff. We reanalyzed the data presented in Figure 3, and only calculated the effect of lateral inhibition for the first 250 ms of spiking. (**a-b**) Example of the analysis in one MC (**a**) and one TC (**b**). (**c**) The range of firing rates that are significantly influenced by lateral inhibition is plotted with respect to the firing rate in light off trials. Outer rectangle for each cell indicates the total range of firing rates evoked during light off trials. Inner (shaded) rectangle indicates the range of firing rates that are reduced during light on trials. Asterisks indicate cells that lack apical dendrites. Gray and pink data indicates analysis of the first 250ms of the trial while black and red data indicate analysis from the full 500ms of the trial.

3.3.3 Differences in the excitability of anatomically defined subclasses of GCs account for differences in the effective activity range of lateral inhibition onto MCs and TCs

This difference in activity-dependent lateral inhibition (ADLI) may arise from differences in the lateral inhibitory circuits engaged by MCs and TCs. Our finding that inhibition is largely unaffected by apical dendrite truncation suggests that differences in ADLI between MCs and TCs most likely involves inhibitory circuitry within the external plexiform layer (EPL). Consistent with MCs and TCs engaging distinct lateral inhibitory circuits within the EPL, classical morphological studies suggest that GCs are subdivided into superficial GCs (sGCs), which innervate the superficial EPL, and deep GCs (dGCs), which innervate the deep EPL(Mori, Kishi et al. 1983, Orona, Scott et al. 1983). This putative morphological subdivision of GCs suggests that sGCs inhibit TC lateral dendrites in the superficial EPL while dGCs inhibit MC lateral dendrites in the deep EPL(Mori, Kishi et al. 1983, Orona, Rainer et al. 1984). Therefore, functional differences between sGCs and dGCs may mechanistically underlie the difference in ADLI observed between MCs and TCs. In particular, given our prior results demonstrating that low firing rates in MCs are unaffected by lateral inhibition because many GCs require cooperative inputs from multiple glomeruli in order to be activated(Arevian, Kapoor et al. 2008), we hypothesized that low firing rates in TCs are affected by lateral inhibition because sGCs are more strongly recruited than dGCs following activation of a single glomerulus.

Supporting our hypothesis, GC soma position correlates with GC subtype (Mori, Kishi et al. 1983, Orona, Scott et al. 1983) and odor-evoked activity *in vivo* (Wellis and Scott 1990). Specifically, GCs located in the MCL and upper GCL tend to exhibit sGC morphologies and suprathreshold odor responses while GCs located in the lower GCL tend to exhibit dGC morphologies and subthreshold odor responses (Mori, Kishi et al. 1983, Orona, Scott et al. 1983,

Wellis and Scott 1990). Whether these differences in odor-evoked activity *in vivo* reflect functional differences between TC-sGC and MC-dGC circuitry remains unclear, however, as: 1) odors activate multiple glomeruli in distinct spatiotemporal patterns, which can evoke a complex array of convergent excitation and inhibition onto individual GCs (Burton and Urban 2014), and 2) GC activity *in vivo* is strongly influenced by centrifugal input (Boyd, Sturgill et al. 2012, Markopoulos, Rokni et al. 2012) and anesthesia (Kato, Chu et al. 2012, Cazakoff, Lau et al. 2014).

Therefore, to more directly test our above hypothesis, we recorded the excitatory synaptic input and spiking response of GCs to activation of single nearby glomeruli, with post-hoc recovery of Neurobiotin-filled cell morphologies. For this experiment, we switched from selective optogenetic stimulation of M72 glomeruli to extracellular stimulation of untagged glomeruli in order to test a large number of GC-glomerulus pairs. While this approach introduces a degree of glomerulus-to-glomerulus variability to our data, we capitalized on the well-established all-or-none nature of glomerular activation at low stimulation intensities(Carlson, Shipley et al. 2000, Gire and Schoppa 2009) to enable across-cell comparisons of synaptic input and spiking responses following glomerular activation. In addition, we and others have previously demonstrated that optogenetic photostimulation and extracellular stimulation of OSN axons trigger comparable sensory-evoked input to both M/TCs and GCs(Gire, Franks et al. 2012, Burton and Urban 2014, Burton and Urban 2015).

Consistent with previous morphological accounts(Mori, Kishi et al. 1983, Orona, Scott et al. 1983), GCs exhibited distinct sGC or dGC morphologies upon visual inspection (Figure 22**a;** Figure 23**a;** Figure 25). Indeed, reconstruction of a large subset of recorded GCs and analysis of the spatial distribution of gemmules – the site of reciprocal dendrodendritic synapse

formation(Rall, Shepherd et al. 1966) – confirmed that sGCs preferentially innervate the superficial EPL while dGCs preferentially innervate the deep EPL (Figure 24**a**). Moreover, somatic depth significantly – but incompletely – predicted GC subtype (Figure 25**;** Table 1), as previously observed(Mori, Kishi et al. 1983, Orona, Scott et al. 1983). To determine whether the observed morphological differences reflect subtypes of GCs rather than a continuum, we additionally performed unbiased clustering of GCs. Specifically, clustering of GCs by the Euclidean distances among their normalized gemmule distributions (using Ward's method) and application of the gap statistic method yielded 3 distinct clusters: dGCs, sGCs, and a small group of sGCs with prominent innervation of the deep glomerular layer (Figure 25). Moreover, these clusters closely aligned with our original classification by visual inspection, with 19 of 19 sGCs and 9 of 11 dGCs correctly assigned (Figure 25**c**). Our results therefore quantitatively confirm the morphological subdivision of GCs into distinct subclasses of sGCs and dGCs.

In agreement with our hypothesis, a strikingly higher percentage of sGCs than dGCs fired in response to activation of a single glomerulus (Figure 22**b,** Figure 23**b,** Figure 24**b**) due, at least partially, to stronger excitatory synaptic input to sGCs than dGCs (Figure 22**c,** Figure 23**c,** Figure 24**c**). As a caveat, we note that the greater recruitment of sGCs following glomerular activation may arise as an artifact of our acute slice preparation. Specifically, as TC circuitry is closer to any given glomerulus than MC circuitry, TC-mediated input to GCs (likely sGCs) may be better preserved than MC-mediated input to GCs (likely dGCs) in the acute slice, leading to stronger sGC excitation and recruitment following glomerular activation. Three lines of evidence argue against this possibility, however, and instead support greater feedforward recruitment of sGCs as a physiological feature of the olfactory bulb circuit. First, our *in vitro* observation of greater sGC firing following glomerular activation (Figure 24**b**) corresponds well with the

previous *in vivo* observation of stronger odor-evoked activity in putative sGCs (Wellis and Scott 1990). Second, examination of GC biophysical properties revealed several intrinsic differences supporting greater recruitment of sGCs than dGCs, including a more hyperpolarized action potential threshold in sGCs (Figure 24**f;** Table 2) and greater intrinsic excitability in sGCs in response to somatic step current injections (Figure 24**d,e;** Table 3), despite equivalent somatodendritic sizes (Figure 25**d**; Table 1) and passive membrane properties (Table 4**)** between sGCs and dGCs. Third, analysis of spontaneous synaptic activity revealed no difference in event frequency or amplitude between sGCs and dGCs (Table 5)**.** Critically, recordings of spontaneous synaptic activity were performed in the absence of TTX and thus contain some degree of action potential-dependent input, which likely originates from intact presynaptic cells. Therefore, equal spontaneous event frequencies between sGCs and dGCs suggests that their respective presynaptic circuits are comparably intact. Moreover, equal spontaneous event amplitudes suggest a comparable contribution of larger action potential-dependent and smaller action potential-independent events between sGCs and dGCs, again consistent with comparably intact presynaptic circuits. In total, our results thus strongly suggest that sGCs are more strongly recruited than dGCs following activation of a single glomerulus due to stronger excitatory input and greater intrinsic excitability.

As an additional test of our hypothesis that differences in the excitability of GCs explain the functional difference in ADLI between MCs and TCs, we measured the effects of lateral inhibition on MC spiking before and after increasing the excitability of GCs with the mGluR agonist (RS)-3,5-dihydroxyphenylglycine (DHPG, 10 µM)(Dong, Hayar et al. 2007, Heinbockel, Laaris et al. 2007). At this concentration, DHPG selectively enhances the excitability of GCs(Heinbockel, Heyward et al. 2004) but not MCs (Figure 28). The effective activity range of

lateral inhibition in MCs (n=6) fell from 31 (± 9) – 73 (± 10) Hz to 16 (± 12) – 49 (± 23) Hz after adding DHPG (Figure 27**a-d**), and the lower and upper bounds of the effective activity range of lateral inhibition were significantly reduced after the addition of DHPG (Figure 27**e**). Additionally, this effect did not depend on whether apical dendrites were intact (Figure 27**d**), and therefore does not reflect effects of DHPG on glomerular layer circuitry. These data (Figure 22**,** Figure 23**,** Figure 24**,** Figure 27**)** provide several strong, independent lines of evidence that differences in GC populations account for differences in the effective activity range of lateral inhibition onto MCs and TCs.

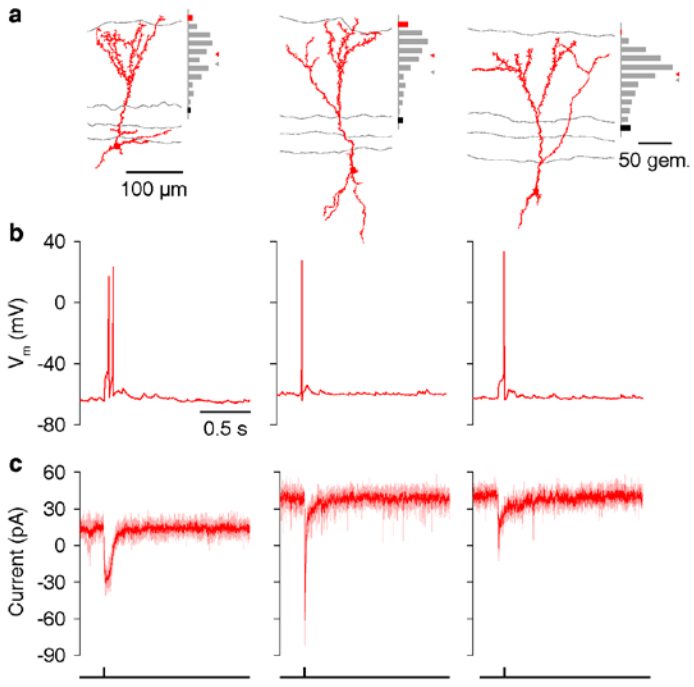

Figure 22: Example of recordings from superficial GCs following glomerular activation.

(**a**) Reconstructed morphologies and distribution of apical dendritic gemmules across the MCL (black bars), EPL (grey bars), and GL (red bars) of 3 representative sGCs. Grey/red ticks represents the midpoint of the EPL/mean of the cell's gemmule distribution. (**b,c**) Spiking response (**b**) and synaptic input (**c**) of the 3 sGCs shown in **a** following activation of a single glomerulus superficial to the targeted GC.

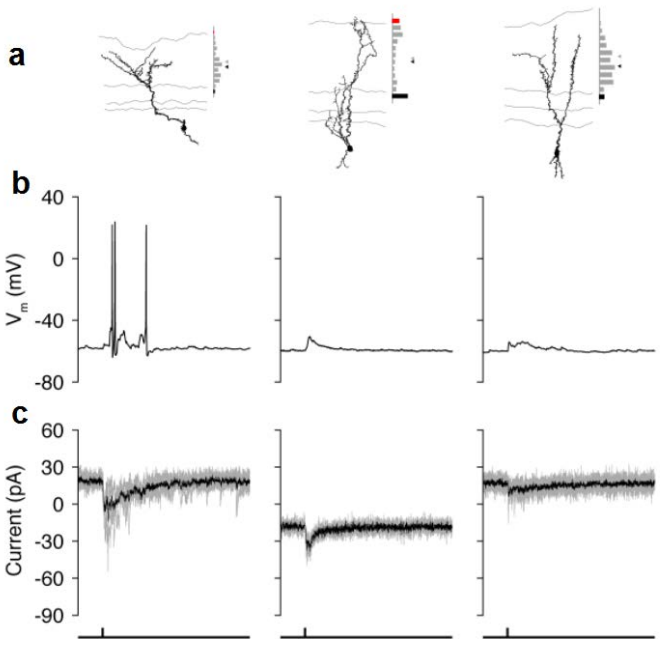

Figure 23: Example of recordings from deep GCs following glomerular activation.

(**a**) Reconstructed morphologies and distribution of apical dendritic gemmules across the MCL (black bars), EPL (grey bars), and GL (red bars) of 3 representative dGCs. Grey/red ticks represents the midpoint of the EPL/mean of the cell's gemmule distribution. (**b,c**) Spiking response (**b**) and synaptic input (**c**) of the 3 dGCs shown in **a** following activation of a single glomerulus superficial to the targeted GC.

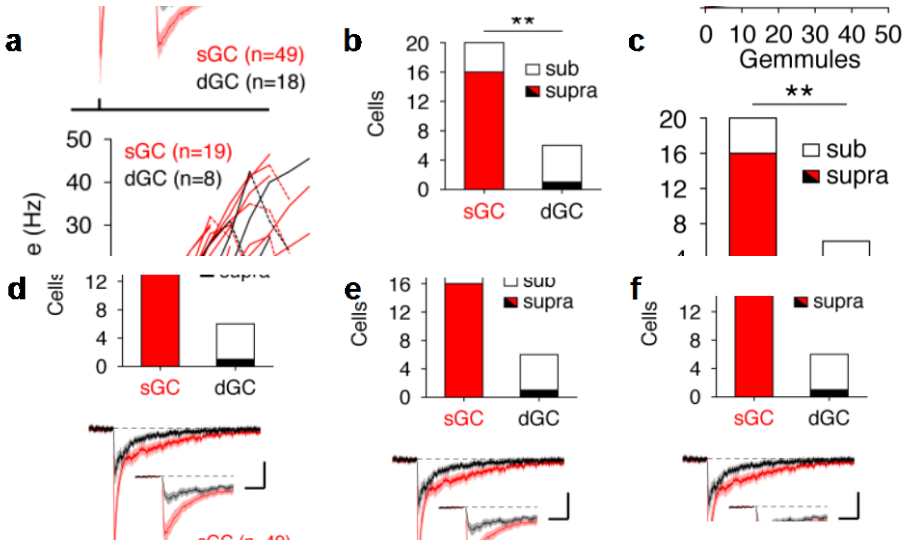

Figure 24: Synaptic and intrinsic differences between superficial and deep GCs regulate recruitment following glomerular activation.

(**a**) Distribution of apical dendritic gemmules across reconstructed sGCs and dGCs. (**b**) A greater proportion of sGCs than dGCs fired in response to glomerular activation (Chi-square test, $p=4.2\times10^{-3}$). (**c**) Excitatory input to sGCs exhibited larger peak currents (rank-sum test, $p=8.5\times10^{-3}$) and charge transferred (rank-sum test, p=0.046) than excitatory input to dGCs. No difference in excitation latency was observed (6.6 ± 11.6 vs. 9.7 ± 11.4 ms; rank-sum test, p=0.12). Scalebar: 0.2 s/10 pA (inset: 40 ms/20 pA). (**j,k**) sGCs and dGCs showed significantly different firing rate-current (FI) curves in response to somatic step current injection (2-way ANOVA, $p=4.1\times10^{-3}$). Individual (**d**) and mean (**e**) FI curves shown. Dashed lines show diminished firing due to depolarization block. (**f**) sGC action potentials exhibited more hyperpolarized thresholds (unpaired *t* test, $p=4.8\times10^{-3}$), larger amplitudes (unpaired *t* test, $p=1.1\times10^{-4}$), and faster rising slopes (unpaired *t* test, $p=2.9\times10^{-4}$) than dGC action potentials. Inset: action potential phase plot. Scalebar: 30mV/100 $mVms^{-1}$; dashed lines show origin. Shaded regions show mean ± SEM.

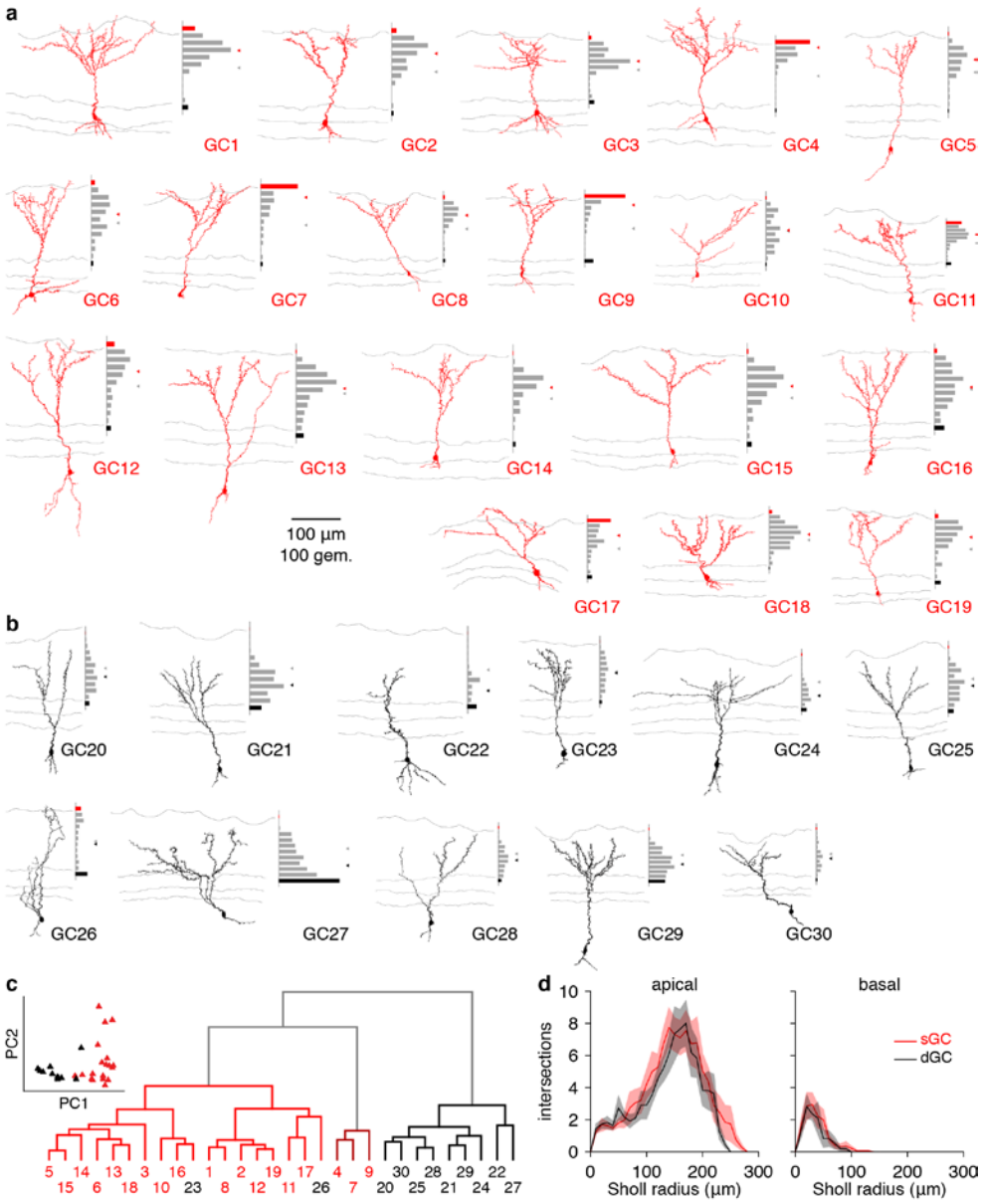

Figure 25: Morphological analysis of superficial and deep GCs.

(**a**) Reconstructed morphologies and distribution of apical dendritic gemmules across the MCL (black bars), EPL (grey bars), and GL (red bars) for 19 sGCs whose response to single glomerular activation was examined (see **Fig. 4**). Grey/red ticks represents the midpoint of the EPL/mean of the cell's gemmule distribution. (**b**) Same as **a** for 11 dGCs. (**c**) Dendrogram of clustered GC morphologies. Line colors correspond to the 3 significant clusters. Numbers correspond to the reconstructed morphologies shown in **a,b**, with number colors reflecting GC classification by visual inspection (sGC: red; dGC: black). Inset: projection of GCs across the first 2 principal components (74.0% of total variance) calculated from the normalized gemmule distributions.(**d**) Sholl analysis of GC dendritic morphologies. sGCs and dGCs exhibited no significant difference in apical (p=0.21) or basal (p=0.56) dendritic complexity (unpaired t-tests of area under Sholl curves). Shaded regions show mean ± SEM.

Table 1: Morphological properties of GCs

	sGC	dGC	*P* value
Soma area (μm^2)	74.9 ± 25.9 (19)	78.6 ± 17.3 (11)	0.67 (n.s.)
Soma depth from MCL (μm)	24.9 ± 26.6 (19)	75.5 ± 21.6 (11)	1.0×10^{-5} ***
Basal dendrites, Σ length (μm)	217.8 ± 186.0 (19)	177.6 ± 121.9 (11)	0.53 (n.s.)
Basal dendrites, Σ volume (μm^3)	70.1 ± 62.3 (19)	65.2 ± 76.0 (11)	0.85 (n.s.)
Apical dendrites, Σ length (μm)	1890.6 ± 477.1 (19)	1642.5 ± 587.0 (11)	0.22 (n.s.)
Apical dendrites, Σ volume (μm^3)	642.5 ± 282.3 (19)	606.7 ± 222.7 (11)	0.72 (n.s.)
Apical dendrites, gemmules	241.9 ± 81.0 (19)	203.1 ± 138.7 (11)	0.34 (n.s.)

Values reported are mean ± standard deviation (*n*). *p<0.05; **p<0.01; ***p<0.001; n.s., not significant (two-tailed unpaired *t* test).

Table 2: Action potential properties of GCs

	sGC	dGC	*P* value
$V_{threshold}$ (mV)	–31.9 ± 6.3 (19)	–23.8 ± 5.7 (8)	4.8×10^{-3} **
Amplitude (mV)	60.6 ± 8.8 (19)	44.3 ± 7.6 (8)	1.1×10^{-4} ***
FWHM (ms)	0.97 ± 0.14 (19)	1.09 ± 0.29 (8)	0.16 (n.s.)
Rising slope (mV ms^{-1})	195.9 ± 53.5 (19)	109.4 ± 33.9 (8)	2.9×10^{-4} ***
Falling slope (mV ms^{-1})	–63.2 ± 12.8 (19)	–53.8 ± 17.2 (8)	0.13 (n.s.)

Values reported are mean ± standard deviation (*n*). *p<0.05; **p<0.01; ***p<0.001; n.s., not significant (two-tailed unpaired *t* test).

Table 3: Spike train properties of GCs

	sGC	dGC	*P* value
Rheobase (pA)	36.3 ± 20.9 (19)	46.2 ± 22.6 (8)	0.28 (n.s.)
Rheobase first-spike latency (ms)	543.6 ± 542.9 (19)	209.0 ± 164.9 (8)	0.10 (n.s.)
Gain (Hz pA^{-1})	0.86 ± 0.33 (19)	0.91 ± 0.34 (7)	0.74 (n.s.)
Peak instantaneous rate (Hz)	59.3 ± 23.5 (19)	42.4 ± 15.2 (8)	0.074 (n.s.)

Values reported are mean ± standard deviation (*n*). *p<0.05; **p<0.01; ***p<0.001; n.s., not significant (two-tailed unpaired *t* test).

Table 4: Passive membrane properties of GCs

	sGC	dGC	*P* value
R_{input} (MΩ)	599.8 ± 397.6 (20)	499.7 ± 248.9 (8)	0.52 (n.s.)
τ_m (ms)	26.6 ± 14.6 (17)	26.1 ± 11.5 (7)	0.94 (n.s.)
C_m (pF)	46.0 ± 12.2 (17)	48.9 ± 11.5 (7)	0.60 (n.s.)
V_{rest} (mV)	–71.3 ± 6.8 (22)	–65.6 ± 10.0 (8)	0.085 (n.s.)

Values reported are mean ± standard deviation (*n*). *p<0.05; **p<0.01; ***p<0.001; n.s., not significant (two-tailed unpaired *t* test).

Table 5: Spontaneous synaptic event properties of GCs

	sGC	dGC	*P* value
sEPSP			
Frequency (Hz)	7.4 ± 3.0 (21)	6.6 ± 2.0 (8)	0.45 (n.s.)
Amplitude (pA)	1.2 ± 0.5 (21)	0.9 ± 0.3 (8)	0.09 (n.s.)
$Rise_{20\text{-}80\%}$ *(ms)*	2.7 ± 0.6 (21)	2.6 ± 0.3 (8)	0.86 (n.s.)
τ_{decay} *(ms)*	19.4 ± 3.9 (21)	26.4 ± 15.8 (8)	0.066 (n.s.)
sEPSC			
Frequency (Hz)	4.2 ± 4.2 (26)	4.0 ± 4.8 (10)	0.87 (n.s.)
Amplitude (pA)	–18.0 ± 7.1 (26)	–14.8 ± 7.1 (10)	0.24 (n.s.)
$Rise_{10\text{-}90\%}$ *(ms)*	1.0 ± 0.2 (26)	1.2 ± 0.4 (10)	0.035 *
τ_{decay} *(ms)*	7.1 ± 4.0 (26)	6.9 ± 3.3 (10)	0.97 (n.s.)
sIPSC			
Frequency (Hz)	1.6 ± 1.4 (26)	1.1 ± 0.7 (10)	0.28 (n.s.)
Amplitude (pA)	25.8 ± 11.6 (26)	21.8 ± 7.3 (10)	0.32 (n.s.)
$Rise_{10\text{-}90\%}$ *(ms)*	1.4 ± 0.7 (26)	1.7 ± 0.7 (10)	0.29 (n.s.)
τ_{decay} *(ms)*	19.6 ± 8.5 (26)	20.9 ± 7.3 (10)	0.67 (n.s.)

Values reported are mean ± standard deviation (*n*). *p<0.05; n.s., not significant (two-tailed unpaired *t* test).

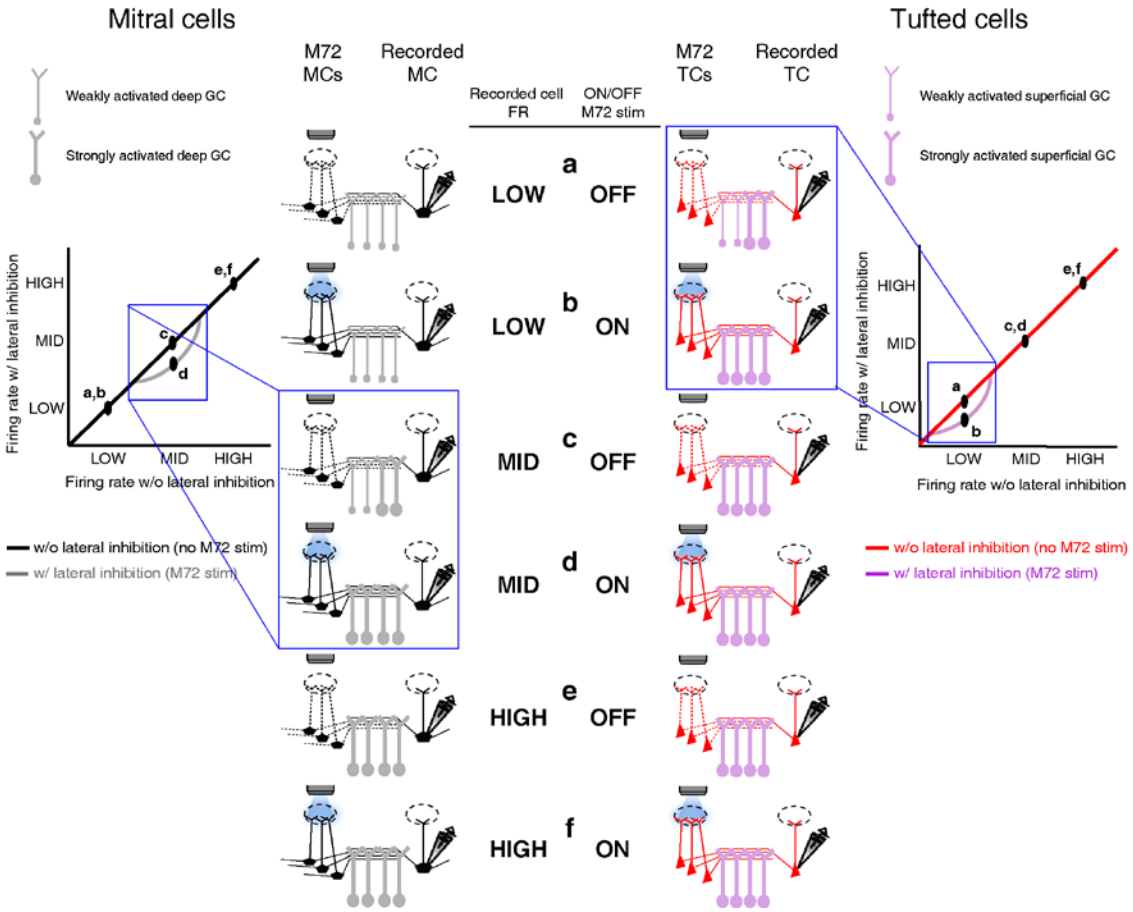

Figure 26: Proposed mechanism of ADLI in mitral (MCs) and tufted cells (TCs).

(**a-f**) Schematics of the levels of activity in the olfactory bulb circuit consisting of M72 M/TCs (presynaptic M/TCs) and the recorded M/TCs (postsynaptic M/TCs) and the associated GCs.

ACTIVITY-DEPENDENT LATERAL INHIBITION IN MCS (LEFT PANELS):
LOW RATES (**a,b**): When the recorded MC is unstimulated or firing at low rates, no additional GCs are recruited during the photostimulation of the M72 glomerulus, so no lateral inhibition is evoked. INTERMEDIATE RATES (**c,d**): When the recorded MC is firing at intermediate firing rates, additional GCs are activated during the photostimulation of the M72 glomerulus and generate lateral inhibition. HIGH RATES (**e,f**): When the recorded MC is firing at high firing rates, all shared GCs are maximally recruited so that M72 photostimulation is unable to activate any additional GCs or generate additional lateral inhibition.

ACTIVITY-DEPENDENT LATERAL INHIBITION IN TCS (RIGHT PANELS):
LOW RATES (**a,b**): When the recorded TC is firing at low firing rates, additional GCs are activated selectively during the photostimulation of the M72 glomerulus and generate lateral inhibition. INTERMEDIATE AND HIGH RATES (**c,d,e,f**): When the recorded TC is firing at intermediate or high firing rates, all shared GCs are maximally recruited so that M72 photostimulation is unable to activate any additional GCs or generate lateral inhibition.

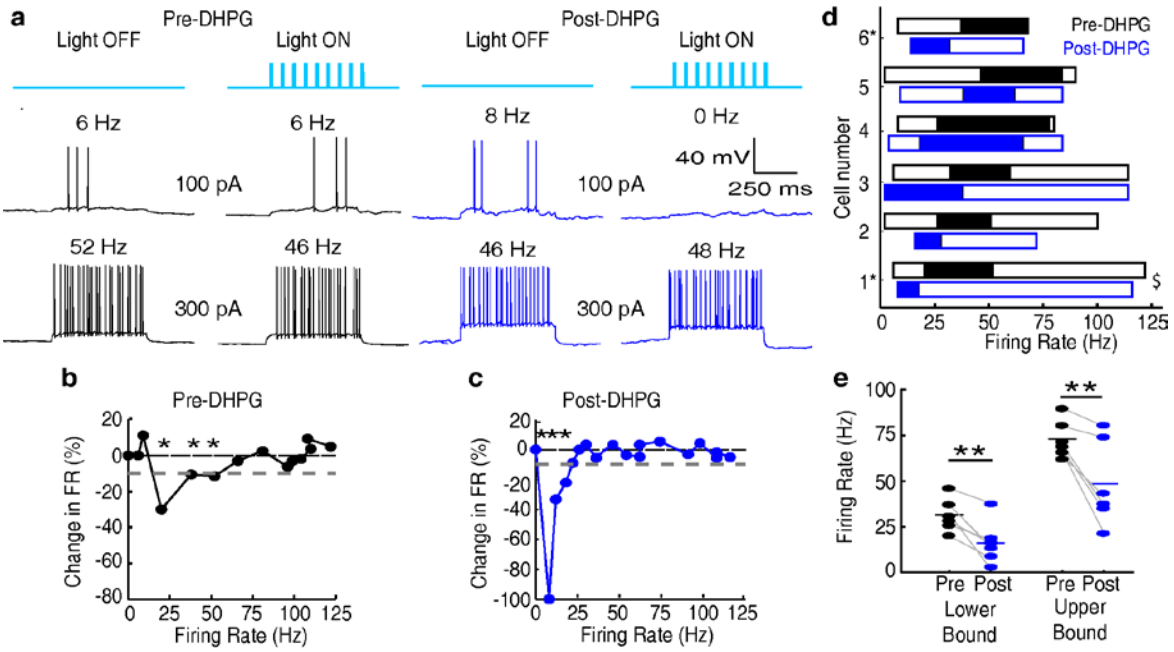

Figure 27: Increasing GC excitability shifts the effective activity range of lateral inhibition in MCs to lower frequencies.

(**a-c**) Example of lateral inhibition in one example MC before and after bath applying mGluR agonist, DHPG (10 µM). (**a**) Example voltage traces from one MC. LEFT: Before application of DHPG, intermediate firing rates are affected by lateral inhibition. RIGHT: After application of DHPG, low firing rates are affected. (**b-c**) The effect of lateral inhibition is illustrated by comparing the FI curves for the light off versus light on trials in a MC before (**b**) and after (**c**) applying DHPG. Plot of the percent decrease in firing rate vs. the firing rate of light off trials. Dotted line in **b,c** represents the 10% threshold used to indicate significant inhibition. Asterisks signify firing rates which are reduced by more than 10% in light on trials. (**d**) Summary of 6 cells recorded before (black) and after (blue) bath application of DHPG ($ - cell depicted in **a-c**). (**e**) The lower (LEFT, paired t-test, p=0.009) and upper bound (RIGHT, paired t-test, p=0.009) of the effective activity range of lateral inhibition are significantly lower after application of DHPG.

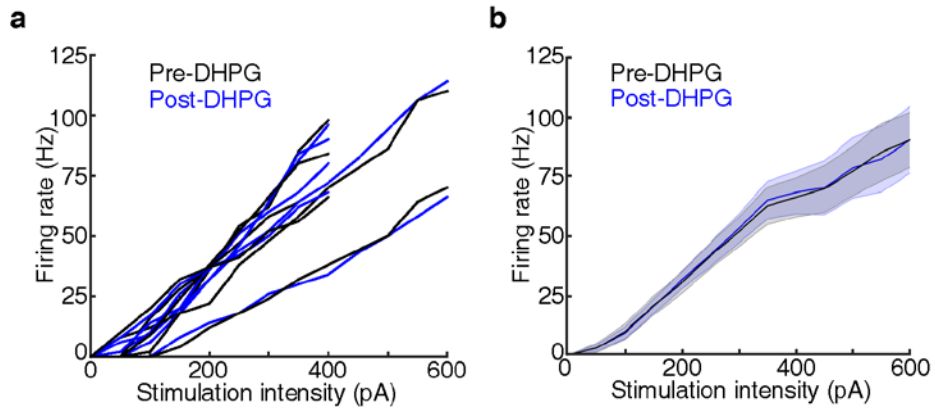

Figure 28: DHPG has no effect on MC excitability.

Data is taken from the LIGHT OFF trials in the MCs recorded in Figure 27 before and after adding 10 μM DHPG. (**a**) MC input-output curves in response to 500 ms somatic current injections of increasing amplitudes before and after bath application of DHPG (n=6 MCs). (**b**) Average Pre-DHPG and Post-DHPG FI curves across 6 MCs indicate that DHPG has no effect on MC excitability (p=0.77; 2-way ANOVA). Shaded regions show mean ± SEM.

3.3.4 Differences in lateral inhibition between MCs and TCs translate into differences in stimulus encoding

Together these data suggest that distinct odor-evoked activity observed in MCs and TCs *in vivo* arises, in part, due to differences in how ADLI affects each cell type (Figure 26). To begin assessing how these circuit-level differences between MCs and TCs impact their ability to encode olfactory information, we performed simulations of MC and TC networks to determine how differences in ADLI may translate into differences in stimulus encoding.

We simulated an olfactory discrimination task in which a presented odor must be identified from a panel of similar odors. Because the goal of the simulations was to understand how the differences in MC and TC circuit properties described above influence population coding, we used simple firing rate models in which we could directly and independently modify lateral inhibition properties without changing other model features. We therefore made relatively few assumptions in performing our simulations, mostly relating to how odor concentration is encoded (as firing rate differences(Cang and Isaacson 2003, Fukunaga, Berning et al. 2012, Igarashi, Ieki et al. 2012, Sirotin, Shusterman et al. 2015) – however see (Meredith 1986)), how lateral inhibitory connectivity is specified (randomly), and how MCs and TCs differ (which was explicitly explored). Each odor was simulated as a pattern of inputs to populations of MCs or TCs, corresponding to activated glomeruli (Figure 29**a,b;** Figure 30**).** Differences in odor concentration were modeled as changes in the number and intensity of activated glomeruli(Rubin and Katz 1999, Meister and Bonhoeffer 2001) (see **Methods**). Additionally, we added trial-to-trial variability in each presentation of a particular odor (Figure 29**b**, see **Methods**) in order to mimic natural fluctuations in the background odors and in the patterns of odor-evoked glomerular activation(Wachowiak, Denk et al. 2004).

In our simulations, we asked how well MC and TC population activity discriminated between similar odors presented at the same odor concentration. While understanding how animals discriminate between odors presented at a variety of concentrations is important, we confined our discriminations to odors presented at the same concentration to more closely match behavioral experiments in mice(Abraham, Egger et al. 2010, Lepousez and Lledo 2013) and to keep from making a number of assumptions about how the representation of individual odors varies with concentration. In this simulation, each MC or TC received excitatory input from one of the 150 glomeruli. On each trial, we randomly presented one odor from the panel to networks comprised entirely of either MCs or TCs. We applied a common decoding algorithm, linear discriminant analysis, to determine the extent to which different odors were discriminable in our simulated MC and TC populations (Figure 29**c**). While the strategy that downstream brain areas use to decode information contained in MC and TC outputs is unknown, linear discriminant analysis is a simple classification algorithm, has some degree of biological plausibility and has been widely applied in similar contexts(Quiroga, Reddy et al. 2007, Quian Quiroga and Panzeri 2009, Giridhar, Doiron et al. 2011).

We first compared the discrimination accuracy of three models: one in which ADLI affected low rates (i.e. an all TC network), one in which ADLI affected intermediate rates (i.e. an all MC network), and a control population that lacked any inhibition. ADLI was modeled by explicitly adjusting the sensitivity of MC and TC firing rates to inhibition without changing other parameters of the model (Figure 29**d-e**). When the odor panel consisted of only 8 odors, both MC and TC populations discriminated between odors with an accuracy that did not differ from the control population that lacked inhibition (Figure 29**f**). However, when we increased the difficulty of the task by increasing the size of the odor panel (to 32 odors), the difference in

accuracy between MCs and TCs dramatically increased (Figure 29**g**). For the set of 32 odors, TCs significantly outperformed MCs and the control population at low odor concentrations (90% accuracy in TCs compared to 70% accuracy in MCs at 30% of maximum concentration) while MCs significantly outperformed TCs and the control population at high concentrations (73% accuracy in TCs compared to 91% accuracy in MCs at 60% of maximum concentration). Therefore, differences in ADLI alone support concentration-dependent differences in odor discrimination.

Next we tested how well different forms of activity-independent inhibition compare to ADLI in their ability to improve discrimination accuracy. Specifically, we compared discrimination accuracy (in panels consisting of 32 odors) between 3 populations of neurons; one with subtractive inhibition (Figure 31**a**), one with divisive inhibition (Figure 31**b**) and a control population that lacked inhibition. We found that populations using subtractive or divisive inhibition performed no better than the control population across all concentrations (Figure 31**c**). These results agree with prior work that showed that ADLI substantially decorrelates MC responses to similar odors while subtractive and divisive forms of lateral inhibition have little effect on MC correlation(Arevian, Kapoor et al. 2008).

Prior work has shown that, in addition to ADLI differences, TCs are more intrinsically excitable(Burton and Urban 2014) and receive stronger OSN inputs than MCs(Gire, Franks et al. 2012, Burton and Urban 2014). Therefore, we next asked how well these differences between MCs and TCs affect odor discrimination. Differences in the strength of OSN input and intrinsic excitability were modeled by altering sigmoid functions that relate the intensity of glomerular inputs to M/TC outputs (Figure 29**h**). These differences in MC vs. TC excitability and OSN input strength also allow TCs and MCs to discriminate odors best at low and high concentrations

respectively (Figure 29**i**). Finally we simulated how all three differences between MCs and TCs – ADLI, intrinsic excitability and glomerular input –affected odor concentration. Intriguingly, TCs were best at discriminating between low concentration odors when all three differences were included in the model (Figure 29**j**). Together, these simulations show that intrinsic and circuit-level differences between MCs and TCs work cooperatively to optimize discrimination between similar odors in separate concentration ranges.

Finally, we asked more generally how sensory systems, including the olfactory system, might benefit from splitting information into multiple channels with distinct ADLI. First, we asked whether models containing a combination of MCs and TCs discriminate odors better than models that have only MCs or TCs. We used a variant of the models presented above: here, each glomerulus provided input to 2 neurons instead of 1. We compared three different output neuron configurations: 2 MCs per glomerulus, 2 TCs per glomerulus, and 1 MC and 1 TC per glomerulus (Figure 29**k,** see **Methods**). Similar to the data presented in Figure 29**g**, TC models discriminated between 32 odors best at low concentrations and MC models were best at high concentrations (Figure 29**l**). However, MC-TC models significantly outperformed other models at intervening odor concentrations. Interestingly, MC-TC models also exhibited the second best performance at high and low concentrations, and after averaging discrimination accuracy across all concentrations tested, we found that models containing a combination of MCs and TCs performed significantly better than models composed of only MCs or only TCs (Figure 29**m**). Second, new features might arise in any brain area that implements ADLI and splits information into parallel channels. Using an image processing analogy, we show that if an image is split into parallel channels and then recombined by a downstream population, new information about the image (i.e. higher contrast), absent in either single channel, emerges (Figure 32). Therefore

systems that split sensory information into multiple pathways can not only outperform single pathway systems at comparable tasks, but are also capable of performing novel computations unlikely to occur in single pathway systems.

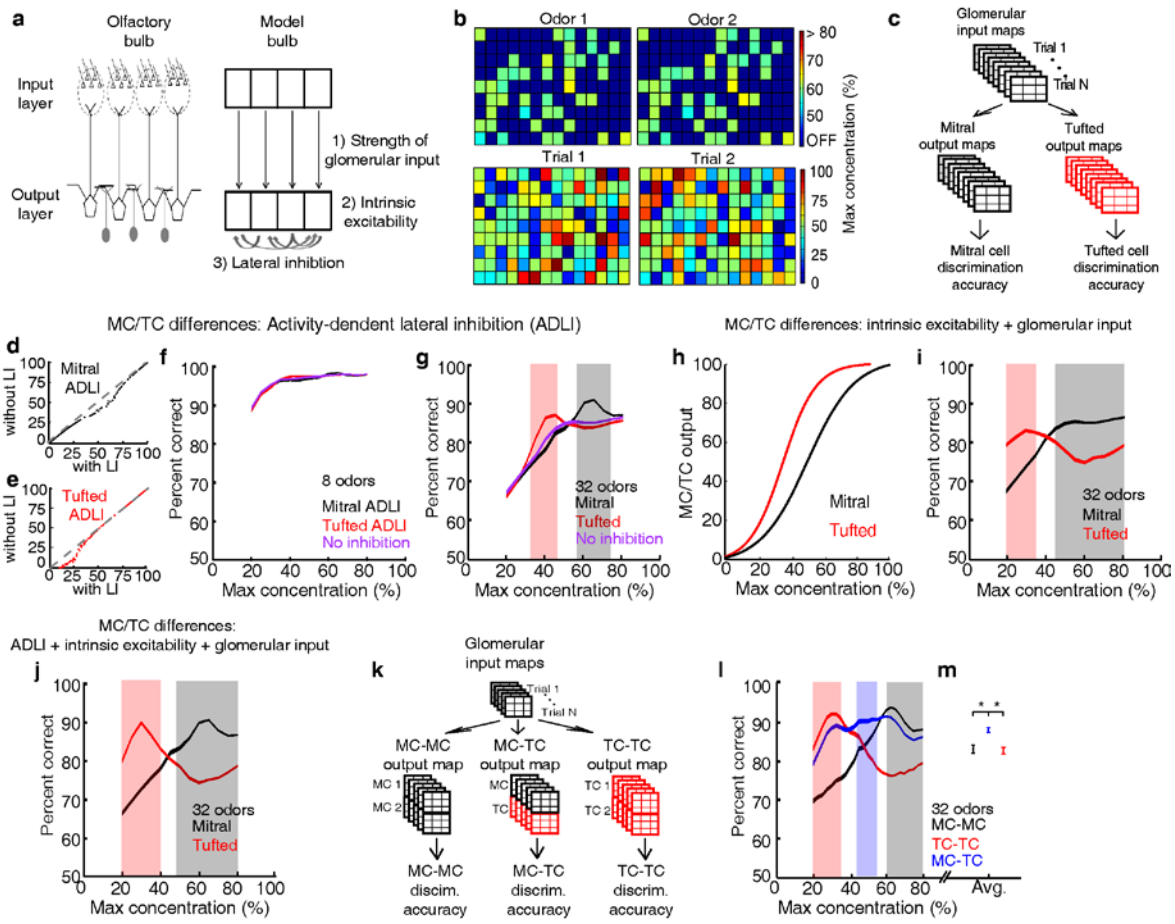

Figure 29: MCs and TCs discriminate between odors best in separate concentration ranges.

(**a**) Odors are defined as the pattern of activated glomeruli (i.e. pixels) in the model. Each glomerulus provides input to only 1 MC/TC. (**b**) TOP: Pattern of activated glomeruli for 2 odors. BOTTOM: Two separate presentations of Odor 1. (**c**) Outputs of MCs or TCs are used to train and test a linear classifier to predict which odors are presented on each trial. (**d-e**) Lateral inhibition differences between MCs and TCs are modeled using Gaussian distributions centered at different firing rates. Firing rates of MCs (**d**) and TCs (**e**) with and without lateral inhibition. (**f-g**) Discrimination accuracy of 8 (**f**) and 32 (**g**) odors in MCs (black), TCs (red) and a control population of neurons that lacked any inhibition (purple). Shaded areas represent concentration ranges where TCs (light red) or MCs (grey) discriminate significantly better (see **Online Methods**). (**h**) Differences in the strength of excitatory inputs and intrinsic excitability between MCs and TCs are modeled using 2 sigmoids to translate glomerular inputs into MC/TC outputs. (**i**) Discrimination accuracy of 32 odors in MCs (black) and TCs (red) that differ in excitability, strength of glomerular input. (**j**) Discrimination accuracy of 32 odors in MCs (black) and TCs (red) that differ in excitability, strength of glomerular input and ADLI. (**k**) Overview of simulations comparing 3 separate output neuron configurations: 2 MCs per glomerulus, 2 TCs per glomerulus or 1 MC and 1TC per glomerulus. (**l**) Discrimination accuracy of 32 odors for MC-MC (black), TC-TC (red) or MC-TC (blue) networks across a range of concentrations. (**m**) Average discrimination accuracy across all concentrations plotted in **l** (* p<1e-4). Width of plots in panels **f,g,i,j,I** reflect the s.e.m.

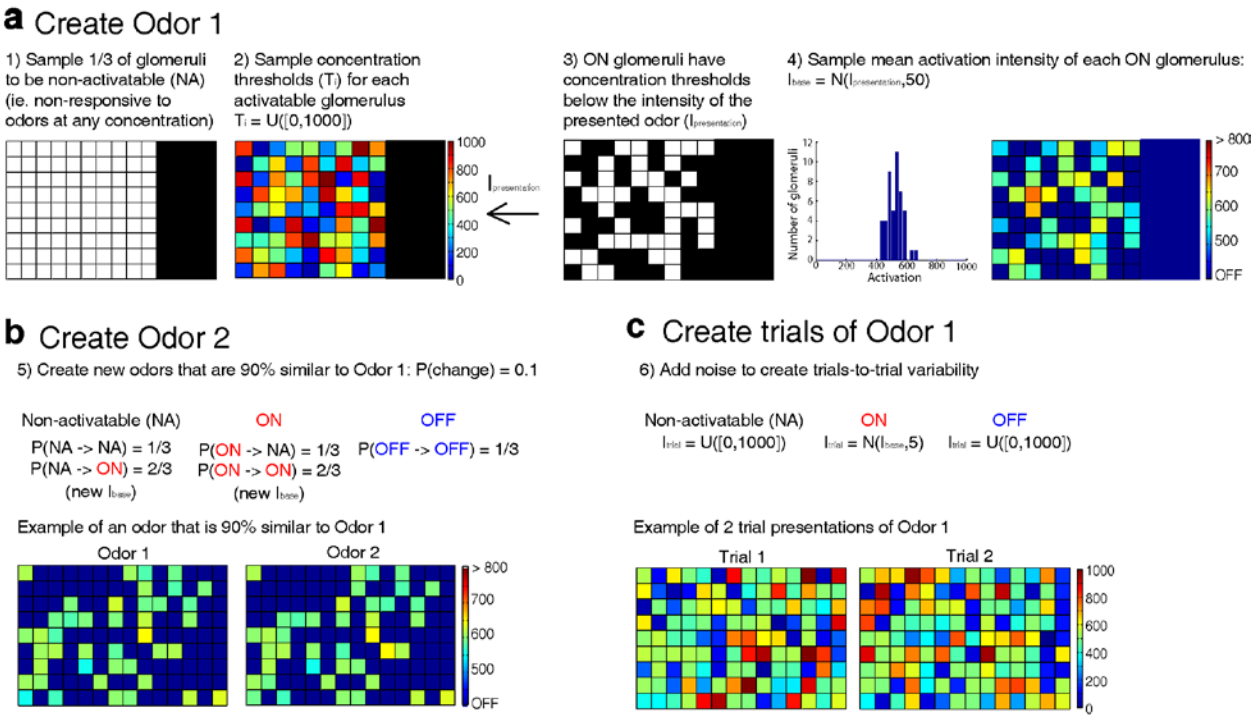

Figure 30: Procedure used to create the odors that served as inputs to simulated mitral and tufted cell networks.

(**a**) The first step in the procedure is the creation of a single odor at a set concentration using the rules outlined in **a**. The odor is defined by a random set of pixels (ON pixels) that will be reliably activated at a set concentration on each presentation of the odor. Pixels that are not ON for a particular odor are either non-activatable (ie not responsive to odors at any concentration) or OFF pixels. This procedure ensures that differences in odor concentration reflect changes in both the number and intensity of activated glomeruli. (**b**) Once a single odor is defined, the rest of the odors in the panel can be created using the rules in **b**. This procedure creates an arbitrary number of odors that are 90% similar to the first odor. Additionally, we ensure that no two odors are identical. (**c**) Lastly the OFF and non-activatable (NA) pixels are sampled randomly from the uniform distribution each time the odor is presented to the MC or TC network in order to add trial-to-trial variability and to mimic the variability in background odor each time an odor is experienced.

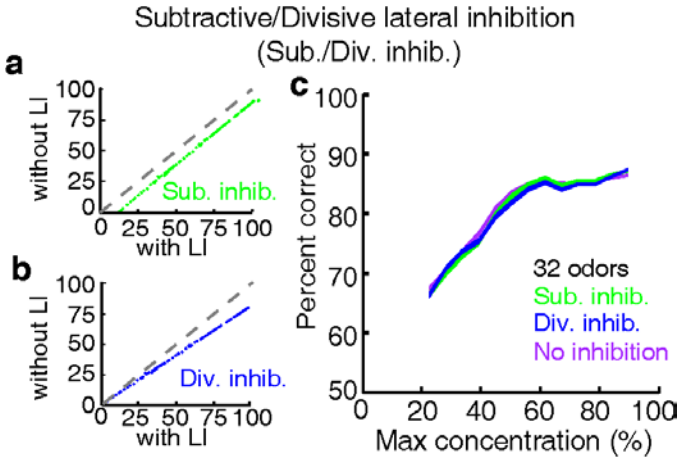

Figure 31: Subtractive or divisive lateral inhibition does not improve discrimination accuracy.

(**a**-**b**) Neural firing rates with and without subtractive (**a**) or divisive (**b**) lateral inhibition. (**c**) Discrimination accuracy of 32 odors in neurons with subtractive (green), divisive (blue) or no inhibition (purple). Width of plots in **c** reflect s.e.m.

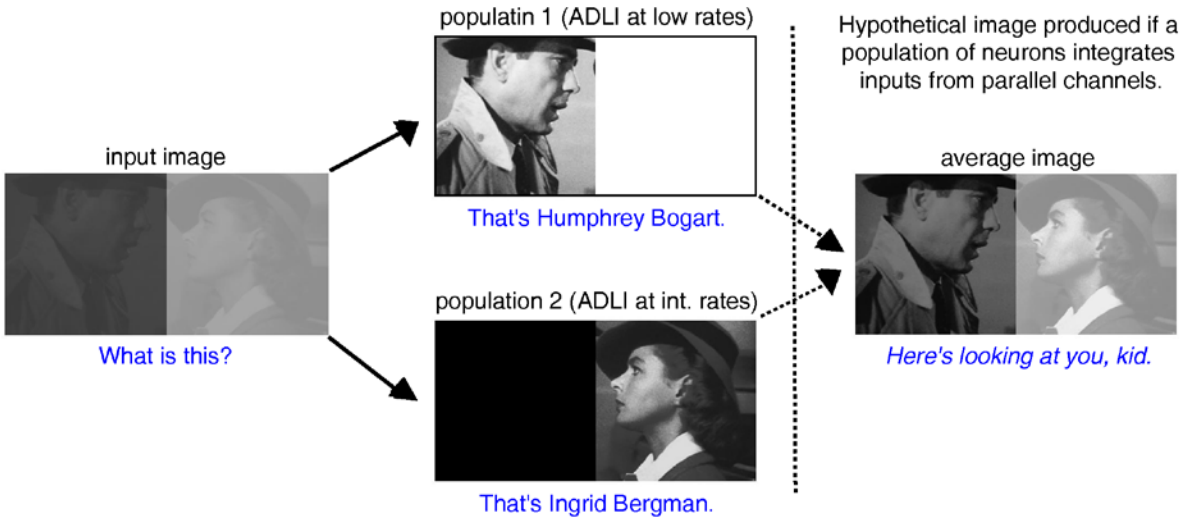

Figure 32: Visual processing example of how the multiple parallel neuron populations can simultaneously enhance the contrast of high and low intensity images.

Digital image before (input image, left) and after processing by two separate populations. One population employs ADLI at low rates (top) and enhances contrast at low intensities. The second employs ADLI at intermediate rates (bottom) and enhances contrast at high intensities. Each image encodes distinct aspects of the input image (who is in the image?), but the overall context of the image remains ambiguous (who is each character talking to?). If a downstream population of neurons integrates inputs from both populations and performs a simple averaging computation (right), then the full context of the image can be perceived (This is a famous scene from the movie, *Casablanca*).

3.4 DISCUSSION

Parallel pathways are a common feature of many sensory systems. Yet how local-circuit activity creates stimulus selectivity in parallel pathways remains poorly understood. Here, we have identified a novel circuit mechanism for generating differential responses across two parallel pathways (formed by MCs and TCs) in the olfactory system and examined the emergence of feature selectivity. We find that differences in ADLI selectively reduce intermediate firing rates in MCs and low firing rates in TCs. We provide evidence that this difference is caused by differences in the excitability of subclasses of GCs that preferentially inhibit TCs vs. MCs. Moreover, using simulations, we show that differences in the effective activity range of lateral inhibition, along with other intrinsic and circuit-level differences between MCs and TCs, work cooperatively to enable MCs and TCs to best discriminate between similar odors in separate concentration ranges. Finally, we show that the combination of MCs and TCs facilitates odor discrimination across a wide range of odor concentrations.

The activity-dependence of lateral inhibition depends on three cell populations – the "presynaptic" M/TCs associated with the M72 glomerulus (which we activate optogenetically via stimulation of OSNs), the inhibitory interneurons and the "postsynaptic" M/TCs. Our prior work has shown that increasing the firing rate of presynaptic MCs (the M72 MCs in this case) shifts the range of MC firing rates influenced by lateral inhibition(Arevian, Kapoor et al. 2008). Given that TCs fire at higher rates than MCs following glomerular activation(Burton and Urban 2014), M72 TCs will fire at higher rates than M72 MCs following M72 photoactivation and, in part, contribute to the decreased lower bound of the effective activity range of lateral inhibition in postsynaptic TCs. However, higher firing rates in M72 TCs alone is insufficient to explain the

differences in both the lower and upper bound in the effective activity range of lateral inhibition between MCs and TCs.

Our analysis supports the hypothesis that TCs and MCs are preferentially connected to dGCs and sGCs respectively. sGCs spike with a higher probability than dGCs following the activation of a single glomerulus. Consequently, postsynaptic TCs can effectively recruit lateral inhibition when firing at low rates. dGCs are less excitable and therefore require more input to be activated. Therefore M72 photostimulation alone causes relatively weak activation of dGCs. However, when the postsynaptic MC fires at intermediate rates, additional dGCs will become activated and mediate lateral inhibition. In support of this mechanism, we show that increasing the excitability of GCs by activating mGluRs(Dong, Hayar et al. 2007, Heinbockel, Laaris et al. 2007) shifts the effective activity range of lateral inhibition in MCs to lower firing rates (Figure 27). Additionally, these differences between sGCs and dGCs explain why the upper bound on the effective activity range of lateral inhibition differs between MCs and TCs. Cells firing above this upper bound recruit the maximum amount of recurrent inhibition such that additional inputs to GCs cannot trigger additional GABA release(Urban and Arevian 2009). Because sGCs are more excitable than dGCs, maximal GABA release, and consequently the upper bound on the effective activity range of lateral inhibition, occurs at lower rates in TCs than in MCs (Figure 26).

While preferential connectivity of TCs with sGCs and MCs with dGCs can explain the observed differences in the activity-dependence of lateral inhibition, other circuit mechanisms may also contribute. In particular, EPL interneurons (EPL-INs) can mediate inhibition onto M/TCs(Huang, Garcia et al. 2013, Kato, Gillet et al. 2013, Miyamichi, Shlomai-Fuchs et al. 2013), and it remains possible that EPL-INs or distinct subclasses of EPL-INs preferentially

inhibit MCs or TCs. However, it is unlikely that EPL-INs predominantly drive the difference in MC vs. TC ADLI given that EPL-INs mediate linear (divisive) but not activity-dependent inhibition of MC/TC outputs(Kato, Gillet et al. 2013, Uchida, Eshel et al. 2013). Glomerular layer circuits have also been shown to play a role in M/TC lateral inhibition(Aungst, Heyward et al. 2003, Liu, Plachez et al. 2013, Whitesell, Sorensen et al. 2013, Banerjee, Marbach et al. 2015), however these circuits likely do not play a role in the differences in ADLI reported here because our results were not influenced by apical dendrite truncation. Therefore, distinct GC populations that differ in excitability are the most parsimonious explanation for the observed differences in ADLI.

Differential connectivity of MCs and TCs with distinct GC subclasses has long been predicted based on the putative morphological subdivisions of GC apical dendritic morphologies(Mori, Kishi et al. 1983, Orona, Scott et al. 1983) and separation of MC and TC lateral dendrites in the deep and superficial EPL(Mori, Kishi et al. 1983, Orona, Rainer et al. 1984), respectively. However, extensive M/TC-GC connectivity along exceedingly long M/TC lateral dendrites has, thus far, precluded a direct demonstration of differential connectivity of MCs and TCs with distinct GC subclasses. Here, we provide quantitative evidence that GCs indeed form two distinct morphological subclasses – sGCs and dGCs – rather than a continuum of morphologies. Moreover, our results provide – to our knowledge – the first functional evidence that MCs and TCs engage distinct lateral inhibitory circuits, likely via differential connectivity with dGCs and sGCs, respectively. Future experiments involving selective manipulation of MCs vs. TCs and dGCs vs. sGCs will ultimately be needed in order to directly demonstrate whether (and the degree to which) these lateral inhibitory circuits overlap.

Our data describe local, circuit-level mechanisms that can account for several differences between MC and TC odor-evoked responses observed *in vivo*. Weaker lateral inhibitory currents may contribute to the finding that TCs are less frequently inhibited by odors(Nagayama, Takahashi et al. 2004). Additionally, the finding that intermediate and high firing rates are unaffected by lateral inhibition in TCs may help explain why TCs show odor-evoked responses that are more highly correlated to OSN input(Adam, Livneh et al. 2014) and less dependent on concentration (Fukunaga, Berning et al. 2012, Igarashi, Ieki et al. 2012). Additionally, TCs firing above the upper bound of the effective activity range of lateral inhibition are shielded, not only from lateral inhibition, but other sources of GC-mediated inhibition as well, such as inhibition triggered by cortical feedback(Boyd, Sturgill et al. 2012, Markopoulos, Rokni et al. 2012), Consequently, the circuit-level differences we describe may explain why MCs but not TCs are decorrelated by cortical feedback(Otazu, Chae et al. 2015).

These circuit-level differences between MCs and TCs likely affect olfactory discrimination (Figure 29). ADLI, but not subtractive or divisive inhibition, allows TCs and MCs to best discriminate between odors at low and high concentrations, respectively. Yet how does this improvement in discrimination occur? Prior work has shown that activity in M/TC populations becomes decorrelated over time(Bathellier, Buhl et al. 2008, Cury and Uchida 2010) and that this decorrelation is driven by GCs(Gschwend, Abraham et al. 2015). Additionally, GC-mediated M/TC decorrelation improves odor discrimination(Gschwend, Abraham et al. 2015). Consequently, ADLI likely improves odor discrimination by driving decorrelation of M/TC firing in ranges that engage lateral inhibition(Arevian, Kapoor et al. 2008). M/TCs firing at rates outside the effective range of lateral inhibition may be encoding complementary olfactory information beyond odor identity.

Performing these experiments in acute slices provides the best opportunity to explore the causes and consequences of differences in lateral inhibition between MCs and TCs. Given the novel features and mechanisms of ADLI, using a reduced and carefully controlled system in which a single glomerulus can be reliably activated is an important first step. Moreover, our *in vitro* approach allowed us to apply pharmacological manipulations that were vital in identifying differences in GC excitability (Figure 24**;** Figure 27) rather than differences in glomerular layer circuitry (Figure 14**e**) as the main mechanism supporting differences in MC vs. TC ADLI.

We note, however, that our *in vitro* approach also has certain limitations. In particular, the slicing procedure may introduce artifacts that could confound our conclusions. Importantly, however, our findings that MCs receive stronger lateral inhibitory currents and are affected at different ranges of firing rates than TCs are unlikely to reflect slicing artifacts. Due to slicing, some MCs and TCs that project to the M72 glomerulus will be truncated, and cells that reside farther from the M72 glomerulus have a higher probability of being truncated. However, our findings do not depend on the cell's distance from the M72 glomerulus (Figure 15; Figure 19). Moreover, the close correspondence of our GC data to previous *in vivo* recordings of odor-evoked GC activity(Wellis and Scott 1990), as well as the equivalent spontaneous synaptic activity – a proxy for circuit intactness – observed between sGCs and dGCs strongly suggests that slicing artifacts cannot explain the differences in excitatory input or intrinsic excitability observed between sGCs and dGCs.

Our *in vitro* approach additionally cannot address multiple important factors that are only present in the intact animal. For instance, respiration and centrifugal feedback likely modulate ADLI *in vivo.* Addressing the extent to which ADLI affects odor-evoked responses in MCs and TCs *in vivo* is thus an important future direction.

Finally, what are the benefits of parallel processing? In other sensory systems, different pathways may arise from functional differences at the initial stages of stimulus detection, which are then maintained through selective feedforward connectivity. In the olfactory system there is no evidence that MCs and TCs are targeted by distinct subsets of OSNs. Rather, we show that differences in bulbar circuitry are sufficient to generate important differences in response properties. Here we show that MCs and TCs perform odor discriminations best at separate concentration ranges and that a combination of MCs and TCs discriminates similar odors better than either population alone. These results suggests that parallel processing may offer similar benefits in other sensory systems in which stimulus intensities can vary over many orders of magnitude. For instance, rods and cones in the retina function best at different ranges of light intensity. Other similarities between the olfactory and visual systems suggest that the mechanisms behind parallel processing may be shared across sensory systems. In the retina, feature selectivity in each ganglion cell type emerges due to its connectivity to specific bipolar and amacrine cell types(Masland 2012). Similarly, differences in odor-evoked responses in MCs and TCs emerge due to differences in connectivity to OSNs, external tufted cells(Najac, De Saint Jan et al. 2011, Gire, Franks et al. 2012) and GCs. Therefore, in these systems, feature selectivity is not inherited but emerges via differential connectivity with distinct neuron types. Similarly, recombining the specific features encoded in individual channels allows new features to emerge. For instance, if populations of neurons in higher order sensory areas integrate inputs from parallel sensory channels, such as the anterior piriform cortex(Nagayama, Enerva et al. 2010, Igarashi, Ieki et al. 2012), and perform simple computations, such as averaging, new features may emerge (Figure 32). More complex integration mechanisms may allow the calculation of

other complex stimulus features using the different information encoded in multiple parallel sensory channels.

4.0 GENERAL DISCUSSION

4.1 SUMMARY OF FINDINGS

In multiple sensory systems, separate neuron types encode distinct features of sensory stimuli. Yet, olfaction has historically been viewed differently: mitral and tufted cells have been thought to play identical roles in odor coding. This view has prevailed despite clear differences in their dendritic and axonal projection patterns. Recently, however, several studies have identified functional differences between MCs and TCs that suggest that the olfactory system segregates olfactory information into parallel pathways, much like in other sensory systems. How circuits in these parallel pathways are composed to maintain or even enhance the coding of specific stimulus features is poorly understood. This question is particularly interesting in the olfactory system because the distinct outputs of MCs and TCs are generated from initially homogeneous sources and so must consequently arise from differences in connectivity with local circuitry. In this thesis, we explored which aspects of the olfactory bulb circuit differ between MCs and TCs to allow them to encode distinct aspects of olfactory information.

Chapter 2 describes differences in feed-forward circuitry onto MCs and TCs. Recent work from other labs has explored differences in how the latency of odor-evoked responses differs between MCs and TCs because response latency has the potential to encode behaviorally relevant information. TCs respond to odors hundreds of milliseconds earlier in the sniff cycle

and show more concentration invariant odor-evoked responses than MCs. These studies suggest that MCs may use spike latency to encode concentration-specific information while TCs may encode concentration-independent information. In light of these emerging differences in the latency of MC and TC responses, determining the circuit-level mechanisms that drive these differences is critical.

We find that MCs display longer latency spiking that is more strongly dependent on stimulus intensity than TCs. Long latency spiking in MCs is a consequence of weaker excitatory and stronger inhibitory currents onto MCs compared to TCs. Stronger inhibitory currents onto MCs are PGC-mediated, so that blocking PGC-mediated, but not GC-mediated, inhibition leads to more reliable and shorter latency responses in MCs, but not TCs. These data suggest that differences in PGC-mediated inhibition, along with differences in intrinsic excitability and excitatory input, work cooperatively to allow TCs to respond to OSN stimulation earlier than MCs.

Chapter 3 describes the causes and consequences of lateral inhibition differences between MCs and TCs. Throughout the brain, lateral inhibitory circuits enhance contrast and facilitate discrimination by decorrelating neural responses. In the olfactory bulb, one type of lateral inhibition occurs between pairs of MCs and TCs via reciprocal dendrodendritic synapses with inhibitory granule cells. Prior work has shown that lateral inhibition most strongly affects MCs firing at intermediate rates because coincident input is required for the activation of GCs. This activity-dependent regulation of the strength of lateral inhibition onto MCs decorrelates MCs responses to similar stimuli more effectively than other forms of inhibition. However, the effects of lateral inhibition onto TCs have yet to be explored.

We find that lateral inhibition onto MCs is larger and more asynchronous than onto TCs.

Additionally, while MCs are affected by lateral inhibition at intermediate firing rates, TCs are affected when firing at lower firing rates. These differences arise, in part, due to differential recruitment of morphologically distinct classes of GCs by MCs and TCs. Using simulations, we show that these differences in lateral inhibition allow TCs and MCs to perform odor discriminations best in separate concentration ranges. Additionally, the combination of both MCs and TCs encodes odors better than either population alone and supports novel computations that are unlikely to occur with a single cell type.

Finally, in Appendix A, we provide a preliminary study of how early postnatal odor exposure affects lateral inhibition onto MCs and TCs. Lateral inhibition is modulated by a variety of inhibitory interneuron subtypes that include superficial short axon cells, external plexiform layer interneurons and granule cells. These circuits influence MC/TC activity in a variety of ways that include controlling gain, decorrelating odor representations, modulating spike timing and synchronizing gamma frequency oscillations. Whether activity-dependent changes in interneurons leads to changes in inter-glomerular lateral inhibition onto MCs and TCs is unknown.

We show that postnatal odor exposure to the M72 ligand, acetophenone, increases the strength of M72-mediated lateral inhibition onto TCs, but not MCs. This differential influence of postnatal odor exposure on TCs is specific to M72 ligands, as TCs from mice exposed to hexanal, a non M72 ligand, did not show increases in the strength of M72-mediated lateral inhibition. Additionally, neither sIPSC frequency nor amplitude were altered by acetophenone or hexanal exposure, indicating that increases in M72-mediated lateral inhibition cannot be explained by increases in the total amount of inhibition onto the recorded MC/TC.

Together, the experiments described here suggest that differences in odor-evoked

responses between MCs and TCs are a consequence of distinct patterns of connectivity to multiple populations of inhibitory interneurons.

What's next? Rather than reiterating the discussion points mentioned in the above chapters, the remainder of the dissertation will look forward. Based on the results presented here, what are the next sets of experiments? Several potential avenues for future work are explored below.

4.2 FINDING BETTER MARKERS FOR MCS AND TCS

The most interesting next steps involve studying whether MCs and TCs control different behaviors. However, in order to perform these experiments, another issue must be addressed. How can the activity of MCs or TCs be manipulated selectively? Currently, this level of selectivity can only be achieved by using genetically engineered lines of mice that express cre recombinase in specific neuron types defined by their molecular identity (Luo, Callaway et al. 2008, Taniguchi, He et al. 2011). Therefore, finding molecules that are selectively expressed in either MCs or TCs is vital.

The neuropeptide cholecystokinin (CCK) is predominately expressed in TCs, but not MC (Seroogy, Brecha et al. 1985, Cheetham, Grier et al. 2015), making the CCK-IRES-Cre line (Taniguchi, He et al. 2011) an excellent candidate to enable reporter expression selectively in TCs. Recently, a study reported that bulk injection of Cre-dependent virus into the olfactory bulb of neonatal CCK-IRES-Cre mice led to specific expression of either fluorescent reporters or calcium indicator in TCs (Cheetham, Grier et al. 2015).

Finding a marker for MCs has proven more difficult. The best available method for

specific labeling of MCs involves retrograde labeling approaches in which Cre-dependent viruses are injected into posterior piriform cortex or cortical amygdala of PCdh21-cre mice (Rothermel, Brunert et al. 2013).

How to find a better marker for MCs? One general approach involves obtaining RNA isolated from either MCs or TCs and performing transcriptome profiling by microarray. MC and TC RNA can be isolated with two different approaches. One involves laser capture microdissection (Emmert-Buck, Bonner et al. 1996, Bonner, Emmert-Buck et al. 1997), which involves dissecting tens to hundreds of individual TCs and MCs from frozen sections. An alternative approach would be to fluorescently label TCs in CCK+ mice and MCs in PCdh21+ mice (using the retrograde labeling approach described above). Once these cells are labeled in two cohorts of mice, fluorescent activated cell sorting would isolate fluorescent labeled cells(Guez-Barber, Fanous et al. 2012). Once TC- and MC-enriched populations have been obtained, RNA could be isolated and transcriptome profiling performed. Once specific transcripts that are differentially expressed between MCs and TCs are identified, further work could determine whether Cre-dependent driver lines exist.

In addition to finding potential markers to differentially target MCs and TCs, this rich data set has the potential to identify other genes that are differentially expressed between MCs and TCs. For instance, MCs and TCs have different biophysical properties (Burton and Urban 2014), and understanding the differential expression on ion channels between them would provide important insights into the molecular mechanisms that create their distinct intrinsic properties.

These approaches can also be used to find markers to target the anatomically distinct subpopulations of GCs described in Chapter 3. Superficial and deep GCs preferentially target

MCs and TCs, and because superficial GCs are more easily activated by glomerular stimulation compared with deep GCs, TCs are affected by lateral inhibition at lower firing rates than MCs. Given these partially segregated circuits, finding other differences between superficial and deep GCs may lead to further insights into the distinct features encoded by MCs and TCs.

4.3 DO MCS AND TCS MEDIATE DIFFERENT BEHAVIORS?

Testing the particular roles of MCs and TCs on behavior will involve performing the same olfactory-guided behavior with and without a particular cell type. Functionally removing a cell from the circuit during behavior is now routine due to the rise of optogenetics (Gradinaru, Thompson et al. 2008, Alivisatos, Andrews et al. 2013, Deisseroth and Schnitzer 2013, Flytzanis, Bedbrook et al. 2014) and DREADDS (designer receptors exclusively activated by designer drugs)(English and Roth 2015, Urban and Roth 2015, Vardy, Robinson et al. 2015). The exact conditions of the experiment will dictate which of these two strategies will be more feasible. For instance, if the task uses natural odors to evoke behaviors, then, all cells of a particular type would need to be silenced. In this case, DREADDS provide the best strategy.

A different strategy would involve expressing channel-rhodopsin2 in a type of OSN (i.e., the M72-ChR2:EYFP mice used in this dissertation) and an inhibitory opsin (halorhodopsin(Gradinaru, Thompson et al. 2008) or archaerhodopsin(Flytzanis, Bedbrook et al. 2014)) in either MCs or TCs. This setup can be obtained by crossing the M72-ChR2:EYFP line with a CCK-IRES-Cre line (followed by an injection of a Cre-dependent inhibitory opsin into the olfactory bulb for TCs) or a PCdh21-Cre line (followed by an injection of the inhibitory opsin into the piriform cortex for MCs). This strategy would allow the exploration of behavior with

and without a particular cell type in a trial-to-trial manner.

Now, which behaviors should be tested with these approaches? The work proposed in this dissertation makes several hypotheses about the differential roles of MCs and TCs on behavior: 1) TCs are necessary for tasks that require fast reactions, and MCs are necessary for difficult tasks that require long periods of odor sampling, and 2) TCs mediate olfactory behaviors when odors are present at low concentrations.

The hypothesis that TCs relay a fast yet crude snapshot of the olfactory world that is necessary for fast decisions while MCs relay a more processed picture that is necessary for difficult decisions is not new (Fukunaga, Berning et al. 2012). Indeed, this view is in line with multiple behavioral findings that a speed-accuracy tradeoff exists in olfaction. If animals are trained to perform a task as quickly as possible, they typically make decisions in about 200ms and perform simple odor discriminations well. However, their performance drops for difficult odor discriminations (Uchida and Mainen 2003). In a different task (go/no-go paradigm), mice can be trained to perform difficult odor discriminations with accuracies that are similar to simple discriminations; however, mice require an additional 100ms to sample the odor (Abraham, Spors et al. 2004). A more recent set of experiments corroborates these prior findings of a speed-accuracy tradeoff in olfaction(Rinberg, Koulakov et al. 2006). When animals are forced to sample odors in an alternative forced choice task for a specified amount of time, performance on difficult discriminations is high if sampling periods are long and low if sampling periods are short. When animals were allowed to decide sampling time, animals typically spent similar amounts of time sampling the odor for both simple and difficult discriminations (~275ms). Consequently, behavioral performance on simple discriminations is better than difficult discriminations(Rinberg, Koulakov et al. 2006).

To test the necessity of MCs and TCs on behavior, experiments similar to the ones performed by Rinberg et al. will be vital. As discussed above, DREADDS can be used to block either MCs or TCs and test their role in performing simple and easy odor discriminations. What are specific hypotheses to test? When mice are forced to sample an odor for short periods of time, blocking TCs should reduce performance of both simple and difficult discriminations; however blocking MCs should not affect performance. When mice are forced to sample an odor for longer periods, blocking TCs should not affect either simple or difficult discriminations; however blocking MCs should reduce performance of difficult discriminations. When mice are allowed to choose how long to sample the odor, blocking MCs should not have any effects on performance on either simple or difficult discriminations. However when TCs are blocked, performance should drop for both simple and difficult discriminations. Alternatively, animals may choose to sample odors for longer periods of time when TCs are blocked in order to achieve similar levels of performance.

The experiments performed in this thesis also suggest that TCs are necessary for identifying odors when presented at low concentrations. To test this hypothesis, animals can be trained on a GO/NO-GO task in which animals must discriminate between the odor in mineral oil and mineral oil. The concentration of the odor can be decreased until the animal's performance approaches 50%. The odor detection threshold can be compared before and after blocking either MCs and TCs. Blocking TCs, but not MCs, should increase the minimal concentration necessary for discrimination.

In addition to these experiments in which behavior is assessed before and after silencing MCs or TCs, similar experiments can be performed by stimulating (via ChR2) either superficial or deep GCs. Prior work shows that stimulating both sGCs and dGCs improves the difficult

discriminations and decorrelates MCs(Gschwend, Abraham et al. 2015). Given work in this thesis showing that MCs and TCs are preferentially inhibited by deep and superficial GCs respectively, stimulating superficial or deep GCs should have the opposite behavioral affects as those listed above.

4.4 FEEDBACK FROM THE CORTEX

MCs and TCs send axons to multiple higher-order cortical areas that include the anterior olfactory nucleus (AON), the anterior (APC) and posterior (PPC) piriform cortex, the olfactory tubericle, the tenia tecta, the cortical amygdaloid nucleus and the lateral entorhinal cortex(Spors, Albeanu et al. 2012). Many of these areas also send dense projections back to the olfactory bulb to form a cortical-bulbar loop(Oswald and Urban 2012). Multiple lines of evidence suggest that these feedback projections are important for associative olfactory learning. Coherent beta oscillations between the APC and OB are prominent during associative learning and this long-range beta synchronization is impaired when cortico-bulbar inputs are lesioned(Neville and Haberly 2003). Additionally, stimulating excitatory synapses onto the proximal region of GC apical dendrites (the region where feedback project from cortex form synapses) can trigger LTP(Gao and Strowbridge 2009, Nissant, Bardy et al. 2009). Recent work has shown that the majority of these feedback projections primarily make excitatory synapses onto granule cells of the bulb(Boyd, Sturgill et al. 2012, Markopoulos, Rokni et al. 2012, Oswald and Urban 2012).

MCs and TCs send axons to largely non-overlapping regions – TCs send axons to the anterior olfactory nucleus (AON) and the anterior piriform cortex (APC) while MCs send axons to the posterior piriform cortex (PPC), the cortical amygdaloid nucleus and the lateral entorhinal

cortex (Nagayama, Enerva et al. 2010, Igarashi, Ieki et al. 2012). Data in Chapter 3 suggest that anatomically distinct subclasses of GCs – superficial and deep GCs – preferentially inhibit TCs and MCs. An interesting question, then, is whether segregated feedback loops onto MCs and TCs exist. For instance, TCs, but not MC, project to AON. Do feedback projections from AON preferentially target superficial GCs and not deep GCs – and consequently inhibit TCs, but not MCs? Similarly do projections from the posterior piriform cortex target deep GCs but not superficial GCs – and consequently inhibit MCs, but not TCs.

To test these hypotheses, ChR2 can be expressed in one of three areas: AON, APC or PPC. AON primarily receives TC input; PPC primarily receives PPC input; and APC receives input from both MCs and TCs. In acute olfactory slices, the strength of inhibitory input onto MCs and TCs (or direct excitatory inputs onto superficial and deep GCs) can be assessed using paired recordings and photostimulation of ChR2 fibers. We expect that feedback from the AON will evoke larger inhibitory currents onto TCs compared with MCs. Similarly we expect feedback from PPC will evoke larger inhibition onto MCs compared with TCs. Feedback from APC should trigger inhibition that is similar in strength between MCs or TCs.

4.5 SEGREGATION OF LATERAL INHIBITION

The data presented in Chapter 3 predict that lateral inhibition between MCs and TCs is, at least partially, segregated. This is supported by our data showing that the output of sGCs and dGCs is partially segregated onto TCs and MCs, respectively. However, our data do not address whether sGCs and dGCs receive overlapping or segregated inputs from MCs and TCs. Given the morphological segregation of sGC apical and TC lateral dendrites in the superficial EPL and

dGC apical and MC lateral dendrites in the deep EPL, it has been suggested that lateral inhibition is segregated (Ezeh, Wellis et al. 1993, Nagayama, Takahashi et al. 2004). However MC and TC axon colatterals could feasibly allow MCs and TCs to excite sGCs and dGCs, respectively (Schoppa 2006, Igarashi, Ieki et al. 2012). Future experiments that can selectively activate either MCs or TCs can clarify the extent to which MCs and TCs exclusively provide excitatory input onto dGCs and sGCs, respectively and, ultimately, whether lateral inhibition is segregated.

For instance, in experiments in which ChR2 is expressed exclusively in TCs or MCs, paired recordings from single sGCs and dGCs can be performed and the size of the excitatory inputs onto each compared. In order to test the overall segregation of lateral inhibition between MCs and TCs, a slight variation to the above experiment must be performed. ChR2 can be expressed exclusively in TCs or MCs. Then, using paired recordings from single MCs and TCs, lateral inhibition can be evoked by photostimulating a single glomerulus so that only MCs or TCs that project to that particular glomerulus are activated. Consequently, the difference in lateral inhibition on TCs and MCs can be compared across a number of individual glomeruli. In addition to measuring the amount of segregation, the dependence of lateral inhibition on distance can also be assessed.

4.6 PLASTICITY OF LATERAL INHIBITION

The data presented in Appendix A provide the first evidence that the strength of inter-glomerular lateral inhibition can be influenced by odor exposure. We show that postnatal odor exposure to the M72-ligand, acetophenone, increases the strength of M72-mediated lateral inhibition onto TCs, but not MCs. This differential influence of postnatal odor exposure on TCs

is specific to M72 ligands, as TCs from mice exposed to hexanal, a non-M72 ligand, did not show increases in the strength of M72-mediated lateral inhibition. Additionally, neither sIPSC frequency nor amplitude were altered by acetophenone or hexanal exposure, indicating that increases in M72-mediated lateral inhibition cannot be explained by increases in the total amount of inhibition onto the recorded M/TC. These experiments raise a number of important questions.

First, does the plasticity of lateral inhibition onto TCs depend on whether the odor exposure paradigm alters the animal's behavior? In our experiments, the mother is painted with the odor once a day. Prior work has shown that pups find the odor aversive after this type of exposure, however painting the odor on the walls of the cage does not change the animal's behavior(Kerr and Belluscio 2006). To test this question, prior work showing that painting the dam, but not the cage's walls, with the odor leads to aversion in the pups must be corroborated. Then, experiments can be performed that explore whether odor exposure (i.e. painting the walls of the cage) leads to increases in the strength of lateral inhibition onto TCs that are similar to the increases caused by odor conditioning (i.e. painting the dam).

Second, does a critical period for plasticity of lateral inhibition onto TCs exist? Similarly, does a separate critical period for plasticity of lateral inhibition onto MCs exist? While a variety of specific changes to the olfactory bulb circuit could explain these activity-dependent increases in lateral inhibition, prior work suggests that GCs are the most plausible source of these changes. Additionally, several lines of evidence suggest that sGCs are more strongly influenced by early odor exposure compared with dGCs. First, subsets of sGCs expressing the glycoprotein 5T4 are known to experience activity-dependent changes in dendritic complexity (Yoshihara, Takahashi et al. 2012). Second, sGCs and dGCs are born at different times during the animal's life –sGCs are typically born during the first few weeks of life (Lemasson, Saghatelyan et al. 2005) while

dGCs are born throughout life (Kelsch, Mosley et al. 2007). Importantly, early odor exposure increases the probability of survival of GCs born in the early postnatal period (P3-7) (mainly sGCs), but not GCs born later (mainly dGCs) (Lemasson, Saghatelyan et al. 2005) while odor discrimination learning during adulthood preferentially increases the probability of survival of adult-born dGCs (Alonso, Viollet et al. 2006). Taken together with the work presented here, these findings suggest that distinct critical windows may exist in which the timing of odor exposure influences the survival of either sGCs or dGCs and consequently the strength of lateral inhibition onto either TCs or MCs.

For the experiments peformed in Appendix A, odor exposure began at P0 and measurements of lateral inhibition were performed between P17-P20. To determine whether the plasticity of lateral inhibition onto TCs only exists during a distinct critical period, odor conditioning can begin later in life (for instance, P10 or P20) and measurements of lateral inhibition can be performed 20 days after the start of conditioning. Measurements of lateral inhibition onto MCs can also be performed during these experiments to determine whether a separate critical period exists for lateral inhibition onto MCs.

An important related question is whether plasticity of lateral inhibition onto TCs persists into adulthood. To test this, odor conditioning can begin at P0 and end at P20. Measurements of lateral inhibition can be performed at multiple time points extending several months after conditioning begins. Control experiments in which odor conditioning persists throughout the entire course of the experiment will also be necessary.

Finally, what mechanisms are responsible for plasticity of lateral inhibition onto TCs? While GCs are the most plausible source of these increases in lateral inhibition, multiple mechanisms can mediate these changes. For instance, more newly-born sGCs could respond to

the conditioned glomerulus. Alternatively, the number of synapses on sGC receiving input from the conditioned glomerulus could increase. To test the first possibility that more sGCs respond to the conditioned glomerulus, calcium-imaging experiments can be performed (either *in vivo* or *in vitro*) to determine whether the number of GCs responsive to a specific glomerulus increases after conditioning. To test the second possibility, whole-cell recordings of GCs can be performed with post-hoc recovery of morphology to test whether GCs that receive input from the conditioned glomerulus have more gemmules or more complex dendritic morphology compared with GCs that do not receive input from the conditioned glomerulus.

4.7 GENERAL CONCLUSIONS

This dissertation provides strong evidence that the olfactory bulb is structured to allow parallel channels of information to encode distinct odor features. Such specialization of functions in mitral and tufted cells emerges due to specific patterns of connectivity to the local inhibitory interneurons. This work challenges the long held assumption that mitral and tufted cells encode redundant information in the olfactory bulb and thus lays the foundation for future work that determines each cell type's unique role in behavior.

APPENDIX A

APPENDIX A: POSTNATAL ODOR EXPOSURE INCREASES THE STRENGTH OF INTER-GLOMERULAR LATERAL INHIBITION ONTO OLFACTORY BULB TUFTED CELLS.

A.1 INTRODUCTION

Determining how past experiences shape sensory responses is vital for understanding how sensory information is processed in specific brain areas. In the olfactory bulb, multiple studies have shown that responses of the two types of projection neurons, mitral cells (MCs) and tufted cells (TCs), depend on prior odor exposure (Buonviso, Gervais et al. 1998, Buonviso and Chaput 2000, Wilson 2000, Spors and Grinvald 2002, Fletcher and Wilson 2003, Wilson and Linster 2008, Chaudhury, Manella et al. 2010, Kato, Chu et al. 2012), yet the specific mechanisms behind these changes remain unknown. Here we focus on how prior odor exposure alters one such circuit element, inter-glomerular lateral inhibition.

MCs and TCs receive excitation from a single glomerulus but inhibition from many – a process known broadly as lateral inhibition. Lateral inhibition is modulated by a variety of inhibitory interneuron subtypes that include superficial short axon cells (sSACs) (Aungst, Heyward et al. 2003, Liu, Plachez et al. 2013, Whitesell, Sorensen et al. 2013, Banerjee,

Marbach et al. 2015), external plexiform layer interneurons (EPL-INs) (Huang, Garcia et al. 2013, Kato, Gillet et al. 2013, Miyamichi, Shlomai-Fuchs et al. 2013) and granule cells (GCs) (Arevian, Kapoor et al. 2008, Fukunaga, Herb et al. 2014, Gschwend, Abraham et al. 2015). These circuits influence MC/TC activity in a variety of ways that include controlling gain (Banerjee, Marbach et al. 2015), decorrelating odor representations (Arevian, Kapoor et al. 2008, Gschwend, Abraham et al. 2015), modulating spike timing (Fukunaga, Herb et al. 2014) and synchronizing gamma frequency oscillations (Lagier, Carleton et al. 2004, Lagier, Panzanelli et al. 2007, Lepousez and Lledo 2013, Fukunaga, Herb et al. 2014). The effects of sensory experience have been studied most extensively in GCs, as previous work has shown that prior odor exposure influences GC survival (Lemasson, Saghatelyan et al. 2005, Saghatelyan, Roux et al. 2005, Alonso, Viollet et al. 2006, Lepousez, Valley et al. 2013), morphology (Saghatelyan, Roux et al. 2005, Yoshihara, Takahashi et al. 2012) and *in vivo* odor responses (Kato, Chu et al. 2012). Whether activity-dependent changes in interneurons leads to changes in inter-glomerular lateral inhibition onto MCs and TCs is unknown.

Although MCs and TCs have distinct morphologies (Mori, Kishi et al. 1983, Orona, Rainer et al. 1984, Burton and Urban 2014) and send axons to largely non-overlapping cortical areas (Haberly and Price 1977, Nagayama, Enerva et al. 2010, Igarashi, Ieki et al. 2012), only recently have their functional differences been described and their distinct roles in odor coding hypothesized. For instance MC and TC odor responses differ in the timing of activation (Fukunaga, Berning et al. 2012, Igarashi, Ieki et al. 2012); concentration-dependence (Nagayama, Takahashi et al. 2004, Fukunaga, Berning et al. 2012, Igarashi, Ieki et al. 2012); and the influence of neuromodulators (Kapoor, Provost et al. 2016), cortical feedback (Otazu, Chae et al. 2015), and lateral inhibition (Nagayama, Takahashi et al. 2004, Geramita, Burton et al.

submitted). Despite this recent push to consider MCs and TCs as functionally distinct, and not equivalent, neuron types, little is known about whether prior sensory experiences differentially impact MCs and TCs. However, lateral inhibition affects spiking in MCs and TCs differently ,in part due to differences in connectivity to superficial GCs (sGCs) and deep GCs (dGCs), respectively – two subclasses of granule cells (Geramita, Burton et al. submitted). Additionally, early olfactory experience increases the survival of GCs born in the early postnatal period (PN 3-14) – the majority of which are sGCs, but has no effect on the survival of GCs born later (PN 14-60) – the majority of which are dGCs (Lemasson, Saghatelyan et al. 2005). Therefore, early postnatal odor exposure may more strongly affect lateral inhibition onto TCs than onto MCs.

Here we show that, in M72-ChR2-YFP mice (Smear, Resulaj et al. 2013), postnatal exposure to the M72 glomerulus ligand, acetophenone, increases the strength of M72-mediated lateral inhibitory currents onto TCs but not MCs. Additionally, we show that this increase in lateral inhibition onto TCs is specific to exposure to M72 ligands and cannot be explained by changes in glomerular layer inhibitory circuitry.

A.2 MATERIALS AND METHODS

A.2.1 Odor exposure

As previously described (Kerr and Belluscio 2006), beginning at P0 and ending at P20, litters of M72-ChR2-YFP (Smear, Resulaj et al. 2013) mice were exposed to one of three odor stimuli through daily application to the nipples of the dam: 1) 50 µl of mineral oil (MO), 2) 50 µl

of a 1:100 (v/v) dilution of acetophenone (Ace) in mineral oil, 3) 50 µl of a 1:100 (v/v) dilution of hexanal (Hex) in mineral oil.

A.2.2 Slice preparation

Postnatal day 17 – 20 M72-ChR2-YFP mice were anaesthetized with isoflurane and decapitated. Brains were dissected into ice-cold oxygenated solution containing (in mM): 125 NaCl, 25 glucose, 2.5 KCl, 25 $NaHCO_3$, 1.25 NaH_2PO_4, 7 $MgCl_2$ and 0.5 $CaCl_2$. Sagittal slices (280 µm thick) of the MOB were prepared using a vibratome (VT1200S; Leica, Nussloch, Germany) and recovered for 15–30 min in 37°C oxygenated Ringer solution that was identical to the dissection solution except for lower Mg^{2+} concentrations (1 mM $MgCl_2$) and higher Ca^{2+} concentrations (2 mM $CaCl_2$). Prior to recording, slices were stored in room temperature oxygenated Ringer solution until recording.

A.2.3 Cell classification

TCs were identified as those cells residing completely in the superficial half of the EPL with large somas (>10 µm in diameter). All TCs had at least 1 lateral dendrite and did not display the rhythmic bursting characteristic of external tufted cells (Hayar, Karnup et al. 2004, Antal, Eyre et al. 2006, Liu and Shipley 2008). MCs were identified as large cells located in the mitral cells layer (MCL). Those cells with somata that only partially reside in the mitral cell layer (‘Displaced MCs (Mori, Kishi et al. 1983)’ or ‘internal TCs (Igarashi, Ieki et al. 2012)’) were excluded from analysis due to their ambiguous identity as MCs or TCs.

A.2.4 Electrophysiology

M/TCs were visualized using infrared differential interference contrast video microscopy. Throughout the recording process, slices were continuously superfused with 37°C oxygenated Ringer solution that contained 0.2 mM Mg^{2+}. Voltage clamp recordings were made using electrodes filled with (in mM): 140 Cs-gluconate, 10 HEPES, 2 KCl, 10 sodium phosphocreatine, 3 Mg-ATP, and 0.3 Na_3GTP,0.25 Alexa Fluor 594 (Life Technologies, Carlsbad, CA, USA) and 0.2% Neurobiotin (Vector Labs, Burlingame, CA, USA). All data were low-pass filtered at 4 kHz and digitized at 10 kHz using a MultiClamp 700A amplifier (Molecular Devices, Sunnyvale, CA, USA) and an ITC-18 acquisition board (Instrutech, Mineola, NY, USA) controlled by custom software written in Igor Pro (WaveMetrics, Lake Oswego, OR, USA). M72 photostimulation was provided by a 250 μm multimode optical fiber (Thorlabs) coupled to a high-intensity light emitting diode (M470F1; Thorlabs) and driver (DC2100: Thorlabs) controlled by TTL pulses.

A.2.5 Data analysis

Inhibitory currents were measured in 7 trials at a holding potential of +10 mV using a single 10 ms light pulse. Spontaneous IPSCs in M/TCs were measured in 4, 30 s trials. Analysis of M72-mediated inhibitory currents was performed using custom Matlab (Mathworks) analysis software. The presence or absence of IPSCs was calculated by taking the average trace of 7 trials and finding the mean and standard deviation of the trace during the second prior to photostimulation. Then the baseline current (mean of the second prior to photostimulation) was subtracted from each trace. Lateral inhibitory currents were present if positive deflections of the

current trace exceeded 3*s.d. for longer than 10 ms in the 500 ms time window following M72 photostimulation. Lateral inhibitory currents were split into early and late phases and the peak current amplitude and charge transfer were calculated in each. As previously described(Geramita, Burton et al. submitted) charge transfer was calculated as the integral of the current trace in either the early phase (0-250ms) or late phase (250-1500ms) following photostimulation. sIPSCs were detected using a standard template-matching function in Axograph (Clements and Bekkers 1997) that included a 21-ms-long double-exponential template with a 5ms baseline, 2ms rise time and 10ms decay constant. All events were detected with a threshold amplitude of 2*SD of the baseline noise. Spurious event detections with rise times >5ms, decay constants >100ms or <2ms were excluded from analysis.

A.3 RESULTS

Isolating the effects of odor-exposure on the strength of inter-glomerular lateral inhibition has proven difficult because it requires the selective activation and identification of the same glomerulus across animals. Here we overcome this challenge by exposing M72-ChR2-YFP mice (Smear, Resulaj et al. 2013) – which express ChR2 exclusively in M72 olfactory sensory neurons (OSNs) – to M72-responsive ligands and then measuring the strength of M72-mediated lateral inhibition via photoactivation of the M72 glomerulus in acute olfactory bulb slices. Beginning at post-natal day 0 (PN0), M72-ChR2-YFP litters were split into 3 groups and exposed to one of three odor stimuli (see **Material and Methods**): mineral oil (MO), acetophenone (Ace) – an odor that activates the M72 glomerulus (Feinstein, Bozza et al. 2004, Zhang, Huang et al. 2012),

or hexanal (Hex) – an odor that does not activate the M72 glomerulus (Smear, Resulaj et al. 2013).

Between PN17-PN20, we cut OB slices and optogenetically activated the M72 glomerulus (10ms light pulse) while recording inhibitory currents in MCs and TCs that innervate nearby glomeruli, as previously described (Geramita, Burton et al. submitted) (Figure 33**a,c**). M72 photostimulation evoked reliable and long lasting inhibitory currents onto MCs and TCs (Figure 33**d**). To quantify the strength of lateral inhibition, we broke lateral inhibitory currents onto MCs and TCs into early (<250 ms) and late (>250 ms) phases. As we have previously shown (Geramita, Burton et al. submitted), MCs from MO-exposed animals received stronger lateral inhibitory currents than TCs from MO-exposed animals (Figure 34**a-d**). The peak amplitude (MC: 34.9 ± 11.9 pA, n=10 cells; TC: 24.2 ± 6.0 pA, n=9; p=0.026, unpaired *t*-test), but not the charge transferred (MC: 2.45 ± 0.92 pA*s; TC: 2.32 ± 0.69 pA*s; p=0.72, unpaired *t*-test) of early phase inhibition was significantly larger in MCs than in TCs from MO-exposed animals. Additionally, both the peak amplitude (MC: 30.9 ± 13.1; TC: 19.4 ± 7.98; p=0.036, unpaired *t*-test) and charge transferred (MC: 7.30 ± 3.39 pA*s; TC: 4.16 ± 1.54 pA*s; p=0.021, unpaired *t*-test) of late phase inhibition was significantly larger in MCs than in TCs from MO-exposed animals. Together these data corroborate prior findings (Geramita, Burton et al. submitted) that M72-mediated lateral inhibition is stronger onto MCs than onto TCs.

Ace-exposure, but not hexanal exposure, increased the strength of M72-mediated lateral inhibition onto TCs, but not MCs. In TCs from Ace-exposed animals, the amplitude (Figure 34**a**; early phase: p=1.5e-6; late phase: p=9.5e-3; one-way ANOVA) and charge (Figure 34**c**; early phase: p=4.0e-4; late phase: p=0.0019; one-way ANOVA) of the early and late phases of inhibition were significantly larger compared with mineral oil or hexanal exposure. In contrast,

neither the amplitude (early phase: p=0.53; late phase: p=0.68 one-way ANOVA) nor charge (early phase: p=0.83; late phase: p=0.96 one-way ANOVA) transferred of the early or late phases of inhibition onto MCs changed following exposure to acetophenone. Therefore postnatal exposure to a ligand that specifically activates the M72 glomerulus increased the strength of M72-mediated lateral inhibition onto TCs, but not MCs.

We next explored other factors that may influence the strength of lateral inhibition. The increase in lateral inhibition onto TCs after acetophenone exposure was maintained when controlling for slice-to-slice variability in the strength of lateral inhibition. The MC/TC ratio of inhibition between cells recorded sequentially in the same slice was significantly reduced in Ace-exposed animals (Figure 34**b**; amplitude: early phase – p=3e-4, late phase – p=0.003; Figure 34**d**; charge: early phase – p=1e-4, late phase – p=0.001; one-way ANOVA). There were no differences in the proportion of MCs (MO – 10/18, 56%; Ace – 9/18, 50%; Hex – 9/20, 45%) and TCs (MO – 9/15, 60%; Ace – 14/25, 56%; Hex – 8/14, 57%) that received lateral inhibition between the 3 odor-exposed groups. Moreover, MCs (MO: 123 ± 86 µm; Ace: 148 ± 97 µm; Hex: 135 ± 75 µm, p=0.72; one-way ANOVA) and TCs (MO: 84 ± 62 µm; Ace: 73 ± 56 µm; Hex: 77 ± 46 µm, p=0.82; one-way ANOVA) from the 3 groups were similar distances from the M72 glomerulus. Additionally, the strength of lateral inhibition did not depend on whether the apical dendrite was intact, as previously described (Geramita, Burton et al. submitted), and TCs without apical dendrites from Ace-exposed mice showed similar increases in the amplitude and charge of lateral inhibition compared with TCs with apical dendrites. Therefore either granule cells or other external plexiform layer interneurons (EPL-INs) are the most likely source of the activity-dependent increases in lateral inhibition described here.

Finally we explored whether increases in M72-mediated lateral inhibition can alternatively be explained as a consequence of increases in the total amount of recurrent inhibition onto the recorded MC/TC. Acetophenone activates many other glomeruli in addition to the M72. Therefore if the recorded M/TCs projected to glomeruli that were also activated during acetophenone exposure and experienced an activity-dependent increase in the total amount of recurrent inhibition (Saghatelyan, Roux et al. 2005), then lateral inhibition triggered by the activation any connected glomerulus – not just the M72 – would increase. To control for this possibility, we measured spontaneous IPSCs (sIPSCs) in MCs and TCs from the 3 odor-exposed groups (Figure 35**a**). Both the amplitude (p=0.038, unpaired t-test) and frequency (p=0.009, unpaired t-test) of sIPSCs are larger in MCs than in TCs from MO-exposed animals. Additionally, neither differed in MCs (amplitude: p=0.65; frequency: p=0.96) and TCs (amplitude: p=0.69; frequency: p=0.95) from acetophenone- or hexanal- exposed animals (Figure 35**b-c**). Therefore increases in the strength of M72-mediated lateral inhibition are most likely due to activity-dependent changes in inhibitory circuitry caused by M72 activation.

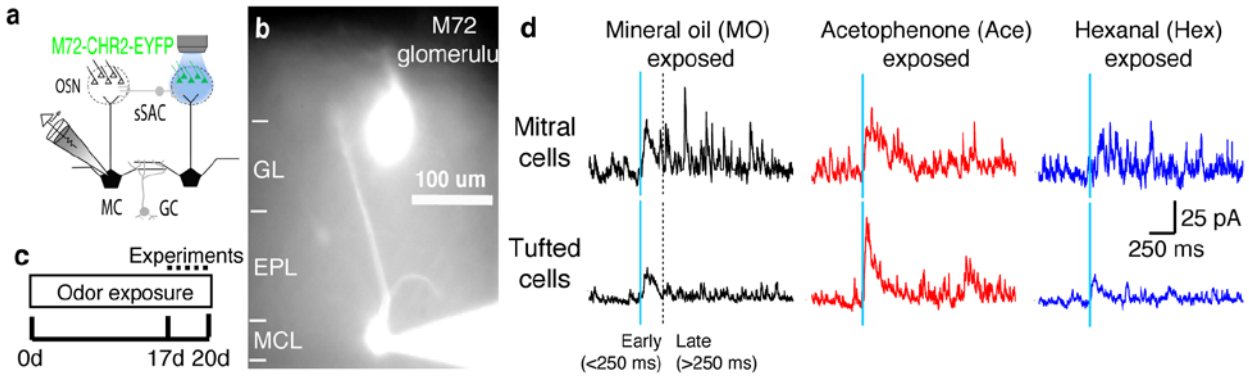

Figure 33: Postnatal exposure to the M72 ligand, acetophenone, increases the strength of M72-mediated lateral inhibition onto TCs, but not MCs.

(**a-b**) Schematic and example of recording from a MC that projects to a glomerulus near the M72 glomerulus in M72-ChR2-YFP mice. (GL: glomerular layer, EPL: external plexiform layer,

MCL: mitral cell layer). Photostimulation of the M72 glomerulus (10 ms light pulse) evokes inhibitory currents. (**c**) Litters are exposed to mineral oil (MO), acetophenone (Ace) or hexanal (Hex) beginning at P0 by daily application of the odor to the nipples of the dam. Experiments measuring M72-mediated lateral inhibition are performed between P17 and P20. (**d**) Examples of M72-mediated lateral inhibition onto MCs (TOP) or TCs (BOTTOM) from MO-exposed mice (LEFT - black); Ace-exposed mice (MIDDLE - red); or Hex-exposed mice (RIGHT - blue). Inhibitory responses were grouped into early phase (<250 ms) and late phase (>250 ms) responses.

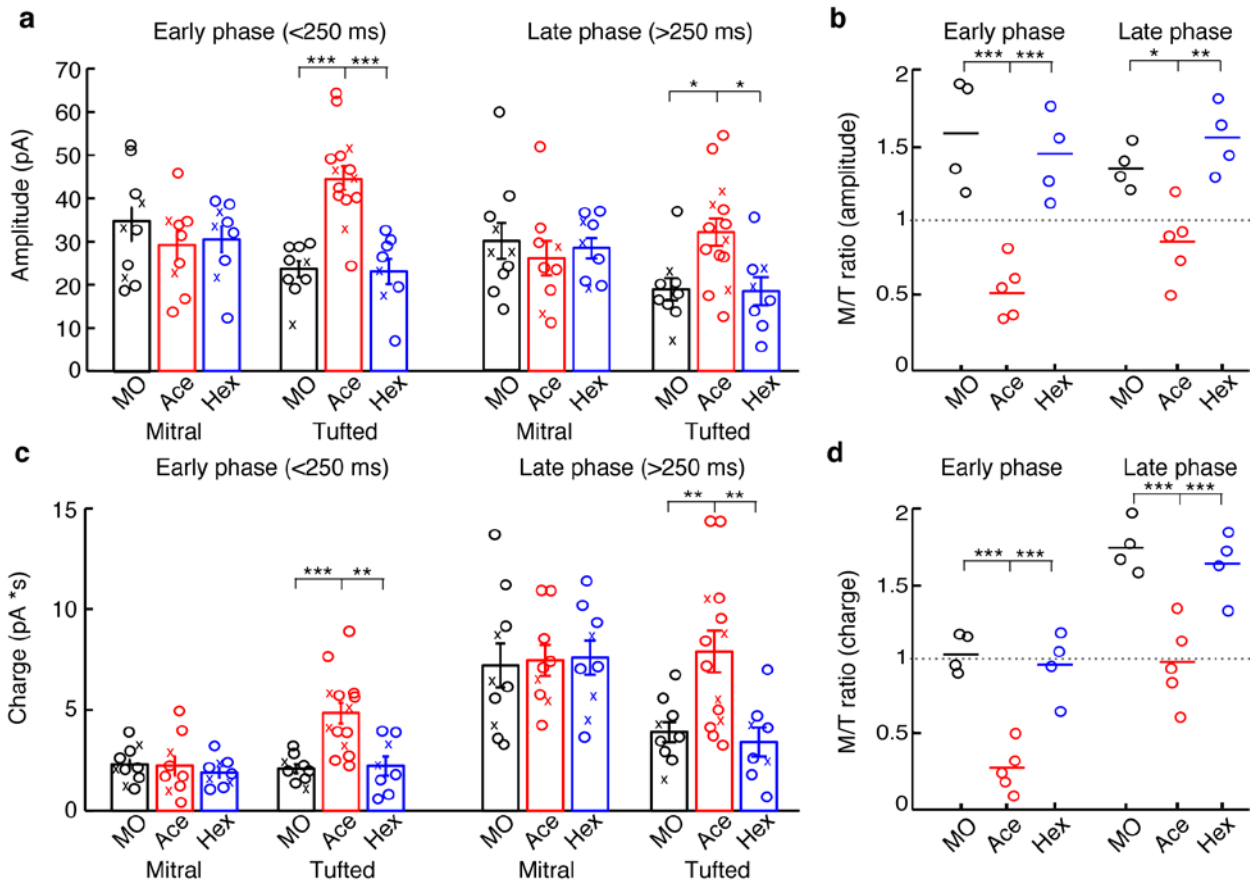

Figure 34: Statistics indicating that postnatal exposure to the M72 ligand, acetophenone, increases the strength of M72-mediated lateral inhibition onto TCs, but not MCs.

(**a-d**) Both the peak amplitude (**a**) and charge transferred (**c**) of early and late phases of inhibition are increased in TCs, but not MCs, from Ace-exposed animals ('x' indicates cells lacking an apical dendrite). The MC/TC ratio of the peak amplitude (**b**) or charge transferred (**d**) between cells recorded sequentially in the same slice was significantly reduced in Ace-exposed animals. Data taken from 24 mitral cells (MO: 10 cells, 8 animals, 2 litters; Ace: 9 cells, 9 animals, 3 litters; Hex: 9 cells, 8 animals, 2 litters) – and 30 tufted cells (Mineral oil: 9 cells, 8 animals, 2 litters; Acetophenone: 14 cells, 10 animals, 3 litters; Hexanal: 8 cells, 5 animals, 2 litters) * $p < 0.05$, ** $p < 0.01$, *** $p < 0.001$. Data presented as mean ± s.e.m.

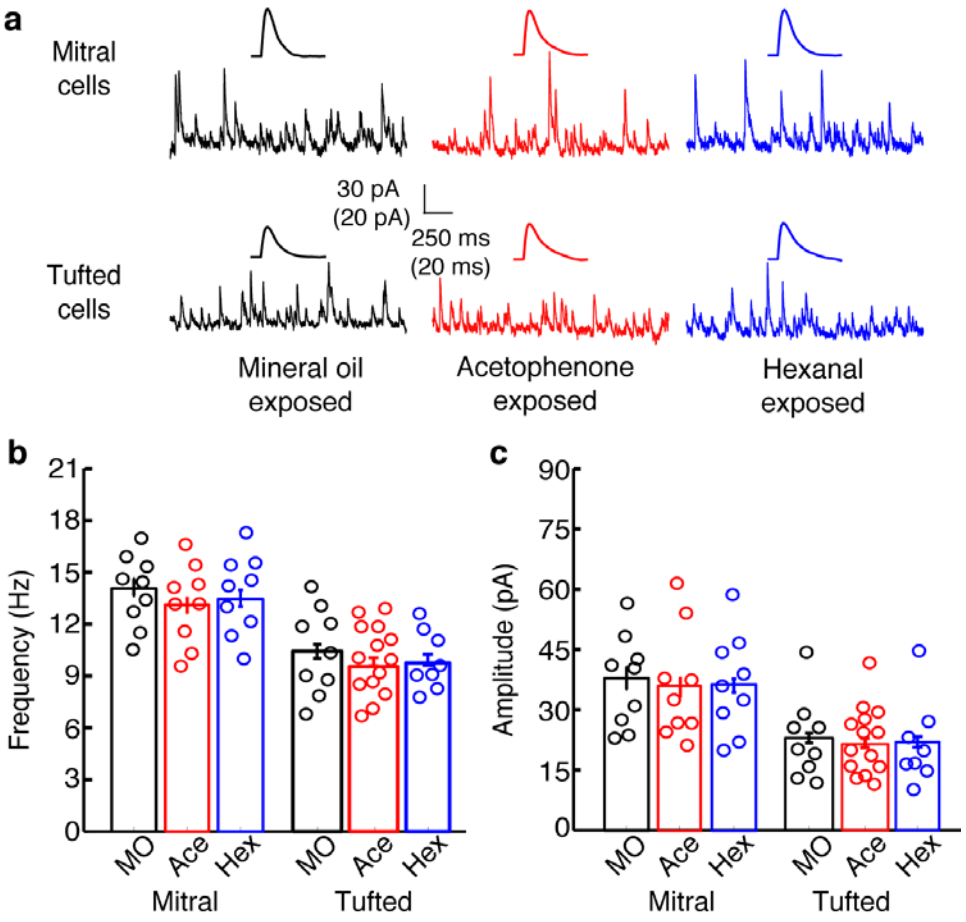

Figure 35: Postnatal exposure to the M72 ligand, acetophenone, increases the strength of M72-mediated lateral inhibition onto TCs, but not MCs.

(**a-b**) Schematic and example of recording from a MC that projects to a glomerulus near the M72 glomerulus in M72-ChR2-YFP mice. (GL: glomerular layer, EPL: external plexiform layer, MCL: mitral cell layer). Photostimulation of the M72 glomerulus (10 ms light pulse) evokes inhibitory currents. (**c**) Litters are exposed to mineral oil (MO), acetophenone (Ace) or hexanal (Hex) beginning at P0 by daily application of the odor to the nipples of the dam. Experiments measuring M72-mediated lateral inhibition are performed between P17 and P20. (**d**) Examples of M72-mediated lateral inhibition onto MCs (TOP) or TCs (BOTTOM) from MO-exposed mice (LEFT - black); Ace-exposed mice (MIDDLE - red); or Hex-exposed mice (RIGHT - blue). Inhibitory responses were grouped into early phase (<250 ms) and late phase (>250 ms) responses. (**e-h**) Both the peak amplitude (**e**) and charge transferred (**g**) of early and late phases of inhibition are increased in TCs, but not MCs, from Ace-exposed animals ('x' indicates cells lacking an apical dendrite). The MC/TC ratio of the peak amplitude (**f**) or charge transferred (**h**) between cells recorded sequentially in the same slice was significantly reduced in Ace-exposed animals. Data taken from 24 mitral cells (MO: 10 cells, 8 animals, 2 litters; Ace: 9 cells, 9 animals, 3 litters; Hex: 9 cells, 8 animals, 2 litters) – and 30 tufted cells (Mineral oil: 9 cells, 8 animals, 2 litters; Acetophenone: 14 cells, 10 animals, 3 litters; Hexanal: 8 cells, 5 animals, 2 litters) * $p < 0.05$, ** $p < 0.01$, *** $p < 0.001$. Data presented as mean ± s.e.m.

A.4 DISCUSSION

Our data provide the first evidence that the strength of inter-glomerular lateral inhibition onto TCs depends on prior odor exposure. We show that postnatal odor exposure to the M72-ligand, acetophenone, increases the strength of M72-mediated lateral inhibition onto TCs, but not MCs. This differential influence of postnatal odor exposure on TCs is specific to acetophenone, as TCs from mice exposed to hexanal did not show increases in the strength of M72-mediated lateral inhibition. Additionally, sIPSC frequency or amplitude was not altered by Ace or Hex exposure, indicating that increases in M72-mediated lateral inhibition cannot be explained by increases in the total amount of inhibition onto the recorded M/TC.

Activity-dependent changes to the strength of inter-glomerular lateral inhibition onto TCs could have multiple physiological roles. First, increasing the strength of lateral inhibition originating from acetophenone-sensitive glomeruli may serve to silence weakly activated TCs and consequently sparsen and/or decorrelate odor representations encoded in populations of TCs. Similarly, prior odor experience in adulthood shifts the tuning curve of individual MCs away from the experienced odors so that MC representations of the experienced odor become sparser (Kato, Chu et al. 2012). Second, increasing the strength of M72-mediated lateral inhibition may serve to shift spike timing or increase gamma synchrony – both of which are mediated by granule cells (Lagier, Carleton et al. 2004, Lagier, Panzanelli et al. 2007, Fukunaga, Herb et al. 2014) and are known to play important roles in olfactory mediated behaviors (Lepousez and Lledo 2013).

While a variety of specific changes to the olfactory bulb circuit could explain the activity-dependent increases in lateral inhibition described here, prior work suggests that GCs are the most plausible source of these changes. Multiple aspects of GC physiology are mediated by olfactory experience: odor deprivation decreases the probability of GC survival, the complexity of GC dendritic arbors and GC spine density (Saghatelyan, Roux et al. 2005) while postnatal odor exposure increases the probability of GC survival (Lemasson, Saghatelyan et al. 2005). Therefore, increases in either the number of GCs activated by M72 activation or the number synapses formed by these GCs could explain the increases in M72-mediated lateral inhibition. However changes to other types of inhibitory interneurons are also possible. In particular, EPL interneurons (EPL-INs) can mediate inhibition onto M/TCs (Huang, Garcia et al. 2013, Kato, Gillet et al. 2013, Miyamichi, Shlomai-Fuchs et al. 2013), and it remains possible that the strength of EPL-IN-mediated inhibition is activity-dependent. Glomerular layer circuits have also been shown to play a role in lateral inhibition (Aungst, Heyward et al. 2003, Liu, Plachez et al. 2013, Whitesell, Sorensen et al. 2013, Banerjee, Marbach et al. 2015), however these circuits most likely do not play a role in the activity-dependence of lateral inhibition reported here because the effects are not influenced by apical dendrite truncation. Finally, any mechanism that increases activity in M72-associated M/TCs could increase activity in interneurons and consequently lateral inhibition onto surrounding TCs. These include activity-dependent increases in the strength of OSN input to M72-M/TCs, the intrinsic excitability of M72-M/TCs, or the number of M72-M/TCs. However, these explanations are unlikely given prior *in vivo* work showing that the vast majority of MCs show reductions in responsiveness following repeated odor exposure (Kato, Chu et al. 2012). These mechanisms also would be unlikely to differentially affect MCs and TCs.

Why is lateral inhibition onto TCs, but not MCs, influenced by postnatal odor exposure? The segregation of TC and sGC dendrites in the superficial EPL and MC and dGC dendrites in the deep EPL (Mori, Kishi et al. 1983, Orona, Scott et al. 1983, Orona, Rainer et al. 1984, Mori 1987) as well as the distinct functional effects of lateral inhibition onto MCs and TCs (Geramita, Burton et al. submitted) suggest that TCs and MCs receive at least partially segregated inhibition from sGCs and dGCs, respectively. Additionally, several lines of evidence suggest that sGCs are more strongly influenced by early odor exposure compared with dGCs. First, subsets of sGCs expressing the glycoprotein 5T4 are known to experience activity-dependent changes in dendritic complexity (Yoshihara, Takahashi et al. 2012). Second, sGCs and dGCs are born at different times during the animal's life –sGCs are typically born during the first few weeks of life (Lemasson, Saghatelyan et al. 2005) while dGCs are born throughout life (Kelsch, Mosley et al. 2007). Importantly, early odor exposure increases the probability of survival of GCs born in the early postnatal period (P3-7) (mainly sGCs), but not GCs born later (mainly dGCs) (Lemasson, Saghatelyan et al. 2005) while odor discrimination learning during adulthood preferentially increases the probability of survival of adult-born dGCs (Alonso, Viollet et al. 2006). Taken together with the work presented here, these findings suggest that distinct critical windows may exist in which the timing of odor exposure influences the survival of either sGCs or dGCs and consequently the strength of lateral inhibition onto either TCs or MCs. Future work involving measurements of lateral inhibition following odor exposure later in life will be needed in order to determine whether the activity-dependence of lateral inhibition persists onto TCs and/or emerges onto MCs.

BIBLIOGRAPHY

Abraham, N. M., V. Egger, D. R. Shimshek, R. Renden, I. Fukunaga, R. Sprengel, P. H. Seeburg, M. Klugmann, T. W. Margrie, A. T. Schaefer and T. Kuner (2010). "Synaptic inhibition in the olfactory bulb accelerates odor discrimination in mice." Neuron **65**(3): 399-411.

Abraham, N. M., H. Spors, A. Carleton, T. W. Margrie, T. Kuner and A. T. Schaefer (2004). "Maintaining accuracy at the expense of speed: stimulus similarity defines odor discrimination time in mice." Neuron **44**(5): 865-876.

Adam, Y., Y. Livneh, K. Miyamichi, M. Groysman, L. Luo and A. Mizrahi (2014). "Functional transformations of odor inputs in the mouse olfactory bulb." Front Neural Circuits **8**: 129.

Alivisatos, A. P., A. M. Andrews, E. S. Boyden, M. Chun, G. M. Church, K. Deisseroth, J. P. Donoghue, S. E. Fraser, J. Lippincott-Schwartz, L. L. Looger, S. Masmanidis, P. L. McEuen, A. V. Nurmikko, H. Park, D. S. Peterka, C. Reid, M. L. Roukes, A. Scherer, M. Schnitzer, T. J. Sejnowski, K. L. Shepard, D. Tsao, G. Turrigiano, P. S. Weiss, C. Xu, R. Yuste and X. Zhuang (2013). "Nanotools for neuroscience and brain activity mapping." ACS Nano **7**(3): 1850-1866.

Alonso, M., C. Viollet, M. M. Gabellec, V. Meas-Yedid, J. C. Olivo-Marin and P. M. Lledo (2006). "Olfactory discrimination learning increases the survival of adult-born neurons in the olfactory bulb." J Neurosci **26**(41): 10508-10513.

Antal, M., M. Eyre, B. Finklea and Z. Nusser (2006). "External tufted cells in the main olfactory bulb form two distinct subpopulations." Eur J Neurosci **24**(4): 1124-1136.

Arevian, A. C., V. Kapoor and N. N. Urban (2008). "Activity-dependent gating of lateral inhibition in the mouse olfactory bulb." Nat Neurosci **11**(1): 80-87.

Aungst, J. L., P. M. Heyward, A. C. Puche, S. V. Karnup, A. Hayar, G. Szabo and M. T. Shipley (2003). "Centre-surround inhibition among olfactory bulb glomeruli." Nature **426**(6967): 623-629.

Banerjee, A., F. Marbach, F. Anselmi, M. S. Koh, M. B. Davis, P. Garcia da Silva, K. Delevich, H. K. Oyibo, P. Gupta, B. Li and D. F. Albeanu (2015). "An Interglomerular Circuit Gates Glomerular Output and Implements Gain Control in the Mouse Olfactory Bulb." Neuron **87**(1): 193-207.

Bathellier, B., D. L. Buhl, R. Accolla and A. Carleton (2008). "Dynamic ensemble odor coding in the mammalian olfactory bulb: sensory information at different timescales." Neuron **57**(4): 586-598.

Bathellier, B., A. Carleton and W. Gerstner (2008). "Gamma oscillations in a nonlinear regime: a minimal model approach using heterogeneous integrate-and-fire networks." Neural Comput **20**(12): 2973-3002.

Bathellier, B., S. Lagier, P. Faure and P. M. Lledo (2006). "Circuit properties generating gamma oscillations in a network model of the olfactory bulb." J Neurophysiol **95**(4): 2678-2691.

Bonner, R. F., M. Emmert-Buck, K. Cole, T. Pohida, R. Chuaqui, S. Goldstein and L. A. Liotta (1997). "Laser capture microdissection: molecular analysis of tissue." Science **278**(5342): 1481,1483.

Boyd, A. M., J. F. Sturgill, C. Poo and J. S. Isaacson (2012). "Cortical feedback control of olfactory bulb circuits." Neuron **76**(6): 1161-1174.

Brody, C. D. and J. J. Hopfield (2003). "Simple networks for spike-timing-based computation, with application to olfactory processing." Neuron **37**(5): 843-852.

Buck, L. B. (1996). "Information coding in the vertebrate olfactory system." Annu Rev Neurosci **19**: 517-544.

Buonviso, N. and M. Chaput (2000). "Olfactory experience decreases responsiveness of the olfactory bulb in the adult rat." Neuroscience **95**(2): 325-332.

Buonviso, N., R. Gervais, M. Chalansonnet and M. Chaput (1998). "Short-lasting exposure to one odour decreases general reactivity in the olfactory bulb of adult rats." Eur J Neurosci **10**(7): 2472-2475.

Burton, S. D. and N. N. Urban (2014). "Greater excitability and firing irregularity of tufted cells underlies distinct afferent-evoked activity of olfactory bulb mitral and tufted cells." J Physiol **592**(Pt 10): 2097-2118.

Burton, S. D. and N. N. Urban (2015). "Rapid Feedforward Inhibition and Asynchronous Excitation Regulate Granule Cell Activity in the Mammalian Main Olfactory Bulb." J Neurosci **35**(42): 14103-14122.

Callaway, E. M. (2005). "Structure and function of parallel pathways in the primate early visual system." J Physiol **566**(Pt 1): 13-19.

Cang, J. and J. S. Isaacson (2003). "In vivo whole-cell recording of odor-evoked synaptic transmission in the rat olfactory bulb." J Neurosci **23**(10): 4108-4116.

Carlson, G. C., M. T. Shipley and A. Keller (2000). "Long-lasting depolarizations in mitral cells of the rat olfactory bulb." J Neurosci **20**(5): 2011-2021.

Cazakoff, B. N., B. Y. Lau, K. L. Crump, H. S. Demmer and S. D. Shea (2014). "Broadly tuned and respiration-independent inhibition in the olfactory bulb of awake mice." Nat Neurosci **17**(4): 569-576.

Chaput, M. A. (1986). "Respiratory-phase-related coding of olfactory information in the olfactory bulb of awake freely-breathing rabbits." Physiol Behav **36**(2): 319-324.

Chaudhury, D., L. Manella, A. Arellanos, O. Escanilla, T. A. Cleland and C. Linster (2010). "Olfactory bulb habituation to odor stimuli." Behav Neurosci **124**(4): 490-499.

Cheetham, C. E., B. D. Grier and L. Belluscio (2015). "Bulk regional viral injection in neonatal mice enables structural and functional interrogation of defined neuronal populations throughout targeted brain areas." Front Neural Circuits **9**: 72.

Christie, J. M., C. Bark, S. G. Hormuzdi, I. Helbig, H. Monyer and G. L. Westbrook (2005). "Connexin36 mediates spike synchrony in olfactory bulb glomeruli." Neuron **46**(5): 761-772.

Cleland, T. A. (2010). "Early transformations in odor representation." Trends Neurosci **33**(3): 130-139.

Clements, J. D. and J. M. Bekkers (1997). "Detection of spontaneous synaptic events with an optimally scaled template." Biophys J **73**(1): 220-229.

Cury, K. M. and N. Uchida (2010). "Robust odor coding via inhalation-coupled transient activity in the mammalian olfactory bulb." Neuron **68**(3): 570-585.

Davidson, S. and G. J. Giesler (2010). "The multiple pathways for itch and their interactions with pain." Trends Neurosci **33**(12): 550-558.

Davison, I. G. and L. C. Katz (2007). "Sparse and selective odor coding by mitral/tufted neurons in the main olfactory bulb." J Neurosci **27**(8): 2091-2101.

De Saint Jan, D., D. Hirnet, G. L. Westbrook and S. Charpak (2009). "External tufted cells drive the output of olfactory bulb glomeruli." J Neurosci **29**(7): 2043-2052.

De Saint Jan, D. and G. L. Westbrook (2007). "Disynaptic amplification of metabotropic glutamate receptor 1 responses in the olfactory bulb." J Neurosci **27**(1): 132-140.

Deisseroth, K. and M. J. Schnitzer (2013). "Engineering approaches to illuminating brain structure and dynamics." Neuron **80**(3): 568-577.

Dhawale, A. K., A. Hagiwara, U. S. Bhalla, V. N. Murthy and D. F. Albeanu (2010). "Non-redundant odor coding by sister mitral cells revealed by light addressable glomeruli in the mouse." Nat Neurosci **13**(11): 1404-1412.

Dong, H. W., A. Hayar and M. Ennis (2007). "Activation of group I metabotropic glutamate receptors on main olfactory bulb granule cells and periglomerular cells enhances synaptic inhibition of mitral cells." J Neurosci **27**(21): 5654-5663.

Egger, V. (2008). "Synaptic sodium spikes trigger long-lasting depolarizations and slow calcium entry in rat olfactory bulb granule cells." Eur J Neurosci **27**(8): 2066-2075.

Egger, V., K. Svoboda and Z. F. Mainen (2003). "Mechanisms of lateral inhibition in the olfactory bulb: efficiency and modulation of spike-evoked calcium influx into granule cells." J Neurosci **23**(20): 7551-7558.

Egger, V., K. Svoboda and Z. F. Mainen (2005). "Dendrodendritic synaptic signals in olfactory bulb granule cells: local spine boost and global low-threshold spike." J Neurosci **25**(14): 3521-3530.

Egger, V. and N. N. Urban (2006). "Dynamic connectivity in the mitral cell-granule cell microcircuit." Semin Cell Dev Biol **17**(4): 424-432.

Emmert-Buck, M. R., R. F. Bonner, P. D. Smith, R. F. Chuaqui, Z. Zhuang, S. R. Goldstein, R. A. Weiss and L. A. Liotta (1996). "Laser capture microdissection." Science **274**(5289): 998-1001.

English, J. G. and B. L. Roth (2015). "Chemogenetics-A Transformational and Translational Platform." JAMA Neurol **72**(11): 1361-1366.

Ezeh, P. I., D. P. Wellis and J. W. Scott (1993). "Organization of inhibition in the rat olfactory bulb external plexiform layer." J Neurophysiol **70**(1): 263-274.

Fantana, A. L., E. R. Soucy and M. Meister (2008). "Rat olfactory bulb mitral cells receive sparse glomerular inputs." Neuron **59**(5): 802-814.

Feinstein, P., T. Bozza, I. Rodriguez, A. Vassalli and P. Mombaerts (2004). "Axon guidance of mouse olfactory sensory neurons by odorant receptors and the beta2 adrenergic receptor." Cell **117**(6): 833-846.

Feng, G., R. H. Mellor, M. Bernstein, C. Keller-Peck, Q. T. Nguyen, M. Wallace, J. M. Nerbonne, J. W. Lichtman and J. R. Sanes (2000). "Imaging neuronal subsets in transgenic mice expressing multiple spectral variants of GFP." Neuron **28**(1): 41-51.

Fletcher, M. L. and D. A. Wilson (2003). "Olfactory bulb mitral-tufted cell plasticity: odorant-specific tuning reflects previous odorant exposure." J Neurosci **23**(17): 6946-6955.

Flytzanis, N. C., C. N. Bedbrook, H. Chiu, M. K. Engqvist, C. Xiao, K. Y. Chan, P. W. Sternberg, F. H. Arnold and V. Gradinaru (2014). "Archaerhodopsin variants with enhanced voltage-sensitive fluorescence in mammalian and Caenorhabditis elegans neurons." Nat Commun **5**: 4894.

Fukunaga, I., M. Berning, M. Kollo, A. Schmaltz and A. T. Schaefer (2012). "Two distinct channels of olfactory bulb output." Neuron **75**(2): 320-329.

Fukunaga, I., J. T. Herb, M. Kollo, E. S. Boyden and A. T. Schaefer (2014). "Independent control of gamma and theta activity by distinct interneuron networks in the olfactory bulb." Nat Neurosci **17**(9): 1208-1216.

Gao, Y. and B. W. Strowbridge (2009). "Long-term plasticity of excitatory inputs to granule cells in the rat olfactory bulb." Nat Neurosci **12**(6): 731-733.

Geramita, M., S. D. Burton and N. N. Urban (submitted). "Distinct lateral inhibitory circuits drive parallel processing of sensory information in the mammalian olfactory bulb.".

Gire, D. H., K. M. Franks, J. D. Zak, K. F. Tanaka, J. D. Whitesell, A. A. Mulligan, R. Hen and N. E. Schoppa (2012). "Mitral cells in the olfactory bulb are mainly excited through a multistep signaling path." J Neurosci **32**(9): 2964-2975.

Gire, D. H. and N. E. Schoppa (2009). "Control of on/off glomerular signaling by a local GABAergic microcircuit in the olfactory bulb." J Neurosci **29**(43): 13454-13464.

Giridhar, S., B. Doiron and N. N. Urban (2011). "Timescale-dependent shaping of correlation by olfactory bulb lateral inhibition." Proc Natl Acad Sci U S A **108**(14): 5843-5848.

Giridhar, S. and N. N. Urban (2012). "Mechanisms and benefits of granule cell latency coding in the mouse olfactory bulb." Front Neural Circuits **6**: 40.

Gradinaru, V., K. R. Thompson and K. Deisseroth (2008). "eNpHR: a Natronomonas halorhodopsin enhanced for optogenetic applications." Brain Cell Biol **36**(1-4): 129-139.

Gschwend, O., N. M. Abraham, S. Lagier, F. Begnaud, I. Rodriguez and A. Carleton (2015). "Neuronal pattern separation in the olfactory bulb improves odor discrimination learning." Nat Neurosci **18**(10): 1474-1482.

Guez-Barber, D., S. Fanous, B. K. Harvey, Y. Zhang, E. Lehrmann, K. G. Becker, M. R. Picciotto and B. T. Hope (2012). "FACS purification of immunolabeled cell types from adult rat brain." J Neurosci Methods **203**(1): 10-18.

Haberly, L. B. and J. L. Price (1977). "The axonal projection patterns of the mitral and tufted cells of the olfactory bulb in the rat." Brain Res **129**(1): 152-157.

Haddad, R., A. Lanjuin, L. Madisen, H. Zeng, V. N. Murthy and N. Uchida (2013). "Olfactory cortical neurons read out a relative time code in the olfactory bulb." Nat Neurosci **16**(7): 949-957.

Hayar, A., S. Karnup, M. Ennis and M. T. Shipley (2004). "External tufted cells: a major excitatory element that coordinates glomerular activity." J Neurosci **24**(30): 6676-6685.

Hayar, A., S. Karnup, M. T. Shipley and M. Ennis (2004). "Olfactory bulb glomeruli: external tufted cells intrinsically burst at theta frequency and are entrained by patterned olfactory input." J Neurosci **24**(5): 1190-1199.

Hayar, A., M. T. Shipley and M. Ennis (2005). "Olfactory bulb external tufted cells are synchronized by multiple intraglomerular mechanisms." J Neurosci **25**(36): 8197-8208.

Heinbockel, T., P. Heyward, F. Conquet and M. Ennis (2004). "Regulation of main olfactory bulb mitral cell excitability by metabotropic glutamate receptor mGluR1." J Neurophysiol **92**(5): 3085-3096.

Heinbockel, T., N. Laaris and M. Ennis (2007). "Metabotropic glutamate receptors in the main olfactory bulb drive granule cell-mediated inhibition." J Neurophysiol **97**(1): 858-870.

Hirsch, J. A. and C. D. Gilbert (1991). "Synaptic physiology of horizontal connections in the cat's visual cortex." J Neurosci **11**(6): 1800-1809.

Hopfield, J. J. (1995). "Pattern recognition computation using action potential timing for stimulus representation." Nature **376**(6535): 33-36.

Huang, L., I. Garcia, H. I. Jen and B. R. Arenkiel (2013). "Reciprocal connectivity between mitral cells and external plexiform layer interneurons in the mouse olfactory bulb." Front Neural Circuits **7**: 32.

Igarashi, K. M., N. Ieki, M. An, Y. Yamaguchi, S. Nagayama, K. Kobayakawa, R. Kobayakawa, M. Tanifuji, H. Sakano, W. R. Chen and K. Mori (2012). "Parallel mitral and tufted cell pathways route distinct odor information to different targets in the olfactory cortex." J Neurosci **32**(23): 7970-7985.

Isaacson, J. S. and B. W. Strowbridge (1998). "Olfactory reciprocal synapses: dendritic signaling in the CNS." Neuron **20**(4): 749-761.

Johnson, B. A. and M. Leon (2000). "Modular representations of odorants in the glomerular layer of the rat olfactory bulb and the effects of stimulus concentration." J Comp Neurol **422**(4): 496-509.

Kapoor, V., A. C. Provost, P. Agarwal and V. N. Murthy (2016). "Activation of raphe nuclei triggers rapid and distinct effects on parallel olfactory bulb output channels." Nat Neurosci **19**(2): 271-282.

Kapoor, V. and N. N. Urban (2006). "Glomerulus-specific, long-latency activity in the olfactory bulb granule cell network." J Neurosci **26**(45): 11709-11719.

Kato, H. K., M. W. Chu, J. S. Isaacson and T. Komiyama (2012). "Dynamic sensory representations in the olfactory bulb: modulation by wakefulness and experience." Neuron **76**(5): 962-975.

Kato, H. K., S. N. Gillet, A. J. Peters, J. S. Isaacson and T. Komiyama (2013). "Parvalbumin-Expressing Interneurons Linearly Control Olfactory Bulb Output." Neuron.

Kelsch, W., C. P. Mosley, C. W. Lin and C. Lois (2007). "Distinct mammalian precursors are committed to generate neurons with defined dendritic projection patterns." PLoS Biol **5**(11): e300.

Kerr, M. A. and L. Belluscio (2006). "Olfactory experience accelerates glomerular refinement in the mammalian olfactory bulb." Nat Neurosci **9**(4): 484-486.

Kikuta, S., M. L. Fletcher, R. Homma, T. Yamasoba and S. Nagayama (2013). "Odorant response properties of individual neurons in an olfactory glomerular module." Neuron **77**(6): 1122-1135.

Kiyokage, E., Y. Z. Pan, Z. Shao, K. Kobayashi, G. Szabo, Y. Yanagawa, K. Obata, H. Okano, K. Toida, A. C. Puche and M. T. Shipley (2010). "Molecular identity of periglomerular and short axon cells." J Neurosci **30**(3): 1185-1196.

Kosaka, K., K. Toida, Y. Aika and T. Kosaka (1998). "How simple is the organization of the olfactory glomerulus?: the heterogeneity of so-called periglomerular cells." Neurosci Res **30**(2): 101-110.

Kosaka, T. and K. Kosaka (2010). "Heterogeneity of calbindin-containing neurons in the mouse main olfactory bulb: I. General description." Neurosci Res **67**(4): 275-292.

Kosaka, T. and K. Kosaka (2011). ""Interneurons" in the olfactory bulb revisited." Neurosci Res **69**(2): 93-99.

Lagier, S., A. Carleton and P. M. Lledo (2004). "Interplay between local GABAergic interneurons and relay neurons generates gamma oscillations in the rat olfactory bulb." J Neurosci **24**(18): 4382-4392.

Lagier, S., P. Panzanelli, R. E. Russo, A. Nissant, B. Bathellier, M. Sassoe-Pognetto, J. M. Fritschy and P. M. Lledo (2007). "GABAergic inhibition at dendrodendritic synapses tunes gamma oscillations in the olfactory bulb." Proc Natl Acad Sci U S A **104**(17): 7259-7264.

Lemasson, M., A. Saghatelyan, J. C. Olivo-Marin and P. M. Lledo (2005). "Neonatal and adult neurogenesis provide two distinct populations of newborn neurons to the mouse olfactory bulb." J Neurosci **25**(29): 6816-6825.

Lepousez, G. and P. M. Lledo (2013). "Odor discrimination requires proper olfactory fast oscillations in awake mice." Neuron **80**(4): 1010-1024.

Lepousez, G., M. T. Valley and P. M. Lledo (2013). "The impact of adult neurogenesis on olfactory bulb circuits and computations." Annu Rev Physiol **75**: 339-363.

Liu, S., C. Plachez, Z. Shao, A. Puche and M. T. Shipley (2013). "Olfactory bulb short axon cell release of GABA and dopamine produces a temporally biphasic inhibition-excitation response in external tufted cells." J Neurosci **33**(7): 2916-2926.

Liu, S. and M. T. Shipley (2008). "Intrinsic conductances actively shape excitatory and inhibitory postsynaptic responses in olfactory bulb external tufted cells." J Neurosci **28**(41): 10311-10322.

Liu, S. and M. T. Shipley (2008). "Multiple conductances cooperatively regulate spontaneous bursting in mouse olfactory bulb external tufted cells." J Neurosci **28**(7): 1625-1639.

Lomber, S. G. and S. Malhotra (2008). "Double dissociation of 'what' and 'where' processing in auditory cortex." Nat Neurosci **11**(5): 609-616.

Luo, L., E. M. Callaway and K. Svoboda (2008). "Genetic dissection of neural circuits." Neuron **57**(5): 634-660.

Ma, J. and G. Lowe (2010). "Correlated firing in tufted cells of mouse olfactory bulb." Neuroscience **169**(4): 1715-1738.

Markopoulos, F., D. Rokni, D. H. Gire and V. N. Murthy (2012). "Functional properties of cortical feedback projections to the olfactory bulb." Neuron **76**(6): 1175-1188.

Masland, R. H. (2012). "The neuronal organization of the retina." Neuron **76**(2): 266-280.

Meister, M. and T. Bonhoeffer (2001). "Tuning and topography in an odor map on the rat olfactory bulb." J Neurosci **21**(4): 1351-1360.

Meredith, M. (1986). "Patterned response to odor in mammalian olfactory bulb: the influence of intensity." J Neurophysiol **56**(3): 572-597.

Merigan, W. H. and J. H. Maunsell (1993). "How parallel are the primate visual pathways?" Annu Rev Neurosci **16**: 369-402.

Miyamichi, K., Y. Shlomai-Fuchs, M. Shu, B. C. Weissbourd, L. Luo and A. Mizrahi (2013). "Dissecting local circuits: parvalbumin interneurons underlie broad feedback control of olfactory bulb output." Neuron **80**(5): 1232-1245.

Mombaerts, P., F. Wang, C. Dulac, S. K. Chao, A. Nemes, M. Mendelsohn, J. Edmondson and R. Axel (1996). "Visualizing an olfactory sensory map." Cell **87**(4): 675-686.

Mombaerts, P., F. Wang, C. Dulac, R. Vassar, S. K. Chao, A. Nemes, M. Mendelsohn, J. Edmondson and R. Axel (1996). "The molecular biology of olfactory perception." Cold Spring Harb Symp Quant Biol **61**: 135-145.

Mori, K. (1987). "Membrane and synaptic properties of identified neurons in the olfactory bulb." Prog Neurobiol **29**(3): 275-320.

Mori, K., K. Kishi and H. Ojima (1983). "Distribution of dendrites of mitral, displaced mitral, tufted, and granule cells in the rabbit olfactory bulb." J Comp Neurol **219**(3): 339-355.

Mori, K., Y. K. Takahashi, K. M. Igarashi and M. Yamaguchi (2006). "Maps of odorant molecular features in the Mammalian olfactory bulb." Physiol Rev **86**(2): 409-433.

Nagayama, S., A. Enerva, M. L. Fletcher, A. V. Masurkar, K. M. Igarashi, K. Mori and W. R. Chen (2010). "Differential axonal projection of mitral and tufted cells in the mouse main olfactory system." Front Neural Circuits **4**.

Nagayama, S., Y. K. Takahashi, Y. Yoshihara and K. Mori (2004). "Mitral and tufted cells differ in the decoding manner of odor maps in the rat olfactory bulb." J Neurophysiol **91**(6): 2532-2540.

Najac, M., D. De Saint Jan, L. Reguero, P. Grandes and S. Charpak (2011). "Monosynaptic and polysynaptic feed-forward inputs to mitral cells from olfactory sensory neurons." J Neurosci **31**(24): 8722-8729.

Najac, M., A. Sanz Diez, A. Kumar, N. Benito, S. Charpak and D. De Saint Jan (2015). "Intraglomerular lateral inhibition promotes spike timing variability in principal neurons of the olfactory bulb." J Neurosci **35**(10): 4319-4331.

Neville, K. R. and L. B. Haberly (2003). "Beta and gamma oscillations in the olfactory system of the urethane-anesthetized rat." J Neurophysiol **90**(6): 3921-3930.

Ngai, J., A. Chess, M. M. Dowling, N. Necles, E. R. Macagno and R. Axel (1993). "Coding of olfactory information: topography of odorant receptor expression in the catfish olfactory epithelium." Cell **72**(5): 667-680.

Ngai, J., M. M. Dowling, L. Buck, R. Axel and A. Chess (1993). "The family of genes encoding odorant receptors in the channel catfish." Cell **72**(5): 657-666.

Nissant, A., C. Bardy, H. Katagiri, K. Murray and P. M. Lledo (2009). "Adult neurogenesis promotes synaptic plasticity in the olfactory bulb." Nat Neurosci **12**(6): 728-730.

Orona, E., E. C. Rainer and J. W. Scott (1984). "Dendritic and axonal organization of mitral and tufted cells in the rat olfactory bulb." J Comp Neurol **226**(3): 346-356.

Orona, E., J. W. Scott and E. C. Rainer (1983). "Different granule cell populations innervate superficial and deep regions of the external plexiform layer in rat olfactory bulb." J Comp Neurol **217**(2): 227-237.

Oswald, A. M. and N. N. Urban (2012). "There and back again: the corticobulbar loop." Neuron **76**(6): 1045-1047.

Otazu, G. H., H. Chae, M. B. Davis and D. F. Albeanu (2015). "Cortical Feedback Decorrelates Olfactory Bulb Output in Awake Mice." Neuron **86**(6): 1461-1477.

Padmanabhan, K. and N. N. Urban (2010). "Intrinsic biophysical diversity decorrelates neuronal firing while increasing information content." Nat Neurosci **13**(10): 1276-1282.

Parrish-Aungst, S., M. T. Shipley, F. Erdelyi, G. Szabo and A. C. Puche (2007). "Quantitative analysis of neuronal diversity in the mouse olfactory bulb." J Comp Neurol **501**(6): 825-836.

Patterson, M. A., S. Lagier and A. Carleton (2013). "Odor representations in the olfactory bulb evolve after the first breath and persist as an odor afterimage." Proc Natl Acad Sci U S A **110**(35): E3340-3349.

Pinching, A. J. and T. P. Powell (1971). "The neuron types of the glomerular layer of the olfactory bulb." J Cell Sci **9**(2): 305-345.

Pinching, A. J. and T. P. Powell (1971). "The neuropil of the glomeruli of the olfactory bulb." J Cell Sci **9**(2): 347-377.

Pinching, A. J. and T. P. Powell (1971). "The neuropil of the periglomerular region of the olfactory bulb." J Cell Sci **9**(2): 379-409.

Quian Quiroga, R. and S. Panzeri (2009). "Extracting information from neuronal populations: information theory and decoding approaches." Nat Rev Neurosci **10**(3): 173-185.

Quiroga, R. Q., L. Reddy, C. Koch and I. Fried (2007). "Decoding visual inputs from multiple neurons in the human temporal lobe." J Neurophysiol **98**(4): 1997-2007.

Rall, W., G. M. Shepherd, T. S. Reese and M. W. Brightman (1966). "Dendrodendritic synaptic pathway for inhibition in the olfactory bulb." Exp Neurol **14**(1): 44-56.

Ressler, K. J., S. L. Sullivan and L. B. Buck (1993). "A zonal organization of odorant receptor gene expression in the olfactory epithelium." Cell **73**(3): 597-609.

Ressler, K. J., S. L. Sullivan and L. B. Buck (1994). "A molecular dissection of spatial patterning in the olfactory system." Curr Opin Neurobiol **4**(4): 588-596.

Rinberg, D., A. Koulakov and A. Gelperin (2006). "Sparse odor coding in awake behaving mice." J Neurosci **26**(34): 8857-8865.

Rinberg, D., A. Koulakov and A. Gelperin (2006). "Speed-accuracy tradeoff in olfaction." Neuron **51**(3): 351-358.

Ronnett, G. V., H. Cho, L. D. Hester, S. F. Wood and S. H. Snyder (1993). "Odorants differentially enhance phosphoinositide turnover and adenylyl cyclase in olfactory receptor neuronal cultures." J Neurosci **13**(4): 1751-1758.

Ross, S. E. (2011). "Pain and itch: insights into the neural circuits of aversive somatosensation in health and disease." Curr Opin Neurobiol **21**(6): 880-887.

Rothermel, M., D. Brunert, C. Zabawa, M. Diaz-Quesada and M. Wachowiak (2013). "Transgene expression in target-defined neuron populations mediated by retrograde infection with adeno-associated viral vectors." J Neurosci **33**(38): 15195-15206.

Rubin, B. D. and L. C. Katz (1999). "Optical imaging of odorant representations in the mammalian olfactory bulb." Neuron **23**(3): 499-511.

Saghatelyan, A., P. Roux, M. Migliore, C. Rochefort, D. Desmaisons, P. Charneau, G. M. Shepherd and P. M. Lledo (2005). "Activity-dependent adjustments of the inhibitory network in the olfactory bulb following early postnatal deprivation." Neuron **46**(1): 103-116.

Schoppa, N. E. (2006). "AMPA/kainate receptors drive rapid output and precise synchrony in olfactory bulb granule cells." J Neurosci **26**(50): 12996-13006.

Schoppa, N. E. and N. N. Urban (2003). "Dendritic processing within olfactory bulb circuits." Trends Neurosci **26**(9): 501-506.

Schoppa, N. E. and G. L. Westbrook (2001). "Glomerulus-specific synchronization of mitral cells in the olfactory bulb." Neuron **31**(4): 639-651.

Schoppa, N. E. and G. L. Westbrook (2002). "AMPA autoreceptors drive correlated spiking in olfactory bulb glomeruli." Nat Neurosci **5**(11): 1194-1202.

Seroogy, K. B., N. Brecha and C. Gall (1985). "Distribution of cholecystokinin-like immunoreactivity in the rat main olfactory bulb." J Comp Neurol **239**(4): 373-383.

Shao, Z., A. C. Puche, E. Kiyokage, G. Szabo and M. T. Shipley (2009). "Two GABAergic intraglomerular circuits differentially regulate tonic and phasic presynaptic inhibition of olfactory nerve terminals." J Neurophysiol **101**(4): 1988-2001.

Shao, Z., A. C. Puche, S. Liu and M. T. Shipley (2012). "Intraglomerular inhibition shapes the strength and temporal structure of glomerular output." J Neurophysiol **108**(3): 782-793.

Shusterman, R., M. C. Smear, A. A. Koulakov and D. Rinberg (2011). "Precise olfactory responses tile the sniff cycle." Nat Neurosci **14**(8): 1039-1044.

Sirotin, Y. B., R. Shusterman and D. Rinberg (2015). "Neural Coding of Perceived Odor Intensity(1,2,3)." eNeuro **2**(6).

Smear, M., A. Resulaj, J. Zhang, T. Bozza and D. Rinberg (2013). "Multiple perceptible signals from a single olfactory glomerulus." Nat Neurosci **16**(11): 1687-1691.

Smear, M., R. Shusterman, R. O'Connor, T. Bozza and D. Rinberg (2011). "Perception of sniff phase in mouse olfaction." Nature **479**(7373): 397-400.

Soucy, E. R., D. F. Albeanu, A. L. Fantana, V. N. Murthy and M. Meister (2009). "Precision and diversity in an odor map on the olfactory bulb." Nat Neurosci **12**(2): 210-220.

Spors, H., D. F. Albeanu, V. N. Murthy, D. Rinberg, N. Uchida, M. Wachowiak and R. W. Friedrich (2012). "Illuminating vertebrate olfactory processing." J Neurosci **32**(41): 14102-14108.

Spors, H. and A. Grinvald (2002). "Spatio-temporal dynamics of odor representations in the mammalian olfactory bulb." Neuron **34**(2): 301-315.

Stockman, A. and L. T. Sharpe (2006). "Into the twilight zone: the complexities of mesopic vision and luminous efficiency." Ophthalmic Physiol Opt **26**(3): 225-239.

Taniguchi, H., M. He, P. Wu, S. Kim, R. Paik, K. Sugino, D. Kvitsiani, Y. Fu, J. Lu, Y. Lin, G. Miyoshi, Y. Shima, G. Fishell, S. B. Nelson and Z. J. Huang (2011). "A resource of Cre driver lines for genetic targeting of GABAergic neurons in cerebral cortex." Neuron **71**(6): 995-1013.

Uchida, N., N. Eshel and M. Watabe-Uchida (2013). "Division of labor for division: inhibitory interneurons with different spatial landscapes in the olfactory system." Neuron **80**(5): 1106-1109.

Uchida, N. and Z. F. Mainen (2003). "Speed and accuracy of olfactory discrimination in the rat." Nat Neurosci **6**(11): 1224-1229.

Uchida, N., C. Poo and R. Haddad (2014). "Coding and transformations in the olfactory system." Annu Rev Neurosci **37**: 363-385.

Uchida, N., Y. K. Takahashi, M. Tanifuji and K. Mori (2000). "Odor maps in the mammalian olfactory bulb: domain organization and odorant structural features." Nat Neurosci **3**(10): 1035-1043.

Urban, D. J. and B. L. Roth (2015). "DREADDs (designer receptors exclusively activated by designer drugs): chemogenetic tools with therapeutic utility." Annu Rev Pharmacol Toxicol **55**: 399-417.

Urban, N. N. (2002). "Lateral inhibition in the olfactory bulb and in olfaction." Physiol Behav **77**(4-5): 607-612.

Urban, N. N. and A. C. Arevian (2009). "Computing with dendrodendritic synapses in the olfactory bulb." Ann N Y Acad Sci **1170**: 264-269.

Vardy, E., J. E. Robinson, C. Li, R. H. Olsen, J. F. DiBerto, P. M. Giguere, F. M. Sassano, X. P. Huang, H. Zhu, D. J. Urban, K. L. White, J. E. Rittiner, N. A. Crowley, K. E. Pleil, C. M. Mazzone, P. D. Mosier, J. Song, T. L. Kash, C. J. Malanga, M. J. Krashes and B. L. Roth (2015). "A New DREADD Facilitates the Multiplexed Chemogenetic Interrogation of Behavior." Neuron **86**(4): 936-946.

Vassar, R., J. Ngai and R. Axel (1993). "Spatial segregation of odorant receptor expression in the mammalian olfactory epithelium." Cell **74**(2): 309-318.

Wachowiak, M. (2011). "All in a sniff: olfaction as a model for active sensing." Neuron **71**(6): 962-973.

Wachowiak, M., W. Denk and R. W. Friedrich (2004). "Functional organization of sensory input to the olfactory bulb glomerulus analyzed by two-photon calcium imaging." Proc Natl Acad Sci U S A **101**(24): 9097-9102.

Wellis, D. P. and J. W. Scott (1990). "Intracellular responses of identified rat olfactory bulb interneurons to electrical and odor stimulation." J Neurophysiol **64**(3): 932-947.

Whitesell, J. D., K. A. Sorensen, B. C. Jarvie, S. T. Hentges and N. E. Schoppa (2013). "Interglomerular lateral inhibition targeted on external tufted cells in the olfactory bulb." J Neurosci **33**(4): 1552-1563.

Wilson, D. A. (2000). "Comparison of odor receptive field plasticity in the rat olfactory bulb and anterior piriform cortex." J Neurophysiol **84**(6): 3036-3042.

Wilson, D. A. and C. Linster (2008). "Neurobiology of a simple memory." J Neurophysiol **100**(1): 2-7.

Yoshihara, S., H. Takahashi, N. Nishimura, H. Naritsuka, T. Shirao, H. Hirai, Y. Yoshihara, K. Mori, P. L. Stern and A. Tsuboi (2012). "5T4 glycoprotein regulates the sensory input-dependent development of a specific subtype of newborn interneurons in the mouse olfactory bulb." J Neurosci **32**(6): 2217-2226.

Zhang, J., G. Huang, A. Dewan, P. Feinstein and T. Bozza (2012). "Uncoupling stimulus specificity and glomerular position in the mouse olfactory system." Mol Cell Neurosci **51**(3-4): 79-88.

Zhang, X. and S. Firestein (2002). "The olfactory receptor gene superfamily of the mouse." Nat Neurosci **5**(2): 124-133.

Zufall, F., T. Leinders-Zufall and C. A. Greer (2000). "Amplification of odor-induced Ca(2+) transients by store-operated Ca(2+) release and its role in olfactory signal transduction." J Neurophysiol **83**(1): 501-512.